Group theoretical analysis of structural instability, vacancy ordering and magnetic transitions in the system troilite (FeS) – pyrrhotite ($Fe_{1-x}S$)

Authors

X**Charles Robert Sebastian Haines[a]*, Christopher J. Howard[b], Richard J. Harrison[a] and Michael A. Carpenter[a]**

[a]Department of Earth Sciences, University of Cambridge, Downing Street, Cambridge, Cambridgeshire, CB3EQ, UK

[b]School of Engineering, The University of Newcastle, University Drive, Callaghan, NSW, 2308, Australia

Correspondence email: crsh2@cam.ac.uk

Funding information Leverhulme Trust.

ynopsis A group-theoretical framework to describe vacancy ordering and magnetism in the $Fe_{1-x}S$ system is developed.

bstract A group-theoretical framework to describe vacancy ordering and magnetism in the $Fe_{1-x}S$ system is developed. This framework is used to determine the sequence of crystal structures consistent with the observed magnetic structures of troilite (FeS), and to determine the crystallographic nature of the low-temperature Besnus transition in $Fe_{0.875}S$. We conclude that the Besnus transition is a magnetically driven transition characterised by the rotation of the moments out of the crystallographic plane to which they are confined above the transition, accompanied by small atomic displacements that lower the symmetry from monoclinic to triclinic at low temperatures. Based on our phase diagram, we predict magnetically driven phase transitions at low temperatures in all the commensurate superstructures of pyrrhotite. The exact nature of the transition is determined by the symmetry of the vacancy ordered state and based on this we predict spin-flop transitions in 3C and 5C pyrrhotite and a transition akin to the Besnus transition in 6C pyrrhotite. Furthermore, we clarify that 3C and 4C pyrrhotite carry a ferrimagnetic moment whereas 5C and 6C are antiferromagnetic.

Keywords: Pyrrhotite; Group Theory; Besnus Transition, Vacancy Ordering, Magnetism

1. Introduction

The mineral pyrrhotite has compositions that are usually expressed in terms of an ideal formula, $Fe_{1-x}S$ ($0 \leq x \leq 0.15$). It adopts the hexagonal NiAs structure at high temperatures, with an increasing concentration of vacancies on the metal cation site (increasing x). Such a simple description belies the remarkable diversity of superstructures and phase transitions that are observed in both natural and synthetic samples. This phenomenological richness is reflected in a complex subsolidus phase diagram (Figure 1; Grønvold and Stølen 1992). The hexagonal structure at high temperatures is labelled as 1C. This gives way to four different commensurate superstructures with repeats along the crystallographic c-axis, corresponding to 3, 4, 5 and 6 times that of the parent structure (3C, 4C, 5C, 6C), and incommensurate superstructures in which a non-rational repeat varies with composition and temperature. Although other compilations differ in detail (Wang & Salveson 2005; Bennett &Graham 1980), it has long been understood that these complex structural relationships arise as a consequence of Fe/vacancy ordering, which, at particular stoichiometries, produce vacancy ordered phases that are more stable than the disordered continuous solid solution (Morimoto & Nakazawa, 1968; Morimoto *et al.* 1970; Carpenter & Desborough, 1964; Andresen *et al.* 1960; Andresen *et al.* 1967). The end member FeS (troilite) has no vacancies but has at least four potential structural instabilities with symmetries relating to the *K*, *M*, *H* and *L* points of the Brillouin zone of the parent primitive hexagonal lattice (Ricci & Bousquet, 2016).

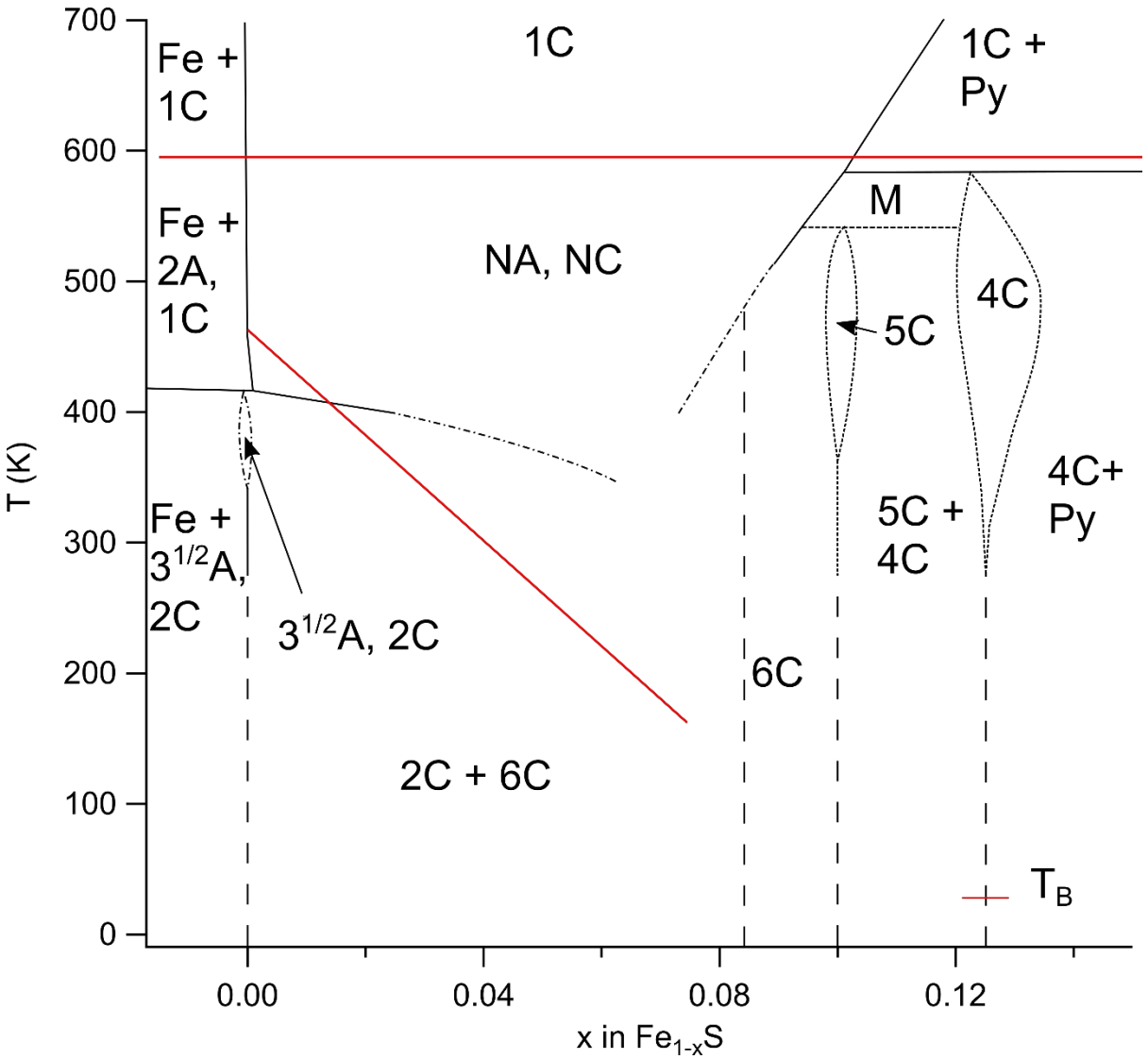

Figure 1 Schematic phase relations, following Grønvold & Stølen (1992), for the system $Fe_{1-x}S$. A and C represent lattice parameters of the parent hexagonal NiAs structure (1C). Commensurate superstructures have multiple repeats of these. Incommensurate superstructures can occur at a wide range of compositions and temperatures, including in the field labelled M (Nakazawa & Morimoto 1971). The stability field at intermediate compositions and temperatures, labelled NA, NC by Grønvold & Stølen (1992), is shown as 1C by Wang & Salveson (2005). Selected magnetic transitions have been added. The red line running horizontally across the whole phase diagram is the magnetic ordering temperature, known in FeS as the β-transition. The red diagonal line shows the FeS spin-flop (Morin) transition at ~450 K, reducing to ~170 K at x = 0.07 (Horwood *et al.* 1976). T_B and the short red line at ~35 K on the 4C line mark the Besnus transition. The line phases for FeS as well as 4C and 5C have been extended to low temperature and a line at the ideal stoichiometry ($Fe_{II}S_{12}$) of 6C has been added (- - -). Py is pyrite (FeS_2)

An equivalent diversity of magnetic structures has also been observed in natural and synthetic pyrrhotite (e.g., Andresen & Torbo 1967, Schwartz & Vaughan 1972, Bennett & Graham 1980, Wang & Salveson 2005, Pearce *et al.* 2006). The first magnetic transition with falling temperature, known as the β-transition, occurs at ~590 K and is from paramagnetic to antiferromagnetic in FeS or to ferrimagnetic or antiferromagnetic across the rest of the solid solution. Additional spin-reorientation transitions occur at lower temperatures and show a high sensitivity to structure type. The best characterised of the low-temperature transitions are a spin-flop (Morin type) transition at ~450 K in

hexagonal FeS (Sparks *et al.* 1962, Andresen & Torbo 1967, Takahashi 1973, Horwood *et al.* 1976, Grønvold, & Stølen 1992), and the Besnus transition at ~35 K in monoclinic Fe_7S_8 (Besnus & Meyer 1964, Fillion & Rochette 1988, Dekkers *et al.* 1989, Rochette *et al.* 1990). The spin-flop transition is a reorientation of individual moments from perpendicular to the crystallographic c-axis above the transition temperature to parallel to the c-axis below it. The transition temperature falls with decreasing Fe content (Horwood *et al.* 1976). The Besnus transition involves more subtle changes of spin orientation in the 4C superstructure (Powell *et al.* 2004, Wolfers *et al.* 2011, Kind *et al.* 2013, Koulialias *et al.* 2016, Volk *et al*. 2016, Koulialias *et al.* 2018, Volk *et al*. 2018) but is not observed in crystals with similar composition when the superstructure type is 3C (Horng & Roberts 2018). Some of these transitions have been added to Figure 1, but the magnetic properties of the superstructure types have not all been determined.

In a geological context, pyrrhotite with stoichiometry ~Fe_7S_8 is an important carrier of palaeomagnetic remanence in terrestrial and extra-terrestrial rocks and has been proposed to be responsible for the strong remanent magnetic anomalies observed in the Martian crust (Rochette *et al.* 2005; Louzada *et al.* 2007). Its remarkable mix of structural transitions, vacancy ordering and magnetic properties, with the further possibility of a magnetoelectric effect (Ricci & Bousquet 2016), makes it of interest in the broader context of multiferroic materials (Eerenstein *et al.* 2006) and in the topical field of domain boundary engineering (Salje 2009 and 2010). Phenomenological mean-field theories provide an effective theoretical framework for relating structural states and physical properties to external fields because of their rigour in defining the form and consequences of coupling between multiple order parameters. Underpinning this approach is the fundamental role of symmetry, as has been used to describe combinations of ferroelectric displacements, octahedral tilting, magnetic ordering, cation order and Jahn-Teller distortions in perovskites (Howard & Stokes 1998; Stokes *et al.* 2002; Howard *et al.* 2003; Howard & Stokes 2004; Carpenter & Howard 2009; Howard & Carpenter 2010; Senn & Bristowe 2018).

The initial objective of the present study was to define the relationships between the crystallographic and magnetic structures of pyrrhotite from the perspective of symmetry. For this, the parental structure is taken to be FeS with the NiAs structure (Fig. 2a), space group $P6_3/mmc$, and the relevant Brillouin zone is that of a hexagonal P lattice (Fig. 2b). In this structure the Fe atom is set at Wyckoff 2*a*, 0, 0, 0 and the S atom at Wyckoff 2*d*, 1/3, 2/3, 3/4. Representative lattice parameters, determined for $Fe_{0.88}S$ at 773 K (Powell *et al.* 2004) are A = 3.5165 Å, C = 5.7142 Å. The structure comprises a distorted hexagonal close packed array of S atoms with the Fe atoms located in the octahedral sites.

The distortions to be considered are of three types: i) purely displacive distortions; ii) vacancy ordering; and iii) magnetic ordering of moments on the Fe atoms. We attempt to associate an irreducible representation (irrep) and corresponding order parameter with each distortion encountered.

To this end we make use of the group theoretical tools available in the ISOTROPY Software Suite (Stokes & Hatch 1988), making particular use of ISOCIF, ISOTROPY, ISODISTORT (Campbell *et al.* 2006) and INVARIANTS (Hatch & Stokes, 2003)[1]. Once the primary and secondary irreps have been identified (using the notation of Miller & Love, 1967, throughout), we list the space groups of the diverse distorted structures and examine the couplings between the different distortions involved. We demonstrate that the known superstructure types can be understood in terms of irreps associated with a line between *L* and *M* points of the Brillouin zone (Fig. 2b), the *U*-line of symmetry (***k*** = 1/2,0,γ), while magnetically ordered structures can be understood in terms of magnetic irreps associated with the Brillouin zone centre. Analysis of the primary and secondary irreps, and the manner in which they can combine, leads to a model for the Besnus transition in 4C pyrrhotite and to a prediction of the likely magnetic behaviour of crystals with different Fe/vacancy ordering schemes. A set of Landau expansions to account for coupling between order parameters, and with strains which accompany the various phase transitions, is included in Appendix B. Group theory tables with the most directly relevant results are given within the text and the complete tables, labelled as Figures S1-S12, are given as Supplementary Material. The magnetoelastic properties of single crystals with 4C and 5C superstructures are set out in two separate experimental papers (Haines *et al.* in preparation).

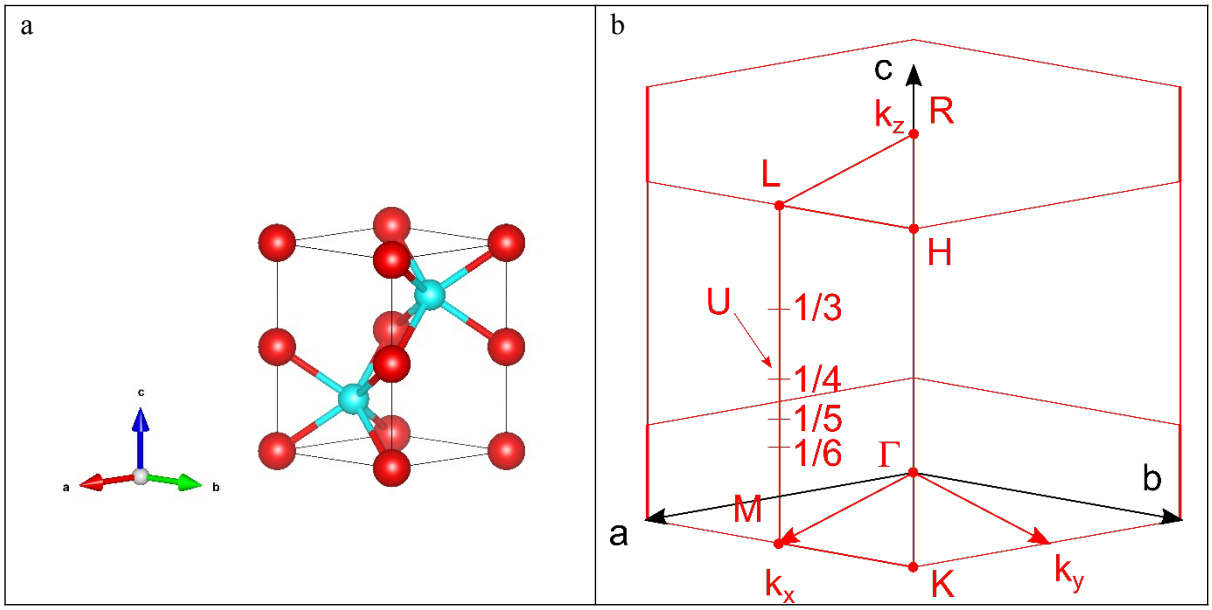

Figure 2 (a) NiAs parent structure of pyrrhotite, stable above $T_\beta \sim 590$ K. Hexagonally close packed sulphur atoms are shown in blue. Fe atoms filling the octahedral sites are shown in red. (b) Brillouin zone for the hexagonal P lattice, with labelling of high symmetry points (filled red circles) and the *U*-line used in the group theoretical analysis. The directions corresponding to the real space unit cell are shown in black. Points on the *U*-line referenced in this work ($\boldsymbol{k}_z = \gamma$ = 1/3, 1/4, 1/5 and 1/6) are shown.

2. Structural relationships and vacancy ordering

Each of the main pyrrhotite superstructure types has lattice geometry that is only slightly distorted from that of the parent hexagonal structure with lattice parameters *A* and *C*. Their lattice parameters

[1] Tabulated results are based on the ISODISTORT Version 6.4.0, April 2018, the OPD assignments can be reproduced using the 'legacy copy' of ISODISTORT.

can be represented as being hexagonal, 2*A*, *NC*, orthorhombic, 2*A*, 2√3*A*, *NC* or monoclinic, *2A*, 2√3*A*, *NC,* $\beta \sim 90°$. From the perspective of group theory, the order parameter must have the symmetry properties of an irreducible representation (irrep) on the *U*-line, $\boldsymbol{k}$ = 1/2, 0, γ, between the *M* point, $\boldsymbol{k}$ = 1/2,0,0, and *L* point, $\boldsymbol{k}$ = 1/2,0,1/2, of the Brillouin zone (Fig. 2b). Irrep U_1 gives the correct structure in each case, with γ = 1/4 for the 4C superstructure, 1/3 for the 3C superstructure, etc. This automatically generates secondary irreps that represent different symmetry adapted combinations of atomic displacements and/or atomic order. It has been found that the observed configurations of vacancies among the crystallographic sites depend on a combination of these secondary irreps in particular proportions. By way of contrast, and as previously shown by Li & Frantzen (1994), the √3*A* by 2*C* structure of FeS develops by the action of an order parameter which has the symmetry properties of an irrep at the *H* point $\boldsymbol{k}$ = 1/3,1/3,1/2 of the Brillouin zone (Ricci & Bousquet 2016).

We start our analysis with the best known of the pyrrhotite structures: 4C. After describing the vacancy ordering in this system in terms of group theory, we apply the same methods to the other pyrrhotite superstructures (working from high to low vacancy concentration) before discussing the case of troilite, FeS, in which there are no vacancies.

2.1. 4C structure

The room temperature structure of 4C pyrrhotite has crystallographic space group *C*2/*c* (Fig. 3; Powell *et al.* 2004). The crystals in which this structure has been observed have stoichiometry close to Fe_7S_8 (e.g. Bertaut 1953; Powell *et al.* 2004). Close packed layers of S in the *ab*-plane alternate with layers of Fe atoms. Vacancies are located in alternate layers of Fe atoms, and within these layers they are found on alternate sites in alternate close-packed rows (Powell *et al.* 2004). This means that one site in four is vacant in the layers containing vacancies. There are four distinct sites for the vacancies: when referred to the parent structure - a vacancy can be located above the 0,0; 1,0; 1,1 or 0,1 positions on the base of the hexagonal unit cell. The layers containing vacancies are stacked up the hexagonal axis in a sequence involving all four distinct vacancy sites (e.g. ABCD), leading to a structure that has a repeat along that axis four times that of the hexagonal parent. This description of the vacancy ordering scheme in terms of stacking up vacancy containing and non-vacancy containing layers was first used by Bertaut (1953) for the 4C structure and subsequently developed for 3C (Fleet 1971, Nakano *et al*. 1979) and 6C (Koto *et al*. 1975) structures before being discussed in detail more generally by Yamamoto & Nakazawa (1982). The 4C structure was first described by Bertaut (1953) in an unconventional space group *F*2/*d*, on a nearly orthorhombic 2√3*A* by 2*A* by 4*C* cell. It was subsequently refined from X-ray data in the same unconventional setting by Tokonami *et al.* (1972). The relationship to the parent NiAs structure is easily visualised (Fig. 3). It was however recognised that the 4C structure could be described in the conventional space group *C*2/*c* on a monoclinic cell

approximately $2\sqrt{3}A$ by $2A$ by $\sqrt{3A^2+4C^2}$ with $\tan(180-\beta)=2C/\sqrt{3}A$ (β ~ 118º), and the structure was refined in this setting by Powell *et al.* (2004).

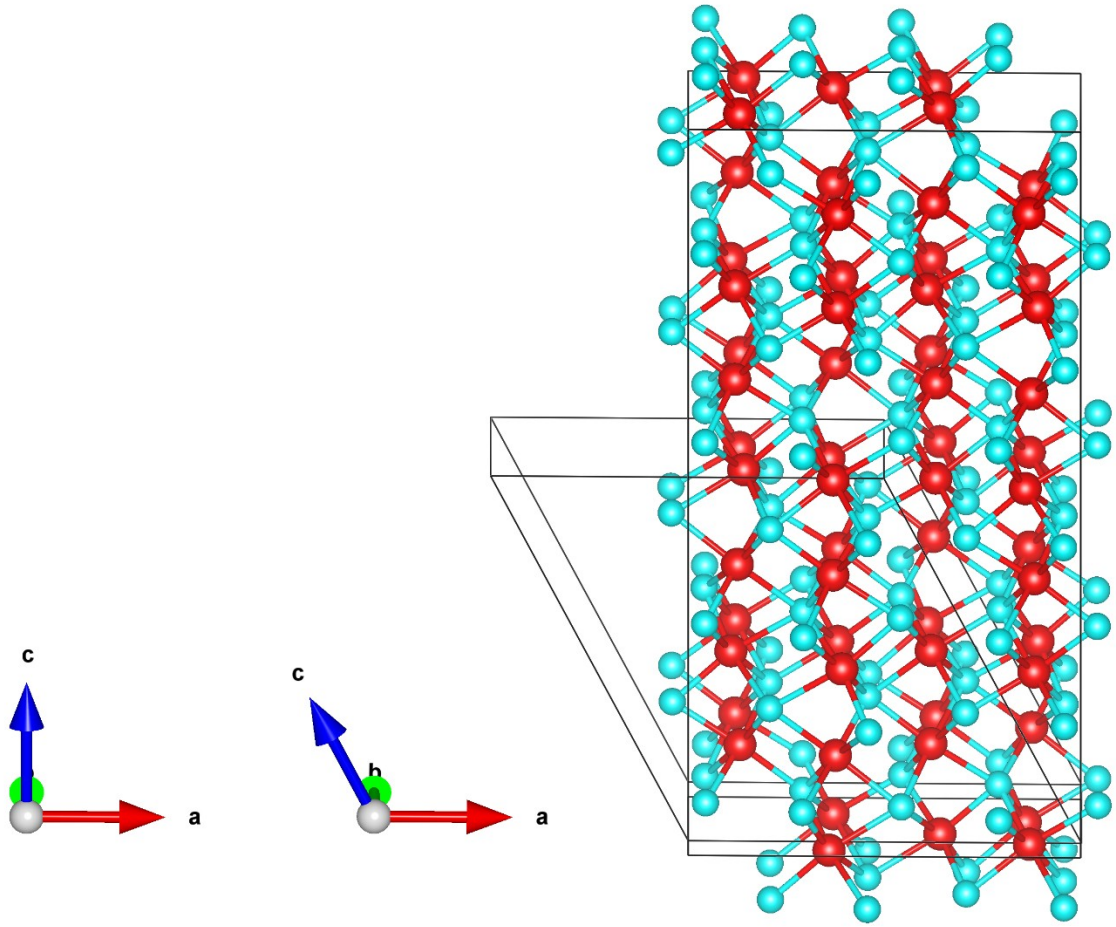

Figure 3 A single unit cell of the structure of 4C Fe_7S_8 at room temperature, after Powell *et al.* (2004). Sulphur atoms are shown in blue. Fully occupied Fe layers alternate with layers in which the vacancies are ordered. The unit cell of the standard setting is also shown. There is a translation of (0,*A*/2,0) between the two cells. The left axes relate to the unconventional *F*2/*d* cell and the right axes to the conventional *C*2/*c* cell.

The order parameter which gives rise to the symmetry change $P6_3/mmc \rightarrow C2/c$ has the symmetry properties of $U_1(1/2,0,1/4)$. It may be helpful to note that a distortion with this ***k***-vector, (1/2,0,1/4), can be thought of as having two distinct effects: the first component (k_x = 1/2) gives the vacancy order within the plane and doubles the repeat in this plane, while the third component (k_z = 1/4) leads to the superstructure repeat along the c-axis of the parent. Table 1 lists possible subgroups, from which it is clear that the order parameter direction (OPD) is P4, (a,0,0,a,0,0). The basis vector is (2,-2,0), (2,2,0), (-1,1,2) and the origin is at (0,1/2,0). U_4 is a secondary order parameter in this case, but the same result would be obtained if U_4 was taken to be primary and U_1 to be secondary. U_1 and U_4 do not appear to be interchangeable in this way for all values of γ, however, and it is therefore assumed that U_1 provides the fundamental primary order parameter.

Table 1 Order parameter components and unit cell configurations for selected subgroups of $P6_3/mmc$ which can arise from phase transitions in which irrep $U_1(1/2,0,1/4)$ is the active representation. The table has been curtailed at the final single component order parameter distortion, P8. The complete set of subgroups is given in Table S1. SGN = space group number. OPD = order parameter direction.

SGN	Space Group	OPD Name	OPD Vector	Basis Vectors	Origin
12	*C*2/*m*	P1	(a,0,0,0,0,0)	(2,1,-4),(0,1,0),(2,1,0)	(0,0,0)
44	*Imm*2	P2	(a,-0.414a,0,0,0,0)	(0,0,4),(0,1,0),(-2,-1,0)	(-7/8,1/16,-7/4)
12	*C*2/*m*	P3	(a,0,a,0,0,0)	(2,-2,0),(2,2,0),(-1,1,2)	(0,0,0)
15	*C*2/*c*	P4	(a,0,0,a,0,0)	(2,-2,0),(2,2,0),(-1,1,2)	(0,1/2,0)
42	*Fmm*2	P5	(a,-0.414a,a,-0.414a,0,0)	(0,0,4),(2,2,0),(-2,2,0)	(-1/8,1/8,1/4)
43	*Fdd*2	P6	(a,-0.414a,0.414a,a,0,0)	(0,0,4),(2,2,0),(-2,2,0)	(-7/8,7/8,7/4)
164	$P\bar{3}m1$	P7	(a,0,a,0,a,0)	(2,0,0),(0,2,0),(0,0,4)	(0,0,0)
187	$P\bar{6}m2$	P8	(a,-0.414a,a,-0.414a,a,-0.414a)	(0,-2,0),(2,2,0),(0,0,4)	(0,0,1/4)

It remains to show that U_1(P4) does indeed lead to the reported ordering scheme. U_1(P4) can impact on the site occupancies, but it does not by itself lead to the observed disposition of vacancies. The space group symmetry allows a number of secondary distortions, some of which also affect the occupancies. It is necessary to invoke these occupation-affecting secondary modes, with amplitudes tied to the amplitude of U_1(P4), to match the observed pattern of vacancy order. In another context, these secondary modes have been described as 'dependent modes' (Campbell *et al.* 2018). An example of the procedure used to determine the dependent modes using ISOTROPY is given in Appendix A. Firstly, all secondary modes related to the symmetry change $P6_3/mmc \rightarrow C2/c$ (P4) were examined to determine which ones define atomic occupancy. Each of these secondary irreps was then examined, as illustrated in Figure A2, to find the set of ratios for their individual contributions which would yield the observed vacancy distribution. Contributions from irreps U_4, L_1, $\Gamma_3^{+¿¿}$ and $\Gamma_1^{+¿¿}$ in the combination $\frac{U1-U4}{4\sqrt{2}}+\frac{L1}{8}+\frac{\Gamma_3^{+¿}}{8}+7\frac{\Gamma_1^{+¿}}{8}¿¿$ give the pattern of vacancy ordering in the 4C structure.

2.2. 3C structure

3C pyrrhotite is metastable at room temperature and is obtained by quenching crystals with compositions in the vicinity of ~Fe_7S_8 from above ~600 K (Fleet 2006). Nakano *et al*. (1979) were able to refine the structure for a Fe_7S_8 crystal that had been quenched from 300 °C as a single phase. They found it to be on a hexagonal cell of dimensions approximately 2*A* by 3*C* and concluded that the space group was $P3_121$ (#154) as did Keller-Besrest *et al.* (1983). As in the 4C structure, vacancies occur on alternate layers, and within the vacancy-containing layers the arrangements are the same as in the 4C structure. The difference is in the stacking of these layers. Again, there are four distinct

possible sites for the vacancies, but in this case the layers are stacked so only three of these are involved. When referred to the parent structure, the vacancies are located successively above the 1,0; 0,1 and -1,-1 (equivalent to 1,1) positions on the base of the hexagonal unit cell; there are no vacancies above the 0,0 position. We concur that this structure is better described in $P3_121$ than in $P3_1$ used by other authors (Fleet, 1971); all positions in $P3_1$ are general and Fleet suggested an arrangement of vacancies on a subset of these positions, whereas in $P3_121$ we can achieve the postulated structure by declaring vacancies to be on one set of Wyckoff 3*a* sites.

The ***k***-vector that will describe this arrangement of vacancies is ***k*** = 1/2,0,1/3 on the *U*-line of symmetry. It follows that U_1 and U_4 are again the irreps of interest. Starting with irrep U_1, we can list details of the structures arising for different 'simple' order parameter directions (Table 2). We find one structure in $P3_121$, from U_1(P7), on a basis (2,0,0), (0,2,0), (0,0,3) and at origin (0,0,1/2). This makes the cell dimensions 2*A* by 2*A* by 3*C*, and we have the structure described just above. It may be worth pointing out that using the P4 direction that describes the distortion in the 4C case would give a symmetry of $P\acute{6}m2$.

Table 2 Order parameter components and unit cell configurations for selected subgroups of $P6_3/mmc$ which can arise from phase transitions in which irrep U_1(1/2,0,1/3) is the active representation. The table has been curtailed at the final single component order parameter direction, P8. The complete set of subgroups is given in Table S10.

SGN	Space Group	OPD Name	OPD Vector	Basis Vectors	Origin
58	*Pnnm*	P1	(a,0,0,0,0,0)	(0,0,3),(2,1,0),(0,1,0)	(0,0,0)
59	*Pmmn*	P2	(0,a,0,0,0,0)	(0,0,3),(0,-1,0),(2,1,0)	(1/2,1/2,0)
164	$P\acute{3}m1$	P3	(a,0,a,0,a,0)	(2,0,0),(0,2,0),(0,0,3)	(0,0,0)
187	$P\acute{6}m2$	P4	(a,-0.577a,a,-0.577a,a,-.577a)	(0,-2,0),(2,2,0),(0,0,3)	(0,0,1/4)
64	*Cmca*	P5	(a,0,0,0,a,0)	(2,0,0),(2,4,0),(0,0,3)	(0,0,0)
63	*Cmcm*	P6	(0,a,0,0,0,-a)	(2,0,0),(2,4,0),(0,0,3)	(1/2,0,0)
152	$P3_121$	P7	(a,1.732a,-2a,0,a,-1.732a)	(2,0,0),(0,2,0),(0,0,3)	(0,0,1/2)
151	$P3_112$	P8	(a,0.577a,a,0.577a,0,-1.155a)	(0,-2,0),(2,2,0),(0,0,3)	(0,0,3/4)

To check that we can reproduce the vacancy ordering scheme, we follow exactly the same procedure as in the 4C case. The combination of model amplitudes indicated by $\frac{\sqrt{3}U4-U1}{12}+\frac{M1-M3}{24}-3\frac{\Gamma_3^{+¿}}{12}+\Gamma_1^{+¿¿}¿$ gives the vacancy ordering arrangement as described.

2.3. 5C structure

De Villiers (2009) reported a *Cmce* (*Cmca*) structure (based on the earlier model of Morimoto *et al*. 1975), Elliot (2010) a $P2_1/c$ structure, Liles & De Villiers (2012) a $P2_1$ structure, and finally recent

work by Haines *et al.* (2019) reports a structure in *Cmce*. The determinations were based on diffraction data from samples with a stoichiometry of approximately Fe_9S_{10}. All these structures are in the table of possible subgroups arising from a *U*-line distortion (Table S4). The most recent determination of the structure of 5C pyrrhotite is in space group $P2_1$ (Liles & de Villiers 2012) using a setting with cell parameters corresponding to 2*A*, 5*C*, 2*A*, $\beta \sim 120°$. We have not determined the necessary combination of irreps that give the vacancy distribution reported because there remains significant uncertainty over the vacancy distribution. In all the other systems (3C, 4C and 6C) the occupancies are set at either 1,0 or ½ and can then be exactly described by occupancies on specific Wyckoff sites. If there is a distribution of occupancy, akin to an 'occupancy wave', then a description starting from an incommensurate vacancy ordering structure may be more illuminating. Table 3 gives distortions described by a single component order parameter.

Table 3 Order parameter components and unit cell configurations for selected subgroups of $P6_3/mmc$ which can arise from phase transitions in which irrep $U_1(1/2,0,1/5)$ is the active representation. The table has been curtailed at the final single component order parameter distortion, P6. The complete set of subgroups is given in Table S4.

SGN	Space Group	OPD Name	OPD Vector	Basis Vectors	Origin
58	*Pnnm*	P1	(a,0,0,0,0,0)	(0,0,5),(2,1,0),(0,1,0)	(0,0,0)
59	*Pmmn*	P2	(0,a,0,0,0,0)	(0,0,5),(0,-1,0),(2,1,0)	(1/2,1/2,0)
164	$P\bar{3}m1$	P3	(a,0,a,0,a,0)	(2,0,0),(0,2,0),(0,0,5)	(0,0,0)
187	$P\bar{6}m2$	P4	(a,-0.325a,a,-0.325a,a,-0.325a)	(0,-2,0),(2,2,0),(0,0,5)	(0,0,1/4)
64	*Cmca*	P5	(a,0,0,0,a,0)	(2,0,0),(2,4,0),(0,0,5)	(0,0,0)
63	*Cmcm*	P6	(0,a,0,0,0,-a)	(2,0,0),(2,4,0),(0,0,5)	(1/2,0,0)

2.4. 6C structure

The 6C structure was first suggested from single crystal XRD by Koto *et al*. (1975) on a crystal of stoichiometry $Fe_{11}S_{12}$. They proposed basis vectors (2,0,0)(2,4,0)(0,0,6) and two possible unconventional space groups: *Fd* (conventional equivalent is *Cc*) or *F*2/*d* (*C*2/*c*). Koto *et al.* (1975) started with the former because it gave 12 independent Fe positions and the possibility of keeping just one of these vacant. However, their analysis suggested that two of these twelve, that is one in six, are half occupied, and that the structure is best described in *F*2/*d*. On the basis of this symmetry, the U_1 irrep in direction P4 (Table 4) gives the correct distortion, and the ordering scheme of the vacancies (or in this case half-filled sites) matches the observed pattern. The combination of irreps needed to give the reported distribution of sites on the *C*2/*c* setting with partial Fe/vacancy order is

$$\frac{(1+\sqrt{3})U1}{24}+\frac{(1-\sqrt{3})U4}{24}+\frac{\sqrt{3}U1(1/2,0,1/3)}{12}+\frac{\Delta 4}{4}-\frac{L1}{24}+11\frac{\Gamma_1^{+i}}{12}i.$$

Table 4 Order parameter components and unit cell configurations for selected subgroups of $P6_3/mmc$ which can arise from phase transitions in which irrep $U_1(1/2,0,1/6)$ is the active representation. The table has been curtailed at the final single component order parameter distortion, P10. The complete set of subgroups is given in Table S7.

SGN	Space Group	OPD Name	OPD Vector	Basis Vectors	Origin
12	*C*2/*m*	P1	(a,0,0,0,0,0)	(2,1,-6),(0,1,0),(2,1,0)	(0,0,0)
44	*Imm*2	P2	(a,-0.268a,0,0,0,0)	(0,0,6),(0,1,0),(-2,-1,0)	(-11/12,1/24,-11/4)
12	*C*2/*m*	P3	(a,0,a,0,0,0)	(2,-2,0),(2,2,0),(-1,1,3)	(0,0,0)
15	*C*2/*c*	P4	(a,0,0,a,0,0)	(2,2,0),(-2,2,0),(1,1,3)	(0,1/2,0)
43	*Fdd*2	P5	(a,-0.268a,0.268a,a,0,0)	(0,0,6),(-2,2,0),(-2,-2,0)	(-4/3,-1/3,1)
42	*Fmm*2	P6	(a,-0.268a,a,-0.268a,0,0)	(0,0,6),(2,2,0),(-2,2,0)	(-1/12,1/12,1/4)
164	$P\bar{3}m1$	P7	(a,0,a,0,a,0)	(2,0,0),(0,2,0),(0,0,6)	(0,0,0)
187	$P\bar{6}m2$	P8	(a,-0.268a,a,-0.268a,a,-0.268a)	(0,-2,0),(2,2,0),(0,0,6)	(0,0,1/4)
152	$P3_121$	P9	(a,1.732a,-2a,0,a,-1.732a)	(2,0,0),(0,2,0),(0,0,6)	(0,0,1)
151	$P3_112$	P10	(a,a,-1.366a,0.366a,0.366a, 1.366a)	(0,-2,0),(2,2,0),(0,0,6)	(0,0,5/4)

We note that de Villiers & Liles (2010) refined the 6C structure from single crystal X-ray data, intending to start from the Koto model but in fact assuming the lower *Fd* (or *Cc*) symmetry. The *Cc* structure would be obtained from the U_1 irrep with one more independent parameter in 2 ways: OPDs C7 and C9 (see Table S7).

2.5. Incommensurate structures

Incommensurate repeat distances in the range ~3.2*C* - 5.75*C* have been observed in crystals with a range of compositions at room temperature and in-situ at high temperatures. There is a tendency for the repeat distance to increase with decreasing vacancy concentration (Nakazawa & Morimoto 1971; Morimoto *et al.* 1975; Yamamoto & Nakazawa 1982). Yamamoto & Nakazawa (1982) proposed an incommensurate model with an 11*C* repeat for the structure of a crystal with composition $Fe_{0.91}S$ which had a repeat distance of 5.54. Use of a U_1 irrep with $\boldsymbol{k}$ = 1/2,0,γ and an irrational value of 1/γ gives the space group of the basic cell as *Cmcm*, in agreement with Yamamoto & Nakazawa (1982). Nakazawa & Morimoto (1971) also reported an incommensurate structure with a range of repeat distances in the *ab*-plane corresponding to ~40-90Å. This requires irreps associated with points close to the Γ-point along the line between Γ and *M* and is not considered further here.

2.6. Troilite, FeS

The paramagnetic–antiferromagnetic transition at T_N ~590 K in troilite is accompanied by a change in crystallographic symmetry. An orthorhombic space group, *Pnma* ($a \sim C$, $b \sim A$, $c \sim \sqrt{3}A$), was proposed by King and Prewitt (1982) on the basis of refinement of diffraction data collected at 463 K,

and a hexagonal space group, $P6_3mc$ (2A, 1C), by Keller-Besrest & Collin (1990) on the basis of data collected at 453 and 429 K. The active irrep for both reductions in symmetry from $P6_3/mmc$ is M_2^- and a list of possible subgroups for different order parameter directions is given in Table 5. Inspection of the OPDs in Table 5 shows that a transition from *Pnma* to $P6_3mc$ would be first order. The magnetic structure has individual magnetic moments aligned perpendicular to the c-axis from T_N down to $T_S \sim 450$ K, where a spin-flop (Morin) transition occurs and the orientation switches to being parallel to the c-axis (Hirahara & Murakami 1958, Andresen 1960, Sparks *et al.* 1962, Andresen & Torbo 1967, Horwood *et al.* 1976). An ordered arrangement of spins within the (001) plane would preclude hexagonal symmetry, favouring the orthorhombic structure, while spins aligned parallel to [001] would fit with hexagonal symmetry. Any distortions from hexagonal lattice geometry are small and the two reported structures may be correct for the temperatures at which the data were collected.

Table 5 Subgroups of space group $P6_3/mmc$ obtained with M_2^- as the active representation.

SGN	Space Group	OPD Name	OPD Vector	Basis Vectors	Origin
62	*Pnma*	P1	(a,0,0)	(0,0,1),(0,-1,0),(2,1,0)	(1/2,0,0)
64	*Cmca*	P2	(a,0,a)	(2,0,0),(2,4,0),(0,0,1)	(1/2,1,0)
186	$P6_3mc$	P3	(a,a,a)	(2,0,0),(0,2,0),(0,0,1)	(0,0,0)
14	$P2_1$/c	C1	(a,0,b)	(0,2,0),(0,0,1),(2,0,0)	(1/2,0,0)
36	*Cmc*21	C2	(a,b,a)	(2,0,0),(2,4,0),(0,0,1)	(0,0,0)
4	$P2_1$	S1	(a,b,c)	(0,2,0),(0,0,1),(2,0,0)	(0,0,0)

An additional structural transition at ~420 K in troilite involves the symmetry change $P6_3mc$ – $P\bar{6}2c$ ($\sqrt{3}A$, 2C) (Keller-Besrest & Collin 1990). $P\acute{6}2c$ is a subgroup of $P6_3/mmc$ but not of $P6_3mc$, so the transition is necessarily first order. The order parameter for $P6_3/mmc$ – $P\acute{6}2c$ belongs to the H point of the Brillouin zone, representing a different distortion to the U-line distortion being considered here (Li & Frantzen 1994; Ricci & Bousquet 2016). There are three H-point irreps which will give the observed space group, although only H_1 produces the reported atomic displacements, i.e. sulphur displaced in the c-axis and iron displaced within the ab-plane. Table 6 lists all structures arising from a distortion to the parent NiAs structure with the active irrep H_1. The first entry is the structure reported for FeS at room temperature.

Table 6 Structures derived from NiAs structure of FeS with active irrep H1

SGN	Space Group	OPD Name	OPD Vector	Basis Vectors	Origin
190	$P\acute{6}2c$	P1	(0,0,0,a)	(2,1,0),(-1,1,0),(0,0,2)	(2/3,1/3,1/4)
189	$P\acute{6}2m$	P2	(0,a,0,0)	(2,1,0),(-1,1,0),(0,0,2)	(2/3,1/3,3/4)
15	$C2/c$	P4	(0,0,a,-a)	(1,2,0),(3,0,0),(0,0,-2)	(2,0,0)
12	$C2/m$	P8	(a,a,0,0)	(1,2,0),(3,0,0),(0,0,-2)	(2,0,0)
174	$P\acute{6}$	C1	(0,a,0,b)	(2,1,0),(-1,1,0),(0,0,2)	(-1/3,1/3,3/4)
9	Cc	C2	(0,0,a,b)	(1,2,0),(3,0,0),(0,0,-2)	(1,1,0)
5	$C2$	C3	(a,0,0,b)	(3,0,0),(1,2,0),(0,0,2)	(1/2,0,1/4)

8	*Cm*	C4	(a,b,0,0)	(1,2,0),(3,0,0),(0,0,-2)	(1,1,0)
2	$P\bar{1}$	C10	(a,a,b,-b)	(1,-1,0),(1,2,0),(0,0,2)	(1,1,0)
5	*C*2	C11	(a,-a,b,-b)	(1,2,0),(3,0,0),(0,0,-2)	(0,0,1/2)
1	*P*1	4D1	(a,b,c,d)	(1,-1,0),(1,2,0),(0,0,2)	(0,0,0)

There had been some discussion in the literature that FeS could be ferroelectric, implying that the room temperature structure has a polar space group (e.g., Van Den Berg *et al.* 1969; Li and Frantzen 1996), but Gosselin *et al.* (1976) demonstrated that this is not the case.

3. Magnetism

Powell *et al.* (2004) determined that the magnetic unit cell of 4C pyrrhotite is the same as the crystallographic cell. Layers of Fe atoms in the *ab*-plane have moments order ferromagnetically with orientations that are reversed between alternate layers to give the antiferromagnetic structure. Ferrimagnetism occurs when vacancies order preferentially onto only one of the sets of layers. Our group theoretical analysis demonstrates that the magnetic ordering is associated with a combination of two Γ-point magnetic irreps, $m\Gamma_4^{+¿¿}$ and $m\Gamma_5^{+¿¿}$, of the space group of the parent structure, $P6_3/mmc$. In order to explore the implications of magnetic order parameters with these symmetries more widely, magnetic structures that would arise as a consequence of magnetic order parameters with all the magnetic Γ-point irreps, $m\Gamma_2^{+¿¿}$, $m\Gamma_4^{+¿¿}$, $m\Gamma_5^{+¿¿}$ and $m\Gamma_6^{+¿¿}$, are listed in Table 7. Irrep $m\Gamma_2^{+¿¿}$ allows alignment of moments parallel to the crystallographic c-axis, but gives only ferromagnetic structures, while $m\Gamma_6^{+¿¿}$ gives ferromagnetic structures with moments predominantly in the *ab*-plane. On their own, $m\Gamma_4^{+}$ and $m\Gamma_5^{+¿¿}$ would give antiferromagnetic structures that are hexagonal ($m\Gamma_4^{+¿¿}$), with moments perpendicular to the *ab*-plane, or orthorhombic ($m\Gamma_5^{+¿¿}$), with moments aligned within the *ab*-plane. The latter can also give a monoclinic structure in which a ferromagnetic component perpendicular to the *ab*-plane is allowed due to $m\Gamma_2^{+¿¿}$ as a secondary irrep. The magnetic gamma point distortions are shown in Figure 4, in which six subfigures correspond to the six independent order parameter directions allowed. The distortions characterised by a C1 order parameter direction in Table 7 are combinations of the two single parameter distortions allowed for that irrep.

Table 7 Magnetic structures arising from Γ-point irreps of the parent $P6_3/mmc$ space group. "Layers" refer to planes of Fe atoms perpendicular to the crystallographic c-axis. Crystallographic directions are given with respect to the parent hexagonal cell. FM = ferromagnetic, AFM = antiferromagnetic.

Active Irrep	OPD	Space Group	Basis Vectors	Magnetic structure
$m\Gamma_2^+$	P1 (a)	$P6_3/mm'c'$	(0,-1,0), (1,1,0), (0,0,1)	FM moments parallel to c-axis
$m\Gamma_4^+$	P1 (a)	$P6_3'/m'm'c$	(0,-1,0), (1,1,0), (0,0,1)	FM layers, moments parallel to c-axis, AFM between layers
$m\Gamma_5^+$	P1 (a,-1.732a)	*Cmcm*	(0,1,0),(-2,-1,0),(0,0,1)	FM layers, moments parallel to [010], AFM between layers
	P2	*Cm'c'm*	(0,1,0),(-2,-1,0),(0,0,1)	FM layers, moments perpendicular to

	(a,0.577a)			(100), AFM between layers. $m\Gamma_2^+$ as secondary order parameter gives FM component along c-axis
	C1 (a,b)	$P2_1/m$	(-1,0,0),(0,0, 1),(0, 1,0)	FM layers, moments have components parallel to [010] and perpendicular to (100), AFM between layers. $m\Gamma_2^+$ as secondary order parameter gives FM component along c-axis
$m\Gamma_6^+$	P1 (a,-1.732a)	$Cm'cm'$	(0,1,0),(-2,-1,0),(0,0,1)	FM, moments perpendicular to (100). $m\Gamma_4^+$ as secondary order parameter gives AFM component along c-axis
	P2 (a,0.577a)	$Cmc'm'$	(0,1,0),(-2,-1,0),(0,0,1)	FM, moments parallel to [010]
	C1 (a,b)	$P2_1'/m'$	(-1,0,0),(0,0,1),(0,1,0)	FM, moments have components parallel to [010] and perpendicular to (100). $m\Gamma_4^+$ as secondary order parameter gives AFM component along c-axis

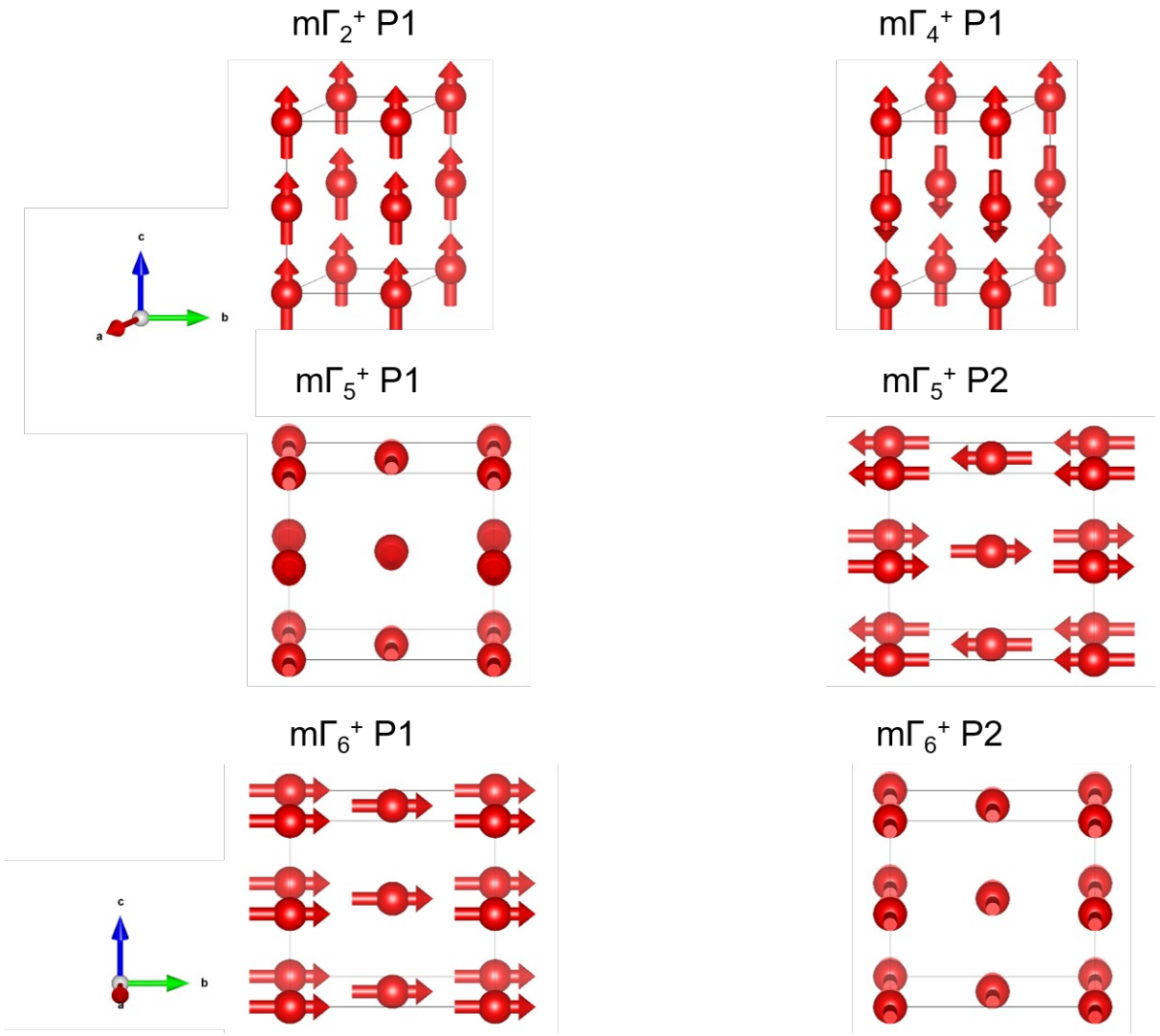

Figure 1 Visualisation of all the allowed gamma point magnetic distortions for FeS with the NiAs structure. Sulphur atoms have been omitted for clarity. $m\Gamma_2^{+¿¿}$ and $m\Gamma_4^{+¿¿}$ do not change the unit cell from the parent NiAs structure (shown in outline). $m\Gamma_5^{+¿¿}$ and $m\Gamma_6^{+¿¿}$ lead to centred structures with doubling in the plane. All views are down the a*-axis with a 15° rotation around the b-axis.

3.1. FeS, troilite

The orientation of individual moments in troilite below T_N is reported as being within the *ab*-plane (Hirahara & Murakami 1958, Andresen 1960, Sparks *et al.* 1962, Andresen & Torbo 1967, Horwood *et al.* 1976), requiring that the relevant magnetic irrep is m$\Gamma_5^{+¿¿}$. As set out in Table 8, combining m $\Gamma_5^{+¿¿}$ with $M_2^{-¿¿}$ gives two possibilities that are consistent with the *Pnma* structure reported by King & Prewitt (1982). These are *Pnma*, and *Pnm*'*a*' from directions P1 (a,-1.732a) and P2 (a,0.577a) of m $\Gamma_5^{+¿¿}$, respectively. Moments are lined up parallel to the crystallographic b-axis of the *Pnma* structure ([0 $\bar{1}$ 0] of the parent hexagonal structure) or to the crystallographic c-axis of the *Pnm*'*a*' structure ([210] of the hexagonal parent). In the latter case, the ferromagnetic moment allowed by m$\Gamma_2^{+¿¿}$ as a secondary irrep could still be zero for thermodynamic reasons. If the m$\Gamma_5^{+¿¿}$ direction is C1 (a,b), the magnetic space group is $P2_1/c$ and the moments are not constrained to any particular orientation within the *ab*-plane of the parent structure.

Table 8 Selected subgroups arising from coupling of irreps m$\Gamma_5^{+¿¿}$ and the P1 direction of $M_2^{-¿¿}$, with respect to the parent space group $P6_3/mmc$. SGN.M = magnetic space group number.

SGN.M	Space Group	OPD Name m $\Gamma_5^{+¿¿}$ $M_2^{-¿¿-}$	OPD Vector m $\Gamma_5^{+¿¿}$, $M_2^{-¿¿}$	Basis Vector	Origin
62.441	*Pnma*	P1(1)P1(1)	(a,-1.732a),(b,0,0)	(0,0,1),(0,-1,0),(2,1,0)	(1/2,0,0)
62.447	*Pnm*'*a*'	P2(1)P1(1)	(a,0.577a),(b,0,0)	(0,0,1),(0,-1,0),(2,1,0)	(1/2,0,0)
14.75	$P2_1/c$	C1(1)P1(1)	(a,b),(c,0,0)	(0,1,0),(0,0,1),(2,0,0)	(1/2,0,0)

Below the spin-flop transition at ~450 K moments lie perpendicular to the *ab*-plane and the structure remains antiferromagnetic (Hirahara & Murakami 1958, Andresen 1960, Sparks *et al.* 1962, Andresen & Torbo 1967, Horwood *et al.* 1976) with spin configurations that are consistent with m $\Gamma_4^{+¿¿}$. Combining m$\Gamma_4^{+¿¿}$ with the P3 direction of $M_2^{-¿¿}$, gives the structure in Table 9, $P6_3'm'c$, which is consistent with the $P6_3mc$ crystal structure reported by Keller-Besrest & Collin (1990). $P6_3'm'c$ is not a subgroup of *Pnma, Pnm*'*a*' or $P2_1/c$ so the spin-flop transition is necessarily first order in character.

Table 9 Order parameter information for subgroup $P6_3'm'c$ arising from coupling of irreps m$\Gamma_4^{+¿¿}$ and the P3 direction of $M_2^{-¿¿}$, with respect to the parent space group $P6_3/mmc$.

SGN.M	Space Group	OPD Name m $\Gamma_4^{+¿¿}$	OPD Vector m$\Gamma_4^{+¿,¿}$ $M_2^{-¿¿}$	Basis Vectors	Origin

		$M_2^{-¿¿}$			
186.205	$P6_3'm'c$	P1(1)P3(1)	(a),(b,b,b)	(0,-2,0),(2,2,0),(0,0,1)	(0,0,0)

The room temperature structure of troilite is also antiferromagnetic, with individual moments parallel to the crystallographic c-axis (Hirahara & Murakami 1958; Andresen 1960; Bertaut 1980). Combining $\mathrm{m}\Gamma_4^+$ with H_1 (as identified in Section 2.6) gives $P\acute{6}'2c'$ as the most likely magnetic space group with properties set out in Table 10.

Table 10 Subgroups arising from coupling of irreps $\mathrm{m}\Gamma_4^{+¿¿}$ and the P1 direction of H_1, with respect to the parent space group $P6_3/mmc$.

SGN.M	Space Group	OPD Name $H_1\mathrm{m}\Gamma_4^{+¿¿}$	OPD Vector $H_1,\mathrm{m}\Gamma_4^{+¿¿}$	Basis Vector	Origin
190.23	$P\acute{6}'2c'$	P1(1)P1(1)	(0,0,0,a),(b)	(1,-1,0),(1,2,0),(0,0,2)	(2/3,1/3,1/4)

3.2. 4C Pyrrhotite

3.2.1. Ferrimagnetism below ~590 K

If the antiferromagnetic ordering which occurs below ~590 K in FeS is essentially the same as occurs at the same temperature all across the $Fe_{1-x}S$ solid solution, it should be possible to obtain the magnetic structure of 4C pyrrhotite reported by Powell *et al.* (2004) by combining $\mathrm{m}\Gamma_5^{+¿¿}$ with $U_1(1/2,0,1/4)$. Table 11 contains selected subgroups of $P6_3/mmc$ that arise by coupling of these two irreps and includes $C2'/c'$ (row 2) as the most appropriate magnetic space group for the reported structure. This has direction P4 of the six component U_1 order parameter, which has one non-zero component as (a,0,0,a,0,0), and direction P2 of the two component $\mathrm{m}\Gamma_5^{+¿¿}$ order parameter, which has one non-zero component as (-b,0.577b). The latter gives the alignment of moments at an angle of 30° to [100] of the hexagonal parent structure, which is also the direction of the crystallographic a-axis of the monoclinic structure (Fig. 3).

Because the symmetry is reduced to monoclinic by the pattern of Fe/vacancy ordering, $\mathrm{m}\Gamma_4^{+¿¿}$ is a secondary order parameter once the magnetic symmetry is broken by $\mathrm{m}\Gamma_5^{+¿¿}$. This allows moments to have a component out of the *ab*-plane, though still constrained to be within the *ac*-plane of the monoclinic structure (Fig. 3). There is a similarity to behaviour observed in hematite with similar group theory underpinnings (Harrison *et al.* 2010). By analogy with the magnetic behaviour of FeS, it should be expected that there will an energetic advantage in a realignment of these moments from parallel to the *ab*-plane at high temperatures ($\mathrm{m}\Gamma_5^{+¿¿}$) to perpendicular to it at low temperatures ($\mathrm{m}\Gamma_4^{+¿¿}$). In this case, all that is required is an increase in the magnitude of the $\mathrm{m}\Gamma_4^{+¿¿}$ component as temperature reduces. The observed angle of rotation of the ferrimagnetic moment out of the *ab*-plane increases from ~6° at room temperature to 25-30° at ~10-30 K (Powell *et al.* 2004, Koulialias 2018).

Table 11 Selected magnetic subgroups arising from coupling of irreps m$\Gamma_5^{+¿¿}$ and the P4 and C5 directions of U_1(1/2,0,1/4), with respect to the parent space group $P6_3/mmc$. The complete set of subgroups is given in Table S3.

SGN.M	Space Group	OPD Name U_1(1/2,0,1/4) m$\Gamma_5^{+¿¿}$	OPD Vector U_1(1/2,0,1/4), m$\Gamma_5^{+¿¿}$	Basis Vectors	Origin
15.85	$C2/c$	P4(1)P1(3)	(a,0,0,a,0,0),(b,1.732b)	(2,-2,0),(2,2,0),(-1,1,2)	(0,1/2,0)
15.89	$C2'/c'$	P4(1)P2(3)	(a,0,0,a,0,0),(-b,0.577b)	(2,-2,0),(2,2,0),(-1,1,2)	(0,1/2,0)
2.4	$P\acute{1}$	C5(1)C1(1)	(a,0,0,b,0,0),(c,d)	(1,1,2),(0,2,0),(-2,0,0)	(0,1/2,0)

Table 12 contains a full list of the magnetic Γ-point irreps which are allowed by symmetry to have non-zero values in the $C2'/c'$ structure. In principle, m$\Gamma_2^{+¿¿}$ (a) and m$\Gamma_6^{+¿¿}$ (a,1.732a) allow ferromagnetic moments parallel to the crystallographic c*- and b-axes of the monoclinic structure, respectively. These have not been observed and must be effectively zero for reasons of thermodynamic stability.

Table 12 Non-zero magnetic irreps arising from the symmetry changes $P6_3/mmc \rightarrow C2'/c'$ and $P6_3/mmc \rightarrow P\bar{1}$.

	U_1(1/2,0,1/4)	m$\Gamma_2^{+¿¿}$	m$\Gamma_4^{+¿¿}$	m$\Gamma_5^{+¿¿}$	m$\Gamma_6^{+¿¿}$
$C2'/c'$	P4 (a,0,0,a,0,0)	P1 (a)	P1 (a)	P2 (-a,0.577a)	P1 (a,1.732a)
$P\acute{1}$	C5 (a,0,0,b,0,0)	P1 (a)	P1 (a)	C1 (a,b)	C1 (a,b)

The full sets of subgroups which arise by coupling of U_1(1/2,0,1/4) with m$\Gamma_4^{+¿¿}$ and m$\Gamma_5^{+¿¿}$ are listed in Tables S2 and S3, respectively.

3.2.2. Besnus transition in 4C Pyrrhotite

The Besnus transition near 35 K in 4C pyrrhotite (~Fe_7S_8) is associated with changes in magnetic properties (Fillion & Rochette 1988, Dekkers *et al.* 1989, Rochette *et al.* 1990, Kind *et al.* 2013; Baranov *et al.* 2015, Koulialias *et al.* 2016, Volk *et al.* 2016, Bazaeva *et al.* 2016, Koulialias *et al.* 2018, Horng & Roberts 2018), an anomaly in heat capacity (Grønvold *et al.* 1959, Volk *et al*. 2018), an anomaly in resistivity (Besnus & Meyer 1964, Charilaou *et al.* 2015), apparently continuous changes in the temperature dependence of lattice parameters (Fillion *et al.* 1992, Koulialias *et al.* 2018), together with small adjustments of Fe-Fe bond lengths and Fe-S-Fe bond angles (Koulialias *et al.* 2018). The evidence from Mössbauer spectroscopy is that the transition is marked by splitting of at least one of the Fe sites into two equally populated subsites (Jeandey *et al.* 1991, Oddou *et al.* 1992, Ferrow *et al.* 2006). In combination, these features are consistent with a phase transition between structures with a group-subgroup relationship. $P1$ and $P\acute{1}$ have been suggested for the crystallographic space group of the low temperature structure (Wolfers *et al.* 2011).

The pattern of vacancy ordering must remain essentially unchanged through the transition because of the slowness of Fe/vacancy diffusion at low temperatures, which implies crystallographic space group $P\acute{1}$ (Table 11) as the only possible subgroup of $C2'/c'$ in Table S3. This has order parameter direction C5 (a,0,0,b,0,0), for U_1(1/2,0,1/4), C1 (c,d) for m$\Gamma_5^{+¿¿}$ and the additional secondary magnetic Γ-point irreps listed in Table 12. Non-zero values of m$\Gamma_2^{+¿¿}$ and m$\Gamma_6^{+¿¿}$ allow ferromagnetic moments parallel to the crystallographic c* and b-axes of the monoclinic structure but there is no experimental evidence suggesting that these develop. In terms of the magnetic structure alone, the transition can be understood as a rotation of the direction of individual moments out of the *ac*-plane of the monoclinic structure. There are no symmetry constraints on the orientation of antiferromagnetic/ferrimagnetic moments in the $P\acute{1}$ structure but, because of the slowness of Fe/vacancy reordering, the U_1 order parameter will effectively remain (a,0,0,a,0,0) instead of relaxing to (a,0,0,b,0,0).

This symmetry analysis does not depend on identification of the driving mechanism for the transition, which might be due primarily to a change in electronic structure (e.g., Besnus & Meyer 1964; Fillion & Rochette 1988; Ferrow *et al.* 2006; Koulialias *et al.* 2016; Koulialias *et al.* 2018) or, more simply, to the normal interactions between spins which give rise to changes in the easy axis of magnetisation.

The sequence of spin orientations is summarised in Figure 5. The magnetic structures at T ~ 300 K and T ~ 590 K are from Powell et. al (2004). The magnetic structure shown for T < T_B is illustrative and based on the allowed freedom that the moments have in the triclinic structure at low temperature.

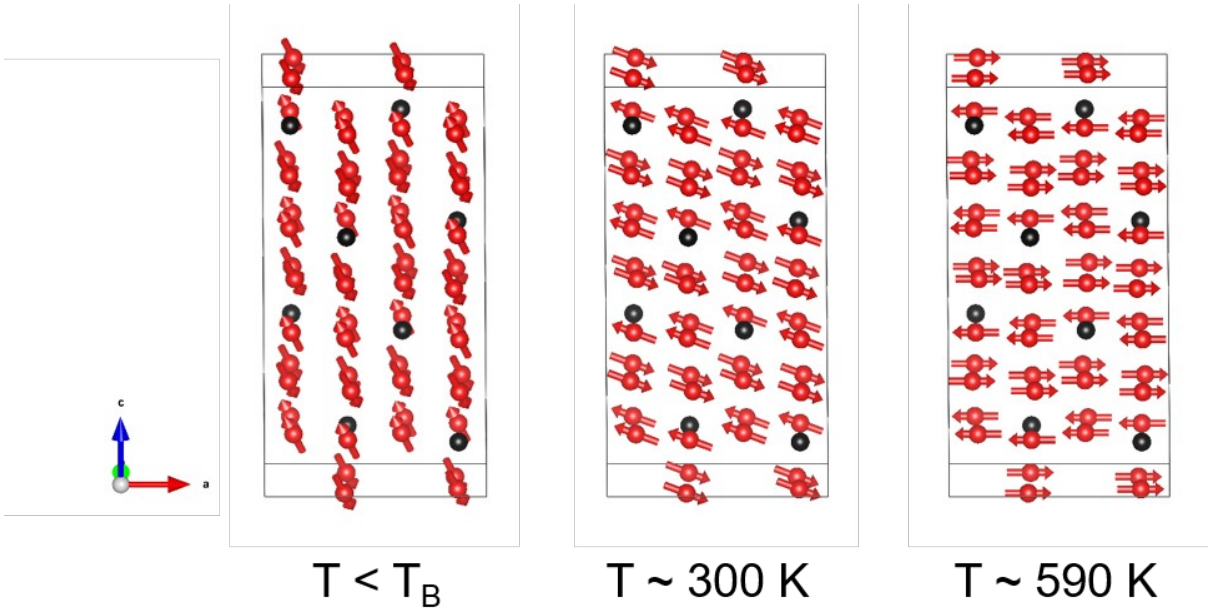

Figure 2 Temperature dependence of the spin orientation in 4C pyrrhotite. Sulphur atoms have been removed for clarity. Iron atoms are red with red arrows for the moment direction. Vacant sites are shown in black.

3.3. Magnetism in 3C pyrrhotite

The 3C structure of pyrrhotite in space group $P3_121$ is similar to that of the 4C structure in the sense that vacancies are confined to alternate Fe-layers. There appears to be little information in the literature for its magnetic structure, but the equivalent phase in Fe_7Se_8 is ferrimagnetic (Kawaminami & Okazaki 1970), as would be expected for this distribution of vacancies. Horng & Roberts (2018) presented magnetic data on 3C pyrrhotite that suggested a remanence of the same order as 4C. This would make sense on the basis of our group theory results as the remanence will come from the imbalance in the distribution of vacancies between the two antiferromagnetic sublattices. This imbalance is the same in both the 3C and 4C structures: one in eight iron sites are vacant and all are situated on one sublattice. Furthermore, it is interesting to note that in all of their samples (which are all multiphase) there are none with both 3C and 4C. They did not observe a transition in 3C pyrrhotite in the range 5 – 300 K.

Combinations of $U_1(1/2,0,1/3)$ $\mathrm{m}\Gamma_5^{+¿¿}$ and $\mathrm{m}\Gamma_4^{+¿¿}$ yield the possible magnetic space groups listed in Tables 13 and 14. Magnetic moments within the *ab*-plane would be produced by $\mathrm{m}\Gamma_5^{+¿¿}$, giving one of the structures seen in Table 13 as the most likely symmetry immediately below ~590 K. The most likely magnetic structure with moments perpendicular to the *ab*-plane would have space group $P3_12'1$ (Table 14). Unlike the case of the monoclinic 4C structure, $\mathrm{m}\Gamma_4^{+¿¿}$ does not become a secondary irrep when the symmetry is broken by $\mathrm{m}\Gamma_5^{+¿¿}$. A change in the orientation of moments with falling temperature from parallel to perpendicular to the *ab*-plane would therefore be expected to occur by a discrete spin-flop transition. This occurs at ~130K in 3C Fe_7Se_8 (Andresen & Leciejewicz 1964; Kawaminami & Okazaki 1970; Ericsson *et al.* 1997). The room temperature structure is only compatible with a magnetic structure in which the moments are perpendicular to the *ab*-plane. On the basis of the sequence of magnetic structures seen in troilite and 4C pyrrhotite, in which the moments lie within the *ab*-plane below 590 K before a transition to a state in which they are perpendicular to it at lower temperature, we would suggest that immediately below ~590 K we might expect a structure other than the $P3_121$ reported. The most likely structures are those listed in Table 13. The single parameter order parameter directions of the combined $\mathrm{m}\Gamma_5^{+¿¿}$ and U_1 irreps produce these structures and none of them contains the $\mathrm{m}\Gamma_4^{+¿¿}$ irrep as a secondary. We therefore predict a first order spin-flop transition between the two magnetic states above room temperature.

Table 13 Selected magnetic subgroups arising from coupling of irreps $\mathrm{m}\Gamma_5^{+¿¿}$ and $U_1(1/2,0,1/3)$, with respect to the parent space group $P6_3/mmc$. Only distortions with single parameter order parameter directions have been included. The complete set of subgroups is given in Table S12.

SGN.M	Space Group	OPD Name $U_1(1/2,0,1/3)\mathrm{m}\Gamma_5^{+¿¿}$	OPD Vector $U_1(1/2,0,1/3),\mathrm{m}\Gamma_5^{+¿¿}$	Basis Vectors	Origin
58.393	*Pnnm*	P1(1)P1(1)	(a,0,0,0,0,0),(b,-1.732b)	(-2,-1,0),(0,0,3),(0,1,0)	(0,0,0)

59.405	*Pmmn*	P2(1)P1(1)	(0,a,0,0,0,0),(b,-1.732b)	(0,1,0),(0,0,3),(2,1,0)	(1/2,0,0)
64.469	*Cmca*	P5(1)P1(2)	(a,0,0,0,a,0),(-2b,0)	(2,0,0),(2,4,0),(0,0,3)	(0,0,0)
63.457	*Cmcm*	P6(1)P1(2)	(0,a,0,0,0,-a),(-2b,0)	(2,0,0),(2,4,0),(0,0,3)	(1/2,0,0)
58.398	*Pnn'm'*	P1(1)P2(1)	(a,0,0,0,0,0),(b,0.577b)	(0,0,3),(2,1,0),(0,1,0)	(0,0,0)
59.41	*Pmm'n'*	P2(1)P2(1)	(0,a,0,0,0,0),(b,0.577b)	(0,0,3),(0,-1,0),(2,1,0)	(1/2,1/2,0)
64.474	*Cm'c'a*	P5(1)P2(2)	(a,0,0,0,a,0),(0,-1.155b)	(2,0,0),(2,4,0),(0,0,3)	(0,0,0)
63.462	*Cm'c'm*	P6(1)P2(2)	(0,a,0,0,0,-a),(0,-1.155b)	(2,0,0),(2,4,0),(0,0,3)	(1/2,0,0)

Table 14 Selected magnetic subgroups arising from coupling of irreps m$\Gamma_4^{+¿¿}$ and U_1(1/2,0,1/3), with respect to the parent space group $P6_3/mmc$. Only distortions with single parameter order parameter directions have been included. The complete set of subgroups is given in Table S11.

SGN.M	Space Group	OPD Name U_1(1/2,0,1/3)m$\Gamma_4^{+¿¿}$	OPD Vector U_1(1/2,0,1/3),m$\Gamma_4^{+¿¿}$	Basis Vectors	Origin
58.398	*Pnn'm'*	P1(1)P1(1)	(a,0,0,0,0,0),(b)	(-2,-1,0),(0,0,3),(0,1,0)	(0,0,0)
59.409	*Pm'm'n*	P2(1)P1(1)	(0,a,0,0,0,0),(b)	(0,0,3),(0,-1,0),(2,1,0)	(1/2,1/2,0)
164.89	$P\bar{3}m'1$	P3(1)P1(1)	(a,0,a,0,a,0),(b)	(0,-2,0),(2,2,0),(0,0,3)	(0,0,0)
187.211	$P\bar{6}'m'2$	P4(1)P1(1)	(a,-0.577a,a,-0.577a,a,-0.577a),(b)	(2,2,0),(-2,0,0),(0,0,3)	(0,0,1/4)
64.476	*Cm'ca'*	P5(1)P1(1)	(a,0,0,0,a,0),(b)	(2,0,0),(2,4,0),(0,0,3)	(0,0,0)
63.464	*Cm'cm'*	P6(1)P1(1)	(0,a,0,0,0,-a),(b)	(2,0,0),(2,4,0),(0,0,3)	(1/2,0,0)
152.35	P312'1	P7(1)P1(1)	(a,1.732a,-2a,0,a,-1.732a),(b)	(0,-2,0),(2,2,0),(0,0,3)	(0,0,0)
151.29	P3112	P8(1)P1(1)	(a,0.577a,-a,0.577a,0,-1.155a),(b)	(2,2,0),(-2,0,0),(0,0,3)	(0,0,1/4)

3.4. Magnetism in 5C pyrrhotite

The crystallographic space groups of the structures of pyrrhotite with 5C and 6C superstructures are perhaps less certain than those of the better-understood 3C and 4C structures. Both are reported to have partially ordered Fe/vacancy sites and monoclinic symmetry: *Cc* for the 6C structure (Koto *et al.* 1975; de Villiers & Liles 2010) and $P2_1$ as the most recent proposal for the 5C structure (Liles & de Villiers 2012). The expected pattern with respect to their magnetic properties would be antiferromagnetic (or ferrimagnetic, depending on the distribution of vacancies), with moments in the *ab*-plane at high temperatures and perpendicular to the *ab*-plane at low temperatures. Whether the change in orientation during cooling occurs by a continuous rotation or abruptly at a spin-flop transition depends on whether the combination of the U_1 order parameter for Fe/vacancy ordering and m$\Gamma_5^{+¿¿}$ for magnetic ordering gives m$\Gamma_4^{+¿¿}$ as a secondary order parameter. U_1(1/2,0,1/5) combined with m$\Gamma_5^{+¿¿}$ does not. U_1(1/2,0,1/6) combined with m$\Gamma_5^{+¿¿}$ does. The energetically preferred orientation of moments within the *ab*-plane will be described, as for the other superstructure types, by P1, P2 or C1 directions of irrep m$\Gamma_5^{+¿¿}$.

In none of the reported 5C structures (nor indeed in any but the triclinic structures) is it possible to have both m$\Gamma_4^{+¿¿}$ and m$\Gamma_5^{+¿¿}$ allowed together. Therefore, it seems likely that 5C pyrrhotite will show an abrupt spin-flop transition from having spins in the *ab*-plane to having the spins

perpendicular to that plane. Evidence for such an abrupt low temperature magnetic transition has recently been reported (Haines *et al.* 2019). The reported structures are all compatible with coupling of the vacancy ordering to either m$\Gamma_4^{+¿¿}$ or m$\Gamma_5^{+¿¿}$. The most likely scenario would be a phase transition from one of the higher symmetry structures, *Cmca* or $P2_1/c$ to the $P2_1$ structure reported by Liles & de Villiers (2012) predominantly using data collected at 120 K. The higher symmetry structure would be due to coupling of the U_1 irrep with the m$\Gamma_5^{+¿¿}$ irrep and Table 15 shows some of the possible distortions. The third entry shows the possible *Cmca* structure whilst the $P2_1/c$ structure is seen in the 5th, 8th and 10th entries. The lower temperature, low symmetry structure would arise from coupling of the U_1 irrep with the m$\Gamma_4^{+¿¿}$ irrep (last entry of Table 16).

Table 15 Selected magnetic subgroups arising from coupling of irreps m$\Gamma_5^{+¿¿}$ and U_1(1/2,0,1/5), with respect to the parent space group $P6_3/mmc$. Some entries have been omitted for clarity and brevity. The complete set of subgroups is given in Table S6.

SGN.M	Space Group	OPD Name U_1(1/2,0,1/5) m$\Gamma_5^{+¿¿}$	OPD Vector U_1(1/2,0,1/5),m$\Gamma_5^{+¿¿}$	Basis Vectors	Origin
58.393	Pnnm	P1(1)P1(1)	(a,0,0,0,0,0),(b,-1.732b)	(-2,-1,0),(0,0,5),(0,1,0)	(0,0,0)
59.405	Pmmn	P2(1)P1(1)	(0,a,0,0,0,0),(b,-1.732b)	(0,1,0),(0,0,5),(2,1,0)	(1/2,0,0)
64.469	*Cmca*	P5(1)P1(2)	(a,0,0,0,a,0),(-2b,0)	(2,0,0),(2,4,0),(0,0,5)	(0,0,0)
63.457	*Cmcm*	P6(1)P1(2)	(0,a,0,0,0,-a),(-2b,0)	(2,0,0),(2,4,0),(0,0,5)	(1/2,0,0)
14.75	$P2_1/c$	P1(1)C1(1)	(a,0,0,0,0,0),(b,c)	(0,1,0),(0,0,5),(2,0,0)	(0,0,0)
11.5	$P2_1/m$	P2(1)C1(1)	(0,a,0,0,0,0),(b,c)	(-2,0,0),(0,0,5),(0,1,0)	(-1/2,0,0)
4.7	$P2_1$	C1(1)C1(1)	(a,b,0,0,0,0),(c,d)	(-2,0,0),(0,0,5),(0,1,0)	(-1/2,0,0)
14.75	$P2_1/c$	C4(1)C1(1)	(0,0,a,0,b,0),(c,d)	(-2,0,0),(0,0,5),(0,2,0)	(0,0,0)
11.5	$P2_1/m$	C5(1)C1(1)	(0,0,0,a,0,b),(c,d)	(-2,0,0),(0,0,5),(0,2,0)	(0,1/2,0)
14.75	$P2_1/c$	C6(1)C1(1)	(a,0,0,0,0,b),(c,d)	(-2,0,0),(0,0,5),(2,2,0)	(0,1/2,0)
4.7	$P2_1$	4D1(1)C1(1)	(0,0,a,b,c,d),(e,f)	(-2,0,0),(0,0,5),(0,2,0)	(0,1/2,0)

Table 16 Selected magnetic subgroups arising from coupling of irreps m$\Gamma_4^{+¿¿}$ and U_1(1/2,0,1/5), with respect to the parent space group $P6_3/mmc$. Some entries have been omitted for clarity and brevity. The complete set of subgroups is given in Table S5.

SGN.M	Space group	OPD Name U_1(1/2,0,1/5) m$\Gamma_4^{+¿¿}$	OPD vector U_1(1/2,0,1/5),m $\Gamma_4^{+¿¿}$	Basis Vectors	Origin
58.398	*Pnn'm'*	P1(1)P1(1)	(a,0,0,0,0,0),(b)	(-2,-1,0),(0,0,5),(0,1,0)	(0,0,0)
59.409	*Pm'm'n*	P2(1)P1(1)	(0,a,0,0,0,0),(b)	(0,0,5),(0,-1,0),(2,1,0)	(1/2,1/2,0)
164.89	$P\acute{3}m'1$ $P\acute{6}'m'2$	P3(1)P1(1)	(a,0,a,0,a,0),(b)	(0,-2,0),(2,2,0),(0,0,5)	(0,0,0)
187.211		P4(1)P1(1)	(a,-0.325a,a,-0.325a,a,-0.325a),(b)	(2,2,0),(-2,0,0),(0,0,5)	(0,0,1/4)
64.476	*Cm'ca'*	P5(1)P1(1)	(a,0,0,0,a,0),(b)	(2,0,0),(2,4,0),(0,0,5)	(0,0,0)
63.464	*Cm'cm'*	P6(1)P1(1)	(0,a,0,0,0,-a),(b)	(2,0,0),(2,4,0),(0,0,5)	(1/2,0,0)

Entries removed. Selected higher order OPD entries listed below

14.79	$P2_1'/c'$	C4(1)P1(1)	(0,0,a,0,b,0),(c)	(-2,0,0),(0,0,5),(0,2,0)	(0,0,0)
11.54	$P2_1'/m'$	C5(1)P1(1)	(0,0,0,a,0,b),(c)	(-2,0,0),(0,0,5),(0,2,0)	(0,1/2,0)
14.79	$P2_1'/c'$	C6(1)P1(1)	(a,0,0,0,0,b),(c)	(-2,0,0),(0,0,5),(2,2,0)	(0,1/2,0)
4.9	$P2_1'$	4D1(1)P1(1)	(0,0,a,b,c,d),(e)	(-2,0,0),(0,0,5),(0,2,0)	(0,1/2,0)

3.5. Magnetism in 6C

The magnetic phase diagram for 6C pyrrhotite could follow very closely that observed in 4C pyrrhotite. The $C2'/c'$ structure attained from the coupled vacancy ordering (the P4 direction of the U_1 distortion) and magnetism (the P2 direction of the m$\Gamma_5^{+¿¿}$ distortion), line 10 of Table 17, can then have a transition to the same $P\acute{1}$ structure (second last entry in Table 17), as seen below the Besnus transition in 4C pyrrhotite. Magnetically this is identical. The m$\Gamma_4^{+¿¿}$ irrep is a secondary distortion, which means that the moments are allowed by symmetry to rotate out of the *ab*-plane. Indeed, similarly to 4C pyrrhotite, the moments can in principle line up parallel to the c-axis of the parent structure. There is therefore no need for an abrupt Morin-type transition. Instead, a transition like the Besnus transition is expected at which moments confined to the *ac*-plane above the transition are free to rotate out of it below the transition. However due to the nature of the vacancy ordering, a vacancy-containing bi-layer separated by a non-vacancy containing layer, the vacancies are evenly distributed on both of the antiferromagnetic sublattices and the overall structure is antiferromagnetic above and below the low-temperature transition.

Table 17 Selected magnetic subgroups arising from coupling of irreps m$\Gamma_5^{+¿¿}$ and $U_1(1/2,0,1/6)$, with respect to the parent space group $P6_3/mmc$. Some entries have been omitted for clarity and brevity. The complete set of subgroups is given in Table S9.

SGN	Space Group	OPD Name $U_1(1/2,0,1/6)$m$\Gamma_5^{+¿¿}$	OPD Vector $U_1(1/2,0,1/6)$,m$\Gamma_5^{+¿¿}$	Basis Vectors	Origin
12.58	C2/m	P1(1)P1(1)	(a,0,0,0,0,0),(b,-1.732b)	(2,1,-6),(0,1,0),(2,1,0)	(0,0,0)
44.229	Imm2	P2(1)P1(1)	(a,-0.268a,0,0,0,0),(b,-1.732b)	(0,1,0),(0,0,6),(2,1,0)	(0,0,1/4)
12.58	C2/m	P3(1)P1(3)	(a,0,a,0,0,0),(b,1.732b)	(2,-2,0),(2,2,0),(-1,1,3)	(0,0,0)
15.85	C2/c	P4(1)P1(3)	(a,0,0,a,0,0),(b,1.732b)	(2,2,0),(-2,2,0),(1,1,3)	(0,1/2,0)
43.224	Fdd2	P5(1)P1(3)	(a,-0.268a,0.268a,a,0,0),(b,1.732b)	(-2,2,0),(0,0,6),(2,2,0)	(5/6,5/6,5/2)
42.219	Fmm2	P6(1)P1(3)	(a,-0.268a,a,-0.268a,0,0),(b,1.732b)	(2,2,0),(0,0,6),(2,-2,0)	(1/12,-1/12,1/4)
12.62	C2'/m'	P1(1)P2(1)	(a,0,0,0,0,0),(b,0.577b)	(2,1,-6),(0,1,0),(2,1,0)	(0,0,0)
44.231	$Im'm2'$	P2(1)P2(1)	(a,-0.268a,0,0,0,0),(b,0.577b)	(0,1,0),(0,0,6),(2,1,0)	(0,0,1/4)
12.62	C2'/m'	P3(1)P2(3)	(a,0,a,0,0,0),(-b,0.577b)	(2,-2,0),(2,2,0),(-1,1,3)	(0,0,0)
15.89	C2'/c'	P4(1)P2(3)	(a,0,0,a,0,0),(-b,0.577b)	(2,2,0),(-2,2,0),(1,1,3)	(0,1/2,0)
43.226	Fd'd2'	P5(1)P2(3)	(a,-0.268a,0.268a,a,0,0),(-b,0.577b)	(-2,2,0),(0,0,6),(2,2,0)	(5/6,5/6,5/2)
42.221	Fm'm2	P6(1)P2(3)	(a,-0.268a,a,-0.268a,0,0),(-	(2,2,0),(0,0,6),(2,-	(1/12,-

	'		b,0.577b)	2,0)	1/12,1/4)
			Entries removed		
9.37	*Cc*	C9(1)P1(3)	(a,b,b,-a,0,0),(c,1.732c)	(2,2,0),(-2,2,0),(1,1,3)	(0,3/2,0)
9.39	*Cc*'	C9(1)P2(3)	(a,b,b,-a,0,0),(-c,0.577c)	(2,2,0),(-2,2,0),(1,1,3)	(0,3/2,0)
9.37	Cc	C7(1)C1(1)	(a,-0.268a,b,3.732b,0,0),(c,d)	(-2,-2,0),(0,0,6),(-2,0,0)	(-7/12,-7/12,7/4)
			Entries removed		
2.4	$P\acute{1}$	C5(1)C1(1)	(a,0,0,b,0,0),(c,d)	(1,1,3),(0,2,0),(-2,0,0)	(0,1/2,0)
1.1	*P*1	4D1(1)C1(1)	(a,b,c,d,0,0),(e,f)	(1,1,3),(0,2,0),(-2,0,0)	(0,0,0)
			Entries removed		

Three different combinations of the U_1 and m$\Gamma_5^{+¿¿}$ irreps could give the vacancy ordered state with a structure in space group *Cc* as suggested by de Villiers & Liles (2010) (see Table 17). Of these three possibilities, one has m$\Gamma_4^{+¿¿}$ as a secondary order parameter (OPD Name: C9(1)P1(3)) and the other two do not. As the vacancy order will not change at the suggested low-temperature spin reorientation transition, the OPD for the vacancy ordering must stay basically unchanged. This suggests *P*1 as the low temperature structure with, OPD Name 4D1(1)C1(1) and OPD Vector (a,b,c,d,0,0),(e,f) (Table 17).

4. Discussion and conclusions

4.1. Fe/vacancy ordering

From the perspective of symmetry, the apparent diversity of pyrrhotite structures observed across the solid solution FeS -~Fe_7S_8 fits with the coherent pattern of structural and magnetic behaviour summarised schematically in Figure 6. *P*6_3*mc* and *Pnma* structures of FeS represent one end-member, and the series as a whole can be thought of as a combination of the *M*-point instability, $M_2^{-¿¿}$ $\boldsymbol{k}$ = (1/2,0,0), combined with vacancy ordering to give a repeat along $\boldsymbol{c}^*$. Divergence from the *M*-point, corresponding to increasing values of γ in irreps of the form $U_1(1/2,0,\gamma)$ along the line between the *M*- and *L*-points, occurs with increasing vacancy concentration. Commensurate ordering schemes develop at particular stoichiometries with values of γ = 1/6, 1/5, 1/4 or 1/3. The precise distribution of vacancies in each case can be described using ratios of the amplitudes of selected secondary irreps. Incommensurate ordering schemes, defined as those with irrational values of $1/\gamma$, appear to be favoured at high temperatures and in crystals with compositions which fall between the nominally rational stoichiometries. Crystals with compositions in between the ideal stoichiometries for commensurate Fe/vacancy ordering schemes are expected to develop exsolution textures and/or stacking mistakes in the *ab*-plane layers.

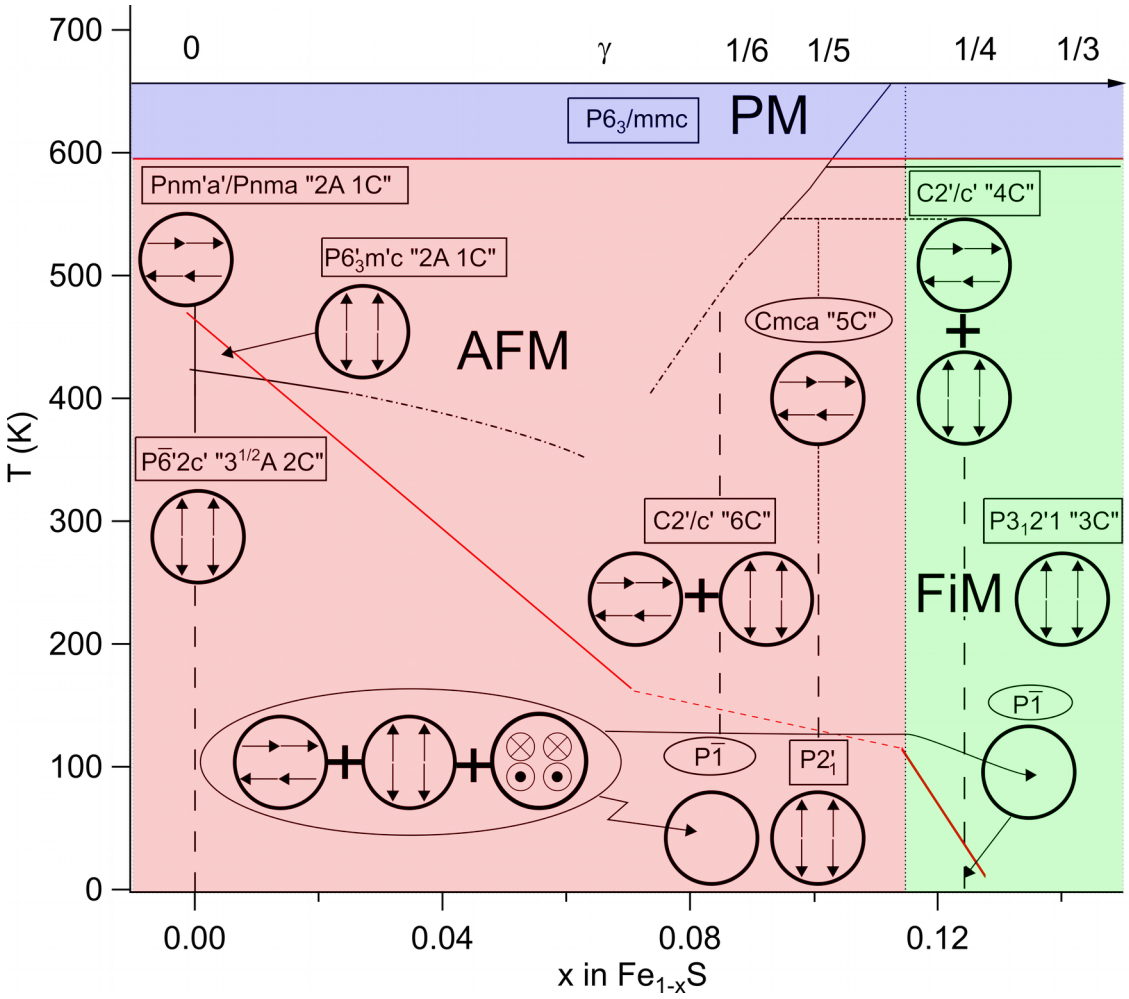

Figure 4 Schematic phase relationships for different structures in the $Fe_{1-x}S$ solid solution after our group theoretical analysis. The phase lines from Fig. 1 have been included to aid comparison. The pink area is antiferromagnetic (AFM), the blue area is paramagnetic (PM) and the green area is ferrimagnetic (FiM). Space groups in rectangles are those known from diffraction experiments and are placed at approximately the temperature that the data used in the refinements were collected. Space groups in ellipses are those we predict based on our group theory framework. Magnetic structures are represented by cartoons showing the three different magnetic ordering schemes: antiparallel vertical arrows represent $m\Gamma_4^{+¿¿}$ ordering, the antiparallel horizontal arrows represent the P2 direction of the $m\Gamma_5^{+¿¿}$ pattern and the two arrows in and two out symbols represent the P1 direction of the $m\Gamma_5^{+¿¿}$ pattern. The horizontal red line at 595 K is the Néel temperature. The red line at the low vacancy concentrations is the spin-flop transition according to Horwood *et al.* (1976). The structural phase transition to the room temperature structure of troilite is associated with an H-point instability rather than the *U*-line irrep, which describes the rest of the phase diagram, as, described in the text. The dashed red line shows the approximate temperatures of the magnetically driven phase transitions predicted for 5C and 6C pyrrhotite.

According to Ricci & Bousquet (2016), there are other possible structural instabilities in this system, but the only one which occurs at low pressures is associated with the H-point, rather than the M-point, of the Brillouin zone, giving the $P\acute{6}2c$ structure of FeS. The FeS phase diagram with respect to pressure and temperature displays considerable phenomenological richness (Fei *et al.* 1995; Terranova & de Leeuw 2017), and the additional possibilities might perhaps be contributing factors to this.

4.2. Magnetic ordering

The overall pattern of magnetic ordering can also be rationalised in a relatively simple manner. Below the Néel point of ~590 K, the stable magnetic structures have moments lined up within the *ab*-plane of the parent hexagonal structure, as represented by the magnetic irrep, $m\Gamma_5^{+¿¿}$. The orientation of moments within this plane generally remains to be determined but there are three possibilities, represented by the order parameter directions P1, P2 and C1 listed in Table 7. The favoured direction in the 4C structure is P2, in which the moments are parallel to the a-axis of the monoclinic cell (or the [120] direction of the parent hexagonal cell). The magnetic space groups shown in Figure 6 are based on the assumption that this will also be preferred in structures with different Fe/vacancy ordering schemes. At low temperatures, the alignment of magnetic moments is perpendicular to the *ab*-plane, as represented by the magnetic irrep, $m\Gamma_4^{+¿¿}$, which has only one direction, P1.

With falling temperature there will be a Morin-type spin-flop transition in structures which do not have $m\Gamma_4^{+¿¿}$ as a secondary order parameter resulting from the combination of $U_1(1/2,0,\gamma)$ and $m\Gamma_5^{+¿¿}$. Two examples of this are the transition near 450 K in FeS and near 130 K in 3C Fe_7Se_8. In structures where the symmetry is broken by vacancy and magnetic ordering such that $m\Gamma_4^{+¿¿}$ is a secondary irrep, rotation of the moments out of the *ab*-plane can occur continuously, as is observed in 4C Fe_7S_8. The subsequent Besnus transition can be understood in terms of a symmetry change $C2'/c'$ – $P\acute{1}$, arising by the change from direction P2 to C1 of irrep $m\Gamma_5^{+¿¿}$ when the moments rotate out of the *ac*-plane of the monoclinic cell. The 6C structure bears a strong similarity to that seen in the 4C case. We expect to see a similar continuous rotation of the spins out of the *ac*-plane. 6C has been reported in the *Cc* structure but inspection of the original determination suggests that the true space group is *C*2/*c*. Therefore, we predict that the magnetic structure is $C2'/c'$ and that the low temperature transition will be to $P\acute{1}$, in the same way as for the Besnus transition in 4C pyrrhotite. We would also predict that the transition temperature will fall between 170 K (seen for off-stoichiometry FeS) and 35 K (the Besnus transition in Fe_7S_8).

The magnetic properties of 5C pyrrhotite will be most closely related to those seen in the 3C case, with an abrupt spin-flop transition. In 5C pyrrhotite the spin-flop transition would be between two antiferromagnetic states, whereas in 3C it is between ferrimagnetic states. The 5C structure is less conclusively determined, however. *Cmca* (*Cmce* in new notation), $P2_1/c$ and $P2_1$ have all been reported. All of these possibilities appear in the Table 15 for the distortions arising from coupled U_1 and $m\Gamma_5^+$ irreps. *Cmca* and $P2_1/c$ arise from a single order parameter distortion and $P2_1$ from a higher order distortion. We therefore suggest that there is a transition from one of *Cmca* or $P2_1$/c to $P2_1$. We would then expect this transition to occur at a lower temperature than the transition in 6C pyrrhotite but above 35 K of the Besnus transition.

4.3. Coupling between Fe/vacancy and magnetic ordering

The overall superposition of structure types in Figure 6 involves interactions between Fe/vacancy and magnetic ordering. In this context, the key issue is the form and strength of coupling between order parameters with symmetries determined by $U_1(1/2,0,\gamma)$, $m\Gamma_4^{+}$ and $m\Gamma_5^{+}$. If the coupling is expressed in terms of two order parameters, Q_V to represent vacancy ordering and $M_{\Gamma 5+}$ to represent magnetic ordering on the basis of $m\Gamma_5^{+}$, the lowest order term permitted by symmetry is biquadratic, $\lambda_{\Gamma 5+} Q_V^2 M_{\Gamma 5+}$. The total excess free energy is given by $G_V + G_M + \lambda_{\Gamma 5+} Q_V^2 M_{\Gamma 5+}$, where G_V is the contribution from vacancy ordering alone and G_M is due to the magnetisation alone. It is notable that the Néel temperature does not vary significantly with composition across the solid solution. There also does not appear to be any correlation between magnetisation on the basis of $m\Gamma_5^{+}$ and the distribution of phase boundaries for the different structure types at high temperatures in the phase diagram (Fig. 1). As a first approximation, therefore, it would appear that the evolution of $M_{\Gamma 5+}$ is overwhelmingly dominated by G_M, ie by interactions between spins in the classic manner for a paramagnetic – antiferromagnetic/ferromagnetic transition.

By way of contrast with the behaviour at the Néel point, subsequent changes in magnetic structure differ between structure types and thus appear to be sensitive to the precise distribution of vacancies. This has been seen, for example, as a change of transition temperature for an antiferromagnetic – ferrimagnetic transition in a hexagonal sample with composition Fe_9S_{10} due to changes in the degree of vacancy order (Bennett & Graham 1981). The driving energy for a spin-flop transition or a continuous rotation of moments out of the *ab*-plane is the difference between $G_V + G_M + \lambda_{\Gamma 5+} Q_V^2 M_{\Gamma 5+}$, and $G_V + G_M + \lambda_{\Gamma 5+} Q_V^2 M_{\Gamma 4+}$. Even if small, the coupling energies can presumably provide a subtle influence on the overall thermodynamic stability of different magnetically ordered structures.

The only possibility for linear-quadratic coupling is associated with the Besnus transition. If it is driven simply by interactions between spins, the coupling is still biquadratic and the monoclinic – triclinic transition will be improper ferroelastic. If, on the other hand, the driving mechanism is a change in electronic structure, a new order parameter, Q_E, would need to be specified. This will have the symmetry of a zone centre irrep, the transition could be pseudoproper ferroelastic, ie with bilinear coupling between Q_E and a symmetry breaking strain and coupling with the magnetic order parameter could be of the form $\lambda Q_E M^2$.

4.4. Coupling with strain

An important mechanism for coupling between two order parameters is by overlap of strains associated with one order parameter and strains associate with the other. Inspection of the lattice

parameters given by Powell *et al.* (2004) for a 4C sample of Fe_7S_8 and by Li and Franzen (1996) or Tenailleau *et al.* (2005) for FeS show changes in linear strains on the order of ~1-3% associated with the transition at ~590 K. In anticipation of a formal strain analysis, selected Landau expansions which include the lowest order coupling terms allowed by symmetry have been set out in Appendix B. Strain coupling with the spin-flop transition at ~450 K in FeS and the Besnus transition near 35 K in Fe_7S_8 is very much weaker, based on the very much smaller changes in lattice parameters given by Li and Franzen (1996), Fillion *et al.* (1992) and Koulialias *et al.* (2018)

Strain coupling effects are also detectable through their influence on elastic constants. For example, an experimental method for distinguishing between linear-quadratic and biquadratic coupling at the Besnus transition, would be to observe the temperature dependence of single-crystal elastic constants. A transition in which the monoclinic symmetry is broken by a structural order parameter, Q, could have coupling with the symmetry-breaking shear strain, e_{sb}, as $\lambda e_{sb}Q$. If the symmetry is broken by a magnetic order parameter, M, the coupling would be $\lambda e_{sb}M^2$. A transition driven by Q would therefore be pseudoproper ferroelastic while a transition driven by M would be improper ferroelastic, and the difference would give rise to quite distinct patterns of evolution for elastic constants C_{44} and C_{66} (see, for example, Figure 4 of Carpenter & Salje 1998). Even the most recent diffraction measurements (Koulialias *et al.* 2018) have not resolved a distortion from monoclinic lattice geometry, however, implying that coupling with e_{sb} is weak.

4.5. Multiferroicity

As an ongoing matter of interest with respect to possible multiferroic sulphides, it is worth noting that structures with $P\acute{6}2c$ (FeS at room temperature) and $P3_121$ (3C pyrrhotite at room temperature) symmetry are expected to be piezoelectric while those with $P6_3mc$ (FeS between ~420 K and 460 K) or $P2_1$ (5C pyrrhotite at low temperature) symmetry could be ferroelectric.

Appendix A. Examples of input/output information for ISOTROPY.

As an example, we consider the 4C structure described in Section 2.1. In that Section we concluded that the structure derived from the parent structure in space group $P6_3/mmc$ (#.194) using irrep U_1 at $\boldsymbol{k}$ = 1/2,0,1/4, was in space group $C2/c$ (#15). To proceed we need first to compile a list of distortions, including secondary distortions. Knowing the space groups of the parent and product structures, and the basis vectors and origin of the product structure in terms of those of the parent (see entries in Table 1) we can use ISOTROPY to compile this list. The dialogue is reproduced in Figure A1, with input choices indicated by the letter v at the start of the line. The output shows all the contributing irreps, including irrep U_1, that we take to effect the primary distortion, along with all the secondary

irreps. The list of irreps shows the pertinent OPD's, along with the subgroups that would develop if each of them acted alone.

```
Isotropy, Version 9.4.1, December 2015
Harold T. Stokes, Dorian M. Hatch, and Branton J. Campbell
Brigham Young University
*DISPLAY SETTING
Current setting is International (new ed.) with conventional basis vectors.
*DISPLAY SETTING IRREP
Current irrep version is 2011
Use "VALUE IRREP VERSION" to change version
*v par 194
*v sub 15
*v bas 2,-2,0 2,2,0 -1,1,2
*v ori 0,1/2,0
*d dir
Irrep (ML) k params Dir                    Subgroup     Size
GM1+                (a)                    194 P6_3/mmc 1
GM3+                (a)                    164 P-3m1    1
GM5+                (a,1.732a)             63 Cmcm      1
GM6+                (a,-0.577a)            12 C2/m      1
A2                  (a,a)                  165 P-3c1    2
A3                  (a,0.577a,-0.577a,a)   15 C2/c      2
L1                  (0,0,0,0,a,a)          12 C2/m      2
M1-                 (0,0,a)                52 Pnna      2
M3-                 (0,0,a)                57 Pbcm      2
U1          1/4     (a,0,0,a,0,0)          15 C2/c      8
U2          1/4     (0,a,a,0,0,0)          15 C2/c      8
U3          1/4     (a,0,0,a,0,0)          15 C2/c      8
U4          1/4     (0,a,a,0,0,0)          15 C2/c      8
```

Figure A1 Example of input/output dialogue from ISOTROPY for determining the irreps responsible for a distortion characterised by a known parent, subgroup and unit cell.

Not all of these irreps relate to the site occupancy and, in order to determine which irreps can influence occupancy, we specify the relevant Wyckoff site (*a*) and use ISOTROPY to give the effect of the irrep on the occupancy by using "show microscopic scalar" (sh mic scal). This is used because the occupancy is a scalar. Figure A2 shows the dialogue for irrep U_1 at $\boldsymbol{k}$ = 1/2,0 ¼ with OPD P4. In the event that the irrep does not affect the occupancy at the Wyckoff a site, the output list is empty. By following this procedure for all the irreps listed in Figure A1, we find that only U_1, U_4, L_1, Γ_3^+ and Γ_1^+ can change occupancy on the relevant iron site. Setting OPD's as appropriate, we can find their effects in the same manner as seen in Figure A2 and, when combined in selected proportions, they give the occupancy of interest. In the case of the 4C structure we add the irreps with mode amplitudes in the following ratios: $\frac{U1-U4}{4\sqrt{2}}+\frac{L1}{8}+\frac{\Gamma_3^{+¿}}{8}+7\frac{\Gamma_1^{+¿}}{8}¿¿$. In this case the contributions of U_1 and U_4 must be opposite and equal.

```
Isotropy, Version 9.4.1, December 2015
Harold T. Stokes, Dorian M. Hatch, and Branton J. Campbell
Brigham Young University
*DISPLAY SETTING
Current setting is International (new ed.) with conventional basis vectors.
*DISPLAY SETTING IRREP
Current irrep version is 2011
Use "VALUE IRREP VERSION" to change version
*v par 194
*v sub 15
*v irrep u1
*v kv 1,1/4
*v dir p4
*v bas 2,-2,0 2,2,0 -1,1,2
*v ori 0,1/2,0
*v wy a
*sh par
*sh sub
*sh mic sc
*v cell 2,0,0 0,2,0 0,0,4
*d dis
Parent          Point     Projected Order Functions
194 P6_3/mmc    (0,0,0)   f
                (0,0,1)   -f
                (0,0,2)   -f
                (0,0,3)   f
                (0,1,0)   f
                (0,1,1)   f
                (0,1,2)   -f
                (0,1,3)   -f
                (1,0,0)   -f
                (1,0,1)   -f
                (1,0,2)   f
                (1,0,3)   f
                (1,1,0)   -f
                (1,1,1)   f
                (1,1,2)   f
                (1,1,3)   -f
                (0,0,1/2) 0
                (0,0,3/2) -1.414f
                (0,0,5/2) 0
                (0,0,7/2) 1.414f
                (0,1,1/2) 1.414f
                (0,1,3/2) 0
                (0,1,5/2) -1.414f
                (0,1,7/2) 0
                (1,0,1/2) -1.414f
                (1,0,3/2) 0
                (1,0,5/2) 1.414f
                (1,0,7/2) 0
                (1,1,1/2) 0
                (1,1,3/2) 1.414f
                (1,1,5/2) 0
                (1,1,7/2) -1.414f
```

Figure A2 Input/output dialogue showing how ISOTROPY can be used to display the effect of an irrep on the occupancy of specific Wyckoff sites within either the conventional cell or any unconventional cell desired. Here, “v bas 2,-2,0 2,2,0 -1,1,2” specifies the unit cell (basis vectors) of the distorted structure and the command “v cell 2,0,0 0,2,0 0,0,4” ensures that the effect of the irrep on the occupancy is listed for all the specified Wyckoff sites within a representative hexagonal column, i.e. all the sites directly above the points within the basal plane of the parent structure. This makes it more intuitive to track the vacancy-ordering scheme through the layers.

Appendix B. Landau expansions for strain and order parameter coupling

The INVARIANTS tool, part of the ISOTROPY suite, gives symmetry allowed terms in the Landau free energy expansion for a phase transition. Here we give an example of the Landau expansion for $U_1(1/2,0,1/4)$ coupled with $m\Gamma_5^{+¿¿}$, as is applicable to 4C pyrrhotite. The chosen (orthogonal) reference axes follow the convention of Nye: X // ***a*** ([100] direction), Z // ***c*** ([001] direction] and Y perpendicular to both ([120] direction). The expansion is given in terms of a vacancy order parameter, Q_{Vac}, a magnetic order parameter, Q_{Mag}, the six components, e_i, of the spontaneous strain tensor, and elastic constants, C_{ik}^0, of the parent hexagonal structure:

$$G=G\left(Q_{Mag}\right)+G\left(Q_{Vac}\right)+G\left(Q_{Mag},Q_{Vac}\right)+G\left(Q_{Mag},e\right)+G\left(Q_{Vac},e\right)+G\left(Q_{Mag},Q_{Vac},e\right)+\frac{1}{2}\sum_{i,k}C_{ik}^{o}e_i e_k,$$

where

$$G\left(Q_{Mag}\right)=\frac{1}{2}a\left(T-T_{CM}\right)\left(M_1^2+M_2^2\right)+\frac{1}{4}b\left(M_1^2+M_2^2\right)^2+\frac{1}{6}c\left(M_1^2+M_2^2\right)^3$$

$$G\left(Q_{Vac}\right)=\frac{1}{2}u\left(T-T_{CV}\right)Q_{Vac}^2+\frac{1}{4}v\,Q_{Vac}^4+\frac{1}{6}w\,Q_{Vac}^6.$$

The lowest order coupling term for the two order parameters is biquadratic:

$$G\left(Q_{Mag},Q_{Vac}\right)=\lambda_{MV}\left(M_1^2+M_2^2\right)Q_{Vac}^2$$

The lowest order allowed coupling terms for strain and the magnetic order parameter are:

$$\lambda_{eM1}\left(e_1+e_2\right)\left(M_1^2+M_2^2\right)+\lambda_{eM2}e_3\left(M_1^2+M_2^2\right)+\lambda_{eM2}\left(\left(e_1-e_2\right)\left(M_1^2-M_2^2\right)+4e_6M_1M_2\right)$$

$$\lambda_{eM3}\left(e_4^2+e_5^2\right)\left(M_1^2+M_2^2\right)+\lambda_{eM4}\left(\left(e_4^2+3e_5^2\right)M_1^2+\left(3e_4^2+e_5^2\right)M_2^2+4e_4e_5M_1M_2\right)$$

The lowest order terms for coupling between strain and the order parameter for vacancy ordering are

$$\lambda_{eV1}\left(e¿¿1+e_2\right)Q_{Vac}^2+\lambda_{eV2}e_3Q_{Vac}^2+\lambda_{eV3}\left(\frac{1}{\sqrt{3}}\left(e_1-e_2\right)-2e_6\right)Q_{Vac}^{2}¿$$

$$\lambda_{eV4}\left(e_4^2+e_5^2\right)Q_{Vac}^2+\lambda_{eV5}\left(\left(2-\frac{\sqrt{2}}{12}\right)e_4^{2}+2e_5^2-\frac{\sqrt{2}}{4\sqrt{3}}e_4e_5\right)Q_{Vac}^{2}+\lambda_{eV6}\left(e_5-\frac{e_4}{\sqrt{3}}\right)Q_{Vac}^{4}.$$

The lowest order allowed terms for coupling of strain with both order parameters are

$$\lambda_{eVM1}(e¿¿1+e_2)Q_{Vac}^2Q_{Mag}^2+\lambda_{eVM2}e_3Q_{Vac}^2Q_{Mag}^2+\lambda_{eVM3}\left(\frac{1}{\sqrt{3}}(e_1-e_2)-2e_6\right)Q_{Vac}^2\left(M_1^2+M_2^2\right)+\lambda_{eVM4}\left((e_1-e_2)\left(\frac{M_1^2}{\sqrt{3}}+M_1\right.\right.$$

and triquadratic for the remaining two:

$$\lambda_{eVM6}\left(e_4^2+e_5^2\right)\left(M_1^2+M_2^2\right)Q_{Vac}^2+\lambda_{eVM7}\left(e_4^2+e_5^2\right)\left(M_1M_2+\frac{M_2^2}{\sqrt{3}}\right)Q_{Vac}^2+\lambda_{eVM8}\left(e_4e_5+\frac{e_4^2}{\sqrt{3}}\right)\left(M_1^2+M_2^2\right)Q_{Vac}^2+\lambda_{eVM9}\left(e_4^2M_1^2+e_5^2\right.$$

Taking these coupling terms and adding the standard Landau expansion terms for the two independent order parameters as well as the elastic energy contribution the final expression becomes

$$G=\frac{1}{2}a(T-T_{CM})\left(M_1^2+M_2^2\right)+\frac{1}{4}b\left(M_1^2+M_2^2\right)^2+\frac{1}{6}c\left(M_1^2+M_2^2\right)^3+\frac{1}{2}u(T-T_{CV})Q_{Vac}^2+\frac{1}{4}vQ_{Vac}^4+\frac{1}{6}wQ_{Vac}^6+\lambda_{MV}\left(M_1^2+M\right.$$

.

For the case of 4C pyrrhotite in the monoclinic phase above T_B the two components of the magnetic order parameter are related. In particular $M_1 = -Q_{Mag}$ and $M_2 = Q_{Mag}/3^{1/2}$ for the P2(3) direction of the mΓ_5^+ distortion. In this case, the expansion simplifies to:

$$G=\frac{1}{2}a(T-T_C)Q_{Mag}^2+\frac{1}{4}bQ_{Mag}^4+\frac{1}{6}cQ_{Mag}^6+\frac{1}{2}u(T-T_C)Q_{Vac}^2+\frac{1}{4}vQ_{Vac}^4+\frac{1}{6}wQ_{Vac}^6+\lambda_{MV}Q_{Mag}^2Q_{Vac}^2+\lambda_{eM1}(e¿¿1+e_2)$$

.

The exact form of the expansion is dependent on the axes chosen. The expressions given here relate to the basis vectors and axis choices used in all the discussion of the 4C structure above.

cknowledgements The authors acknowledge funding from the Leverhulme Foundation, grant number RPG-2016-298.

References

Andresen, A. F., Hofman-Bang, N., Bak, T. A., Varde, E. & Westin, G. (1960). *Acta Chemica Scandinavica*, **14**, 919–926.

Andresen, A., & Leciejewicz, J. (1964). *Journal De Physique,* **25**(5), 574-578.

Andresen, A. F., Torbo, P., Ostlund, E., Bloom, G. & Hagen, G. (1967). *Acta Chemica Scandinavica*, **21**, 2841–2848.

Baranov, N V., Ibrahim, P. N. G., Selezneva, N. V., Gubkin, A. F., Volegov, A. S., Shishkin, D. A., Keller, L., Sheptyakov, D. & Sherstobitova, E. A. (2015). *Journal of Physics: Condensed Matter,* **27**(28), 12.

Bennett, C. E. G. & Graham, J. (1980) *American Mineralogist* **65** 800-807

Bennett, C. E. G. & Graham, J. (1981) *American Mineralogist* ; **66** (11-12): 1254–1257

Bertaut, E. F. (1953). *Acta Crystallographica,* **6**, 557-561

Bertaut, E. F. (1980). *Pure and Applied Chemistry,* **52**(1), 73-92

Besnus, M. J. & Meyer, A. J. P. (1964) *Proceedings of the International Conference on Magnetism Nottingham* 507-511

Bezaeva, N. S., Chareev, D. A., Rochette, P., Kars, M., Gattacceca, J., Feinberg, J. M., Sadykov, R. A., Kuzina, D. M & Axenov, S. N. (2016). *Physics of the Earth and Planetary Interiors*, **257**, 79-90.

Campbell, B. J., Stokes, H. T., Tanner, D. E. & Hatch, D. M. (2006). *Journal of Applied Crystallography,* **39**(4), 607-614.

Carpenter, M. A, & Salje, E. (1998). *European Journal of Mineralogy,* **10**(4), 693-812.

Carpenter, M. A. & Howard, C. J. (2009). *Acta Crystallographica Section B*, **65**(2), 134–146. *https://doi.org/10.1107/S0108768109000974

Carpenter, R. & Desborough, G. (1964). *American Mineralogist*, **49**(9-1), 1350–&.

Charilaou, M., Kind, J., Koulialias, D., Weidler, P. G., Mensing, C., Löffler, J. F. & Gehring. A. U. (2015). *Journal of Applied Physics,* **118** 083903

Dekkers, M. J., Mattéi, J.-L., Fillion, G. and Rochette, P. (1989). *Geophysical Research Letters* **16** 855-858.

De Villiers, J. P. R. & Liles, D. C. & Becker, M. (2009). *American Mineralogist,* **94**(10), 1405-1410.

De Villiers, J. P. R. & Liles, D. C. (2010). *American Mineralogist,* **95**(1), 148-152.

Eerenstein, W., Mathur, N. D. & Scott, J. F. (2006). *Nature, **442***(7104), 759-765.

Elliot, A. D. (2010). *Acta Crystallographica Section B,* **66**(3), 271-279.

Ericsson, T., Amcoff, Ö. & Nordblad, P. (1997). *European Journal of Mineralogy,* **9**(6), 1131-1146.

Fei, Y., Prewitt, C., Mao, H., & Bertka, C. (1995). *Science,* **268**(5219), 1892-1894.

Ferrow, E., Adetunji, J., & Nkoma, J. (2006). *European Journal of Mineralogy,* **18**(5), 653-664.

Fillion, G. & Rochette, P. (1988) *Journal de Physique Colloques* **49** C8 907-908.

Fillion, G., Mattei, J., Rochette, P. & Wolfers, P. (1992). *Journal of Magnetism and Magnetic Materials*, **104-107**, 1985 – 1986.

*http://www.sciencedirect.com/science/article/pii/0304885392916335

Fleet, M. E. (1971). *Acta Crystallographica Section B,* **27**(10), 1864-1867.

Fleet, M. (2006). *Reviews in Mineralogy and Geochemistry,* **61(**1), 365-419.

Gosselin, J. R., Townsend, M. G. & Tremblay, R. J. (1976). *Solid State Communications,* **19(**8), 799-803.

Grønvold, F. & Westrum Jr, E. F. (1959). *The Journal of Chemical Physics* **30** 528-531

Grønvold, F. & Stølen, S. (1992). *The Journal of Chemical Thermodynamics* **24** 913-936

* https://doi.org/10.1016/S0021-9614(05)80003-5

Haines, C. R. S., Lampronti G. I., Klooster W. T., Coles S. J., Dutton S. E. & Carpenter, M. A. C. (2019) *American Mineralogist,* Submitted

Harrison, R. J., Mcenroe, S. A., Robinson, P. & Howard, C. J., (2010). *American Mineralogist* **95**, 974–979.

Stokes, H. T., & Hatch, D. M. (2003). *Journal of Applied Crystallography,* 36(3-2), 951-952.

Hirahara, E. & Murakami, M. (1958). *Journal of Physics and Chemistry of Solids,* **7**(4), 281-289.

Horng, C., & Roberts, A. (2018). *Geochemistry, Geophysics, Geosystems, 19*(9), 3364-3375.

Horwood, J. L., Townsend, M. G. & Webster, A. H. (1976) *Journal of Solid State Chemistry* **17** 17-42.

Howard, C., & Stokes, H. (1998). *Acta Crystallographica, Section B: Structural Science,* **54**, 782-789.

Howard, C. J. & Carpenter, M. A. (2010). *Acta Crystallographica Section B*, **66**(1), 40–50. *https://doi.org/10.1107/S0108768109048010

Howard, C. J., Kennedy, B. J. & Woodward, P. M. (2003). *Acta Crystallographica Section B*, **59**(4), 463–471.
*https://doi.org/10.1107/S0108768103010073

Howard, C. J. & Stokes, H. T. (2004). *Acta Crystallographica Section B*, **60**(6), 674–684.
*https://doi.org/10.1107/S0108768104019901

Jeandey, C., Oddou, J., Mattei, J. & Fillion, G. (1991). *Solid State Communications*, **78**(3), 195 – 198.
*http://www.sciencedirect.com/science/article/pii/003810989190282Z

Kawaminami, M. & Okazaki, A. (1967). *Journal of the Physical Society of Japan*, **22**(3), 924–924.
*https://doi.org/10.1143/JPSJ.22.924

Kawaminami, M. & Okazaki, A. (1970). *Journal of the Physical Society of Japan*, **29**(3), 649–655.
*https://doi.org/10.1143/JPSJ.29.649

Keller-Besrest, F., Collin, G. & Comes, R. (1983). *Acta Crystallographica Section B* **39**, 296-303.

Keller-Besrest, F. & Collin, G. (1990). *Journal of Solid State Chemistry*, **84**(2), 194 – 210.
*http://www.sciencedirect.com/science/article/pii/002245969090319S

Kind, J., García-Rubio, I., Charilaou, M., Nowaczyk, N., Löffler, J., & Gehring, A. (2013). *Geophysical Journal International, 195*(1), 192-199.

King, Jnr, H. E. & Prewitt, C. T. (1982). *Acta Crystallographica Section B*, **38**(7), 1877–1887.
*https://doi.org/10.1107/S0567740882007523

Koto, K., Morimoto, N., & Gyobu, A. (1975). *Acta Crystallographica Section B,* **31(**12), 2759-2764.

Koulialias, D., Kind, J., Charilaou, M., Weidler, P., Löffler, J., & Gehring, A. (2016). *Geophysical Journal International*, **204**(2), 961-967.

Koulialias, D., Schäublin, R., Kurtuldu, G., Weidler, P. G., Löffler, J. F., & Gehring, A. U. (2018). *Journal of Geophysical Research: Solid Earth*, **123**, 6236–6246.
*https://doi.org/10.1029/2018JB015548

Li, F. & Franzen. H. F. (1994). *Journal of Alloys and Compounds,* **215**(1), L3-L6.

Li, F. & Franzen. H. F. (1996). *Journal of Alloys and Compounds,* **238**(1), 73-80.

Liles, D. C. & De Villiers, J. P. R. (2012). *American Mineralogist*, **97**(2), 257-261.

Louzada, K. L., S. T. Stewart, & B. P. Weiss (2007), *Geophyics. Research Letters*, **34**, L05204, *doi:10.1029/2006GL027685.

Miller, S. C. & Love W. F. (1967). Boulder, Colo.: Pruett Press.

Morimoto, N. & Nakazawa, H. (1968). *Science*, **161**(3841), 577–579.

*http://science.sciencemag.org/content/161/3841/577

Morimoto, N., Nakazawa, H., Nishigucmi, K. & Tokonami, M. (1970). *Science*, **168**(3934), 964–966.

*http://science.sciencemag.org/content/168/3934/964

Morimoto, N., Gyobu, A, Tsukuma, K, & Koto, K. (1975). *The American Mineralogist.,* **60**(3-4), 240-248.

Morimoto, N., Gyobu, A., Mukaiyama, H., & Izawa, E. (1975). *Economic Geology and the Bulletin of the Society of Economic Geologists,* **70**(4), 824-833.

Nakano, A., Tokonami, M. & Morimoto, N. (1979). *Acta Crystallographica Section B*, **35**(3), 722–724.

*https://onlinelibrary.wiley.com/doi/abs/10.1107/S0567740879004532

Nakazawa, H. & Morimoto, N. (1971). *Material Research Bulletin* Morimoto, **6** 345-358.

Oddou, J. L., Jeandey, C., Mattei, J. L. & Fillion. G. (1992). *Journal of Magnetism and Magnetic Materials, 104*(3), 1987-1988.

Okazaki, A. (1961). *Journal of the Physical Society of Japan*, **16**(6), 1162–1170.

*https://doi.org/10.1143/JPSJ.16.1162

Pearce, C. I., Pattrick, R. & Vaughan, D. J. (2006) *Reviews in Mineralogy and Geochemistry* **61** 127-180.

Powell, A., Vaqueiro, P., Knight, K., Chapon, L. & Sanchez, R. (2004). *Physical Review B*, **70**(1).

Ricci, F. & Bousquet, E. (2016). *Physical Review Letters* **116** 227601

Rochette, P., Fillion, G., Mattéi, J. & Dekkers, M. J. (1990) *Earth and Planetary Science Letters* **98** 319-328.

Rochette, P., Gattacceca, J., Chevrier, V., Hoffmann, V., Lorand, J., Funaki, M., & Hochleitner, R. (2005). *Meteoritics & Planetary Science, 40*(4), 529-540.

Salje, E., & Zhang, H. (2009). *Phase Transitions,* **82**(6), 452-469.

Salje, E. (2010). *Phase Transitions,* **83**(9), 657-669.

Schwarz, E. J. & Vaughan, D. J. (1972) *Journal of Geomagnetism and Geoelectricity* **24** 441-458.

Senn, M., & Bristowe, N. (2018). *Acta Crystallographica Section A,* **74**(4), 308-321.

Sparks, J. T., Mead, W., Kirschbaum, A. J. & Marshall, W. (1960). *Journal of Applied Physics*, **31**(5), S356–S357.

Sparks, J. T., Mead, W. & Komoto, T. (1962) *Journal of the Physical Society of Japan* **17(Suppl. B-I)** 249-252.

Stokes H. T. and Hatch, D. M. (1988) Isotropy Subgroups of the 230 Crystallographic Space Groups (World Scientific, Singapore), 624 pages.

Stokes, H., Kisi, E., Hatch, D., & Howard, C. (2002). *Acta Crystallographica Section B, **58***(6), 934-938.

Takahashi, T. (1973) *Solid State Communications* **13** 1335-1337.

Tenailleau, C., Etschmann, B., Wang, H., Pring, A., Grguric, B. A. & Studer, A. (2015) *Mineralogical Magazine,* **69**, 205-216.

Terranova, U. & De Leeuw, N. H. (2017). *Journal of Physics and Chemistry of Solids,* **111**(C), 317-323.

Van den Berg, C. B., Van Delden, J. & Bouman, J. (1969). *Physica Status Solidi (b),* **36**(2), K89-K93.

Van Den Berg, C. B. (1972). *Ferroelectrics*, **4**(1), 117–120.
*https://doi.org/10.1080/00150197208235752

Volk, M. W., Gilder, S. A. & Feinberg, J. M. (2016). *Geophysical Journal International*, **207**(3), 1783–1795.
*http://dx.doi.org/10.1093/gji/ggw376

Volk, M. W., McCall, E., Voigt, B., Manno, M. A., Leighton, C. & Feingerg J. M. (2018) American Mineralogist, 103, 1674-1689.

Wang, H. & Salveson, I. (2005) *Phase Transitions* **78** 547-567

Wolfers, P., Fillion, G., Ouladdiaf, B., Ballou, R. & Rochette, P. (2011). In *Solid Compounds of Transition Elements*, vol. 170 of *Solid State Phenomena*, pp. 174–179. Trans Tech Publications.

Yamamoto, A. & Nakazawa, H. (1982). *Acta Crystallographica Section A*, **38**(1), 79–86.
*https://doi.org/10.1107/S0567739482000151

Supplementary Material

S1. Tables in full

S2. 4C

S3. 4C U_1 (1/2,0,1/4)

Table S1 Order parameter components and unit cell configurations for subgroups of $P6_3/mmc$ which can arise from phase transitions in which irrep $U_1(1/2,0,1/4)$ is the active representation. SGN = space group number.

SGN	Space Group	NOPD NName	OPD Vector	Basis Vectors	Origin
12	*C*2/*m*	P1	(a,0,0,0,0,0)	(2,1,-4),(0,1,0),(2,1,0)	(0,0,0)
44	*Imm*2	P2	(a,-0.414a,0,0,0,0)	(0,0,4),(0,1,0),(-2,-1,0)	(-7/8,1/16,-7/4)
12	*C*2/*m*	P3	(a,0,a,0,0,0)	(2,-2,0),(2,2,0),(-1,1,2)	(0,0,0)
15	*C*2/c	P4	(a,0,0,a,0,0)	(2,-2,0),(2,2,0),(-1,1,2)	(0,1/2,0)
42	*Fmm*2	P5	(a,-0.414a,a,-0.414a,0,0)	(0,0,4),(2,2,0),(-2,2,0)	(-1/8,1/8,1/4)
43	*Fdd*2	P6	(a,-0.414a,0.414a,a,0,0)	(0,0,4),(2,2,0),(-2,2,0)	(-7/8,7/8,7/4)
164	$P\bar{3}m1$	P7	(a,0,a,0,a,0)	(2,0,0),(0,2,0),(0,0,4)	(0,0,0)
187	$P\bar{6}m2$	P8	(a,-0.414a,a,-0.414a,a,-0.414a)	(0,-2,0),(2,2,0),(0,0,4)	(0,0,1/4)
8	*Cm*	C1	(a,b,0,0,0,0)	(2,1,-4),(0,1,0),(2,1,0)	(0,0,0)
5	*C*2	C2	(a,b,a,-b,0,0)	(2,-2,0),(2,2,0),(-1,1,2)	(0,0,0)
5	*C*2	C3	(a,b,0.707a0.707b,-0.707a0.707b,0,0)	(2,2,0),(-2,2,0),(1,1,2)	(1/8,15/8,1/4)
2	$P\bar{1}$	C4	(a,0,b,0,0,0)	(1,1,2),(0,2,0),(-2,0,0)	(0,0,0)
2	$P\bar{1}$	C5	(a,0,0,b,0,0)	(1,1,2),(0,2,0),(-2,0,0)	(0,1/2,0)
8	*Cm*	C6	(a,-0.414a,b,-0.414b,0,0)	(-2,-2,0),(0,0,4),(-2,0,0)	(-1/8,-1/8,1/4)
9	*Cc*	C7	(a,-0.414a,b,2.414b,0,0)	(-2,-2,0),(0,0,4),(-2,0,0)	(-5/8,-5/8,5/4)
8	*Cm*	C8	(a,b,a,b,0,0)	(2,-2,0),(2,2,0),(-1,1,2)	(0,0,0)
9	*Cc*	C9	(a,b,b,-a,0,0)	(2,-2,0),(2,2,0),(-1,1,2)	(3/2,0,0)
156	*P*3*m*1	C10	(a,b,a,b,a,b)	(2,0,0),(0,2,0),(0,0,4)	(0,0,0)
12	*C*2/*m*	C11	(a,0,b,0,a,0)	(-2,-4,0),(2,0,0),(0,0,4)	(0,0,0)
12	*C*2/*m*	C12	(0,a,b,0,0,-a)	(-2,-4,0),(2,0,0),(0,0,4)	(1/2,0,0)
38	*Amm*2	C13	(a,-0.414a,b,-0.414b,b,-0.414b)	(0,0,4),(0,2,0),(-4,-2,0)	(0,0,1/4)
39	*A*b*m*2	C14	(a,-0.414a,b,2.414b,-b,2.414b)	(0,0,4),(0,2,0),(-4,-2,0)	(0,0,1/4)
5	*C*2	S1	(a,b,c,0,a,-b)	(-2,-4,0),(2,0,0),(0,0,4)	(0,0,0)
5	*C*2	S2	(a,-0.414a,b,c,0.707b0.707c,-0.707b0.707c)	(0,-2,0),(4,2,0),(0,0,4)	(0,0,1/4)
2	$P\bar{1}$	S3	(a,0,b,0,c,0)	(0,0,4),(0,2,0),(-2,0,0)	(0,0,0)
2	$P\bar{1}$	S4	(a,0,0,b,0,c)	(0,0,4),(0,2,0),(-2,0,0)	(0,1/2,0)

6	*Pm*	S5	(a,-0.414a,b,-0.414b,c,-0.414c)	(-2,0,0),(0,0,4),(0,2,0)	(0,0,1/4)
7	*Pc*	S6	(a,-0.414a,b,2.414b,c,2.414c)	(-2,0,0),(0,0,4),(0,2,0)	(0,0,1/4)
1	*P*1	4D1	(a,b,c,d,0,0)	(1,1,2),(0,2,0),(-2,0,0)	(0,0,0)
8	*Cm*	4D2	(a,b,c,d,a,b)	(-2,-4,0),(2,0,0),(0,0,4)	(0,0,0)
1	*P*1	6D1	(a,b,c,d,e,f)	(0,0,4),(0,2,0),(-2,0,0)	(0,0,0)

S4. 4C mΓ_4^+ with U_1

Table S2 Magnetic subgroups arising from coupling of irreps $m\Gamma_4^{+¿¿}$ and $U_1(1/2,0,1/4)$, with respect to the parent space group $P6_3/mmc$. SGN.M = magnetic space group number.

SGN.M	Space Group	OPD Name $U_1(1/2,0,1/4)$ $m\Gamma_4^{+¿¿}$	OPD Vector $U_1(1/2,0,1/4)$, $m\Gamma_4^{+¿¿}$	Basis Vectors	Origin
12.62	C2'/m'	P1(1)P1(1)	(a,0,0,0,0,0),(b)	(2,1,-4),(0,1,0),(2,1,0)	(0,0,0)
44.232	Im'm'2	P2(1)P1(1)	(a,-0.414a,0,0,0,0),(b)	(0,0,4),(0,1,0),(-2,-1,0)	(-7/8,1/16,-7/4)
12.62	C2'/m'	P3(1)P1(1)	(a,0,a,0,0,0),(b)	(2,-2,0),(2,2,0),(-1,1,2)	(0,0,0)
15.89	C2'/c'	P4(1)P1(1)	(a,0,0,a,0,0),(b)	(2,-2,0),(2,2,0),(-1,1,2)	(0,1/2,0)
42.222	Fm'm'2	P5(1)P1(1)	(a,-0.414a,a,-0.414a,0,0),(b)	(0,0,4),(2,2,0),(-2,2,0)	(-1/8,1/8,1/4)
43.227	Fd'd'2	P6(1)P1(1)	(a,-0.414a,0.414a,a,0,0),(b)	(0,0,4),(2,2,0),(-2,2,0)	(-7/8,7/8,7/4)
164.89	P$\bar{3}$*m*'1	P7(1)P1(1)	(a,0,a,0,a,0),(b)	(0,-2,0),(2,2,0),(0,0,4)	(0,0,0)
187.211	*P*$\bar{6}$'*m*'2	P8(1)P1(1)	(a,-0.414a,a,-0.414a,a,-0.414a),(b)	(2,2,0),(-2,0,0),(0,0,4)	(0,0,1/4)
8.34	Cm'	C1(1)P1(1)	(a,b,0,0,0,0),(c)	(2,1,-4),(0,1,0),(2,1,0)	(0,0,0)
5.15	C2'	C2(1)P1(1)	(a,b,a,-b,0,0),(c)	(2,-2,0),(2,2,0),(-1,1,2)	(0,0,0)
5.13	C2	C3(1)P1(1)	(a,b,0.707a-0.707b,-0.707a-0.707b,0,0),(c)	(2,2,0),(-2,2,0),(1,1,2)	(1/8,15/8,1/4)
2.4	P$\bar{1}$	C4(1)P1(1)	(a,0,b,0,0,0),(c)	(1,1,2),(0,2,0),(-2,0,0)	(0,0,0)
2.4	P$\bar{1}$	C5(1)P1(1)	(a,0,0,b,0,0),(c)	(1,1,2),(0,2,0),(-2,0,0)	(0,1/2,0)
8.34	Cm'	C6(1)P1(1)	(a,-0.414a,b,-0.414b,0,0),(c)	(-2,-2,0),(0,0,4),(-2,0,0)	(-1/8,-1/8,1/4)
9.39	Cc'	C7(1)P1(1)	(a,-0.414a,b,2.414b,0,0),(c)	(-2,-2,0),(0,0,4),(-2,0,0)	(-5/8,-5/8,5/4)
8.34	Cm'	C8(1)P1(1)	(a,b,a,b,0,0),(c)	(2,-2,0),(2,2,0),(-1,1,2)	(0,0,0)
9.39	Cc'	C9(1)P1(1)	(a,b,b,-a,0,0),(c)	(2,-2,0),(2,2,0),(-1,1,2)	(3/2,0,0)
156.51	P3m'1	C10(1)P1(1)	(a,b,a,b,a,b),(c)	(0,-2,0),(2,2,0),(0,0,4)	(0,0,0)
12.62	C2'/m'	C11(1)P1(1)	(a,0,b,0,a,0),(c)	(-2,-4,0),(2,0,0),(0,0,4)	(0,0,0)
12.62	C2'/m'	C12(1)P1(1)	(0,a,b,0,0,-a),(c)	(-2,-4,0),(2,0,0),(0,0,4)	(1/2,0,0)
38.191	Am'm'	C13(1)P1(1)	(a,-0.414a,b,-0.414b,b,-	(0,0,4),(0,2,0),(-4,-	(0,0,1/4)

	2		0.414b),(c)	2,0)	
39.199	Ab'm'2	C14(1)P1(1)	(a,-0.414a,b,2.414b,-b,-2.414b),(c)	(0,0,4),(0,2,0),(-4,-2,0)	(0,0,1/4)
5.15	C2'	S1(1)P1(1)	(a,b,c,0,a,-b),(d)	(-2,-4,0),(2,0,0),(0,0,4)	(0,0,0)
5.13	C2	S2(1)P1(1)	(a,-0.414a,b,c,0.707b-0.707c,-0.707b-0.707c),(d)	(0,-2,0),(4,2,0),(0,0,4)	(0,0,1/4)
2.4	P$\bar{1}$	S3(1)P1(1)	(a,0,b,0,c,0),(d)	(0,0,4),(0,2,0),(-2,0,0)	(0,0,0)
2.4	P$\bar{1}$	S4(1)P1(1)	(a,0,0,b,0,c),(d)	(0,0,4),(0,2,0),(-2,0,0)	(0,1/2,0)
6.2	Pm'	S5(1)P1(1)	(a,-0.414a,b,-0.414b,c,-0.414c),(d)	(-2,0,0),(0,0,4),(0,2,0)	(0,0,1/4)
7.26	Pc'	S6(1)P1(1)	(a,-0.414a,b,2.414b,c,2.414c),(d)	(-2,0,0),(0,0,4),(0,2,0)	(0,0,1/4)
1.1	P1	4D1(1)P1(1)	(a,b,c,d,0,0),(e)	(1,1,2),(0,2,0),(-2,0,0)	(0,0,0)
8.34	Cm'	4D2(1)P1(1)	(a,b,c,d,a,b),(e)	(-2,-4,0),(2,0,0),(0,0,4)	(0,0,0)
1.1	P1	6D1(1)P1(1)	(a,b,c,d,e,f),(g)	(0,0,4),(0,2,0),(-2,0,0)	(0,0,0)

S5. 4C mΓ_5^+ and U_1

Table S3 Magnetic subgroups arising from coupling of irreps $m\Gamma_5^{+¿¿}$ and U_1(1/2,0,1/4), with respect to the parent space group $P6_3/mmc$.

SGN. M	Space Group	OPD Name U_1(1/2,0,1/4) $m\Gamma_5^{+¿¿}$	OPD Vector U_1(1/2,0,1/4), $m\Gamma_5^{+¿¿}$	Basis Vectors	Origin
12.58	*C*2/*m*	P1(1)P1(1)	(a,0,0,0,0,0),(b,-1.732b)	(2,1,-4),(0,1,0),(2,1,0)	(0,0,0)
44.229	*Imm*2	P2(1)P1(1)	(a,-0.414a,0,0,0,0),(b,-1.732b)	(0,1,0),(0,0,4),(2,1,0)	(0,0,1/4)
12.58	*C*2/*m*	P3(1)P1(3)	(a,0,a,0,0,0),(b,1.732b)	(2,-2,0),(2,2,0),(-1,1,2)	(0,0,0)
15.85	*C*2/*c*	P4(1)P1(3)	(a,0,0,a,0,0),(b,1.732b)	(2,-2,0),(2,2,0),(-1,1,2)	(0,1/2,0)
42.219	*Fmm*2	P5(1)P1(3)	(a,-0.414a,a,-0.414a,0,0),(b,1.732b)	(2,2,0),(0,0,4),(2,-2,0)	(1/8,-1/8,1/4)
43.224	*Fdd*2	P6(1)P1(3)	(a,-0.414a,0.414a,a,0,0),(b,1.732b)	(2,2,0),(0,0,4),(2,-2,0)	(11/8,-3/8,3/4)
8.32	*Cm*	C1(1)P1(1)	(a,b,0,0,0,0),(c,-1.732c)	(2,1,-4),(0,1,0),(2,1,0)	(0,0,0)
5.13	*C*2	C2(1)P1(3)	(a,b,a,-b,0,0),(c,1.732c)	(2,-2,0),(2,2,0),(-1,1,2)	(0,0,0)
5.13	*C*2	C3(1)P1(3)	(a,b,0.707a-0.707b,-0.707a-0.707b,0,0),(c,1.732c)	(2,2,0),(-2,2,0),(1,1,2)	(1/8,15/8,1/4)
8.32	*Cm*	C8(1)P1(3)	(a,b,a,b,0,0),(c,1.732c)	(2,-2,0),(2,2,0),(-1,1,2)	(0,0,0)
9.37	*Cc*	C9(1)P1(3)	(a,b,b,-a,0,0),(c,1.732c)	(2,-2,0),(2,2,0),(-1,1,2)	(3/2,0,0)
12.58	*C*2/*m*	C11(1)P1(2)	(a,0,b,0,a,0),(-2c,0)	(-2,-4,0),(2,0,0),(0,0,4)	(0,0,0)
12.58	*C*2/*m*	C12(1)P1(2)	(0,a,b,0,0,-a),(-2c,0)	(-2,-4,0),(2,0,0),(0,0,4)	(1/2,0,0)
38.187	*Amm*2	C13(1)P1(1)	(a,-0.414a,b,-0.414b,b,-0.414b),(c,-1.732c)	(0,0,4),(0,2,0),(-4,-2,0)	(0,0,1/4)
39.195	*Abm*2	C14(1)P1(1)	(a,-0.414a,b,2.414b,-b,-	(0,0,4),(0,2,0),(-4,-	(0,0,1/4)

			2.414b),(c,-1.732c)	2,0)	
5.13	*C*2	S1(1)P1(2)	(a,b,c,0,a,-b),(-2d,0)	(-2,-4,0),(2,0,0), (0,0,4)	(0,0,0)
5.13	*C*2	S2(1)P1(1)	(a,-0.414a,b,c,0.707b-0.707c,-0.707b-0.707c),(d,-1.732d)	(0,-2,0),(4,2,0), (0,0,4)	(0,0,1/4)
8.32	*Cm*	4D2(1)P1(2)	(a,b,c,d,a,b),(-2e,0)	(-2,-4,0),(2,0,0), (0,0,4)	(0,0,0)
12.62	*C*2'/*m*'	P1(1)P2(1)	(a,0,0,0,0,0),(b,0.577b)	(2,1,-4),(0,1,0), (2,1,0)	(0,0,0)
44.231	*Im*'*m*2'	P2(1)P2(1)	(a,-0.414a,0,0,0,0),(b,0.577b)	(0,1,0),(0,0,4), (2,1,0)	(0,0,1/4)
12.62	*C*2'/*m*'	P3(1)P2(3)	(a,0,a,0,0,0),(-b,0.577b)	(2,-2,0),(2,2,0),(-1,1,2)	(0,0,0)
15.89	*C*2'/*c*'	P4(1)P2(3)	(a,0,0,a,0,0),(-b,0.577b)	(2,-2,0),(2,2,0),(-1,1,2)	(0,1/2,0)
42.221	*Fm*'*m*2'	P5(1)P2(3)	(a,-0.414a,a,-0.414a,0,0),(-b,0.577b)	(2,2,0),(0,0,4),(2,-2,0)	(1/8,-1/8,1/4)
43.226	*Fd*'*d*2'	P6(1)P2(3)	(a,-0.414a,0.414a,a,0,0),(-b,0.577b)	(2,2,0),(0,0,4),(2,-2,0)	(11/8,-3/8,3/4)
8.34	*Cm*'	C1(1)P2(1)	(a,b,0,0,0,0),(c,0.577c)	(2,1,-4),(0,1,0), (2,1,0)	(0,0,0)
5.15	*C*2'	C2(1)P2(3)	(a,b,a,-b,0,0),(-c,0.577c)	(2,-2,0),(2,2,0),(-1,1,2)	(0,0,0)
5.15	*C*2'	C3(1)P2(3)	(a,b,0.707a-0.707b,-0.707a-0.707b,0,0),(-c,0.577c)	(2,2,0),(-2,2,0), (1,1,2)	(1/8,15/8,1/4)
8.34	*Cm*'	C8(1)P2(3)	(a,b,a,b,0,0),(-c,0.577c)	(2,-2,0),(2,2,0),(-1,1,2)	(0,0,0)
9.39	*Cc*'	C9(1)P2(3)	(a,b,b,-a,0,0),(-c,0.577c)	(2,-2,0),(2,2,0),(-1,1,2)	(3/2,0,0)
12.62	*C*2'/*m*'	C11(1)P2(2)	(a,0,b,0,a,0),(0,-1.155c)	(-2,-4,0),(2,0,0), (0,0,4)	(0,0,0)
12.62	*C*2'/*m*'	C12(1)P2(2)	(0,a,b,0,0,-a),(0,-1.155c)	(-2,-4,0),(2,0,0), (0,0,4)	(1/2,0,0)
38.19	*Amm*'2'	C13(1)P2(1)	(a,-0.414a,b,-0.414b,b,-0.414b),(c,0.577c)	(0,0,4),(0,2,0),(-4,-2,0)	(0,0,1/4)
39.198	*Abm*'2'	C14(1)P2(1)	(a,-0.414a,b,2.414b,-b,-2.414b),(c,0.577c)	(0,0,4),(0,2,0),(-4,-2,0)	(0,0,1/4)
5.15	*C*2'	S1(1)P2(2)	(a,b,c,0,a,-b),(0,-1.155d)	(-2,-4,0),(2,0,0), (0,0,4)	(0,0,0)
5.15	*C*2'	S2(1)P2(1)	(a,-0.414a,b,c,0.707b-0.707c,-0.707b-0.707c),(d,0.577d)	(0,-2,0),(4,2,0), (0,0,4)	(0,0,1/4)
8.34	*Cm*'	4D2(1)P2(2)	(a,b,c,d,a,b),(0,-1.155e)	(-2,-4,0),(2,0,0), (0,0,4)	(0,0,0)
2.4	$P\acute{1}$	P1(1)C1(1)	(a,0,0,0,0,0),(b,c)	(1,0,2),(0,1,0),(-2,0,0)	(0,0,0)
8.32	*Cm*	P2(1)C1(1)	(a,-0.414a,0,0,0,0),(b,c)	(-2,0,0),(0,0,4), (0,1,0)	(-1/8,0,1/4)
1.1	*P*1	C1(1)C1(1)	(a,b,0,0,0,0),(c,d)	(1,0,2),(0,1,0),(-2,0,0)	(0,0,0)
2.4	$P\acute{1}$	C4(1)C1(1)	(a,0,b,0,0,0),(c,d)	(1,1,2),(0,2,0),(-2,0,0)	(0,0,0)
2.4	$P\acute{1}$	C5(1)C1(1)	(a,0,0,b,0,0),(c,d)	(1,1,2),(0,2,0),(-2,0,0)	(0,1/2,0)
8.32	*Cm*	C6(1)C1(1)	(a,-0.414a,b,-0.414b,0,0),(c,d)	(-2,-2,0),(0,0,4),(-2,0,0)	(-1/8,-1/8,1/4)
9.37	*Cc*	C7(1)C1(1)	(a,-0.414a,b,2.414b,0,0),(c,d)	(-2,-2,0),(0,0,4),(-2,0,0)	(-5/8,-5/8,5/4)
2.4	$P\acute{1}$	S3(1)C1(1)	(a,0,b,0,c,0),(d,e)	(0,0,4),(0,2,0),(-2,0,0)	(0,0,0)
2.4	$P\acute{1}$	S4(1)C1(1)	(a,0,0,b,0,c),(d,e)	(0,0,4),(0,2,0),(-	(0,1/2,0)

				2,0,0)	
6.18	*Pm*	S5(1)C1(1)	(a,-0.414a,b,-0.414b,c,-0.414c),(d,e)	(-2,0,0),(0,0,4),(0,2,0)	(0,0,1/4)
7.24	*Pc*	S6(1)C1(1)	(a,-0.414a,b,2.414b,c,2.414c),(d,e)	(-2,0,0),(0,0,4),(0,2,0)	(0,0,1/4)
1.1	*P*1	4D1(1)C1(1)	(a,b,c,d,0,0),(e,f)	(1,1,2),(0,2,0),(-2,0,0)	(0,0,0)
1.1	*P*1	6D1(1)C1(1)	(a,b,c,d,e,f),(g,h)	(0,0,4),(0,2,0),(-2,0,0)	(0,0,0)

S6. 5C

S7. U_1

Table S4 Order parameter components and unit cell configurations for subgroups of $P6_3/mmc$ which can arise from phase transitions in which irrep $U_1(1/2,0,1/5)$ is the active representation.

SGN	Space Group	OPD Name	OPD Vector	Basis Vectors	Origin
58	*Pnnm*	P1	(a,0,0,0,0,0)	(0,0,5),(2,1,0),(0,1,0)	(0,0,0)
59	*Pmmn*	P2	(0,a,0,0,0,0)	(0,0,5),(0,-1,0),(2,1,0)	(1/2,1/2,0)
164	$P\bar{3}m1$	P3	(a,0,a,0,a,0)	(2,0,0),(0,2,0),(0,0,5)	(0,0,0)
187	$P\bar{6}m2$	P4	(a,-0.325a,a,-0.325a,a,-0.325a)	(0,-2,0),(2,2,0),(0,0,5)	(0,0,1/4)
64	*Cmca*	P5	(a,0,0,0,a,0)	(2,0,0),(2,4,0),(0,0,5)	(0,0,0)
63	*Cmcm*	P6	(0,a,0,0,0,-a)	(2,0,0),(2,4,0),(0,0,5)	(1/2,0,0)
31	$Pmn2_1$	C1	(a,b,0,0,0,0)	(0,-1,0),(2,1,0),(0,0,5)	(1/2,1/4,0)
156	*P*3*m*1	C2	(a,b,a,b,a,b)	(2,0,0),(0,2,0),(0,0,5)	(0,0,0)
20	$C222_1$	C3	(a,b,0,0,a,-b)	(2,0,0),(2,4,0),(0,0,5)	(1/2,0,0)
14	$P2_1/c$	C4	(0,0,a,0,b,0)	(-2,0,0),(0,0,5),(0,2,0)	(0,0,0)
11	$P2_1/m$	C5	(0,0,0,a,0,b)	(-2,0,0),(0,0,5),(0,2,0)	(0,1/2,0)
14	$P2_1/c$	C6	(a,0,0,0,0,b)	(-2,0,0),(0,0,5),(2,2,0)	(0,1/2,0)
12	*C*2/*m*	C7	(a,0,b,0,a,0)	(-2,-4,0),(2,0,0),(0,0,5)	(0,0,0)
12	*C*2/*m*	C8	(0,a,b,0,0,-a)	(-2,-4,0),(2,0,0),(0,0,5)	(1/2,0,0)
38	Amm2	C9	(a,-0.325a,b,-0.325b,b,-0.325b)	(0,0,5),(0,2,0),(-4,-2,0)	(0,0,1/4)
39	Abm2	C10	(a,-0.325a,b,3.078b,-b,-3.078b)	(0,0,5),(0,2,0),(-4,-2,0)	(0,0,1/4)
36	$Cmc2_1$	C11	(a,b,0,0,a,b)	(2,0,0),(2,4,0),(0,0,5)	(1/2,-1,0)
5	*C*2	S1	(a,b,c,0,a,-b)	(-2,-4,0),(2,0,0),(0,0,5)	(0,0,0)
5	C2	S2	(a,-0.325a,b,c,0.809b-0.588c,-0.588b-0.809c)	(0,-2,0),(4,2,0),(0,0,5)	(0,0,1/4)
2	$P\bar{1}$	S3	(a,0,b,0,c,0)	(0,0,5),(0,2,0),(-2,0,0)	(0,0,0)
2	$P\bar{1}$	S4	(a,0,0,b,0,c)	(0,0,5),(0,2,0),(-2,0,0)	(0,1/2,0)
6	Pm	S5	(a,-0.325a,b,-0.325b,c,-0.325c)	(-2,0,0),(0,0,5),(0,2,0)	(0,0,1/4)
7	Pc	S6	(a,-0.325a,b,3.078b,c,3.078c)	(-2,0,0),(0,0,5),(0,2,0)	(0,0,1/4)
4	$P2_1$	4D1	(0,0,a,b,c,d)	(-2,0,0),(0,0,5),(0,2,0)	(0,1/2,0)

8	*Cm*	4D2	(a,b,c,d,a,b)	(-2,-4,0),(2,0,0),(0,0,5)	(0,0,0)
1	*P*1	6D1	(a,b,c,d,e,f)	(0,0,5),(0,2,0),(-2,0,0)	(0,0,0)
58	*Pnnm*	P1	(a,0,0,0,0,0)	(0,0,5),(2,1,0),(0,1,0)	(0,0,0)
59	*Pmmn*	P2	(0,a,0,0,0,0)	(0,0,5),(0,-1,0),(2,1,0)	(1/2,1/2,0)
164	$P\bar{3}m1$	P3	(a,0,a,0,a,0)	(2,0,0),(0,2,0),(0,0,5)	(0,0,0)

S8. U_1 and mΓ_4^+

Table S5 Magnetic subgroups arising from coupling of irreps $m\Gamma_4^{+¿¿}$ and U_1(1/2,0,1/5), with respect to the parent space group $P6_3/mmc$.

SGN.M	Space Group	OPD Name U_1(1/2,0,1/5) $m\Gamma_4^{+¿¿}$	OPD Vector U_1(1/2,0,1/5), $m\Gamma_4^{+¿¿}$	Basis Vectors	Origin
58.398	*Pnn*'*m*'	P1(1)P1(1)	(a,0,0,0,0,0),(b)	(-2,-1,0),(0,0,5),(0,1,0)	(0,0,0)
59.409	Pm'm'n	P2(1)P1(1)	(0,a,0,0,0,0),(b)	(0,0,5),(0,-1,0),(2,1,0)	(1/2,1/2,0)
164.89	$P\bar{3}m'1$	P3(1)P1(1)	(a,0,a,0,a,0),(b)	(0,-2,0),(2,2,0),(0,0,5)	(0,0,0)
187.211	$P\bar{6}'m'2$	P4(1)P1(1)	(a,-0.325a,a,-0.325a,a,-0.325a),(b)	(2,2,0),(-2,0,0),(0,0,5)	(0,0,1/4)
64.476	*Cm*'*ca*'	P5(1)P1(1)	(a,0,0,0,a,0),(b)	(2,0,0),(2,4,0),(0,0,5)	(0,0,0)
63.464	*Cm*'*cm*'	P6(1)P1(1)	(0,a,0,0,0,-a),(b)	(2,0,0),(2,4,0),(0,0,5)	(1/2,0,0)
31.125	Pm'n21'	C1(1)P1(1)	(a,b,0,0,0,0),(c)	(0,-1,0),(2,1,0),(0,0,5)	(1/2,1/4,0)
156.51	*P*3*m*'1	C2(1)P1(1)	(a,b,a,b,a,b),(c)	(0,-2,0),(2,2,0),(0,0,5)	(0,0,0)
20.34	C22'21'	C3(1)P1(1)	(a,b,0,0,a,-b),(c)	(2,4,0),(-2,0,0),(0,0,5)	(3/2,2,5/4)
14.79	$P2_1'/c'$	C4(1)P1(1)	(0,0,a,0,b,0),(c)	(-2,0,0),(0,0,5),(0,2,0)	(0,0,0)
11.54	$P2_1'/m'$	C5(1)P1(1)	(0,0,0,a,0,b),(c)	(-2,0,0),(0,0,5),(0,2,0)	(0,1/2,0)
14.79	$P2_1'/c'$	C6(1)P1(1)	(a,0,0,0,0,b),(c)	(-2,0,0),(0,0,5),(2,2,0)	(0,1/2,0)
12.62	*C*2'/*m*'	C7(1)P1(1)	(a,0,b,0,a,0),(c)	(-2,-4,0),(2,0,0),(0,0,5)	(0,0,0)
12.62	*C*2'/*m*'	C8(1)P1(1)	(0,a,b,0,0,-a),(c)	(-2,-4,0),(2,0,0),(0,0,5)	(1/2,0,0)
38.191	Am'm'2	C9(1)P1(1)	(a,-0.325a,b,-0.325b,b,-0.325b),(c)	(0,0,5),(0,2,0),(-4,-2,0)	(0,0,1/4)
39.199	Ab'm'2	C10(1)P1(1)	(a,-0.325a,b,3.078b,-b,-3.078b),(c)	(0,0,5),(0,2,0),(-4,-2,0)	(0,0,1/4)
36.174	*Cm*'*c*2$_1$'	C11(1)P1(1)	(a,b,0,0,a,b),(c)	(2,0,0),(2,4,0),(0,0,5)	(1/2,-1,0)
5.15	*C*2'	S1(1)P1(1)	(a,b,c,0,a,-b),(d)	(-2,-4,0),(2,0,0),(0,0,5)	(0,0,0)
5.13	C2	S2(1)P1(1)	(a,-0.325a,b,c,0.809b-0.588c,-0.588b-0.809c),(d)	(0,-2,0),(4,2,0),(0,0,5)	(0,0,1/4)
2.4	$P\bar{1}$	S3(1)P1(1)	(a,0,b,0,c,0),(d)	(0,0,5),(0,2,0),(-2,0,0)	(0,0,0)
2.4	$P\bar{1}$	S4(1)P1(1)	(a,0,0,b,0,c),(d)	(0,0,5),(0,2,0),(-2,0,0)	(0,1/2,0)
6.2	Pm'	S5(1)P1(1)	(a,-0.325a,b,-0.325b,c,-0.325c),(d)	(-2,0,0),(0,0,5),(0,2,0)	(0,0,1/4)

7.26	Pc'	S6(1)P1(1)	(a,-0.325a,b,3.078b,c,3.078c),(d)	(-2,0,0),(0,0,5),(0,2,0)	(0,0,1/4)
4.9	$P2_1$'	4D1(1)P1(1)	(0,0,a,b,c,d),(e)	(-2,0,0),(0,0,5),(0,2,0)	(0,1/2,0)
8.34	*Cm*'	4D2(1)P1(1)	(a,b,c,d,a,b),(e)	(-2,-4,0),(2,0,0),(0,0,5)	(0,0,0)
1.1	*P*1	6D1(1)P1(1)	(a,b,c,d,e,f),(g)	(0,0,5),(0,2,0),(-2,0,0)	(0,0,0)

S9. U_1 and mΓ_5^+

Table S6 Magnetic subgroups arising from coupling of irreps $m\Gamma_5^{+¿¿}$ and U_1(1/2,0,1/5), with respect to the parent space group $P6_3/mmc$.

SGN.M	Space Group	OPD Name U_1(1/2,0,1/5) $m\Gamma_5^{+¿¿}$	OPD Vector U_1(1/2,0,1/5),$m\Gamma_5^{+¿¿}$	Basis Vectors	Origin
58.393	*Pnnm*	P1(1)P1(1)	(a,0,0,0,0,0),(b,-1.732b)	(-2,-1,0),(0,0,5),(0,1,0)	(0,0,0)
59.405	*Pmmn*	P2(1)P1(1)	(0,a,0,0,0,0),(b,-1.732b)	(0,1,0),(0,0,5),(2,1,0)	(1/2,0,0)
64.469	*Cmca*	P5(1)P1(2)	(a,0,0,0,a,0),(-2b,0)	(2,0,0),(2,4,0),(0,0,5)	(0,0,0)
63.457	*Cmcm*	P6(1)P1(2)	(0,a,0,0,0,-a),(-2b,0)	(2,0,0),(2,4,0),(0,0,5)	(1/2,0,0)
31.123	$Pmn2_1$	C1(1)P1(1)	(a,b,0,0,0,0),(c,-1.732c)	(0,-1,0),(2,1,0),(0,0,5)	(1/2,1/4,0)
20.31	$C222_1$	C3(1)P1(2)	(a,b,0,0,a,-b),(-2c,0)	(2,0,0),(2,4,0),(0,0,5)	(1/2,0,0)
12.58	*C*2/*m*	C7(1)P1(2)	(a,0,b,0,a,0),(-2c,0)	(-2,-4,0),(2,0,0),(0,0,5)	(0,0,0)
12.58	*C*2/*m*	C8(1)P1(2)	(0,a,b,0,0,-a),(-2c,0)	(-2,-4,0),(2,0,0),(0,0,5)	(1/2,0,0)
38.187	Amm2	C9(1)P1(1)	(a,-0.325a,b,-0.325b,b,-0.325b),(c,-1.732c)	(0,0,5),(0,2,0),(-4,-2,0)	(0,0,1/4)
39.195	Abm2	C10(1)P1(1)	(a,-0.325a,b,3.078b,-b,-3.078b),(c,-1.732c)	(0,0,5),(0,2,0),(-4,-2,0)	(0,0,1/4)
36.172	$Cmc2_1$	C11(1)P1(2)	(a,b,0,0,a,b),(-2c,0)	(2,0,0),(2,4,0),(0,0,5)	(1/2,-1,0)
5.13	*C*2	S1(1)P1(2)	(a,b,c,0,a,-b),(-2d,0)	(-2,-4,0),(2,0,0),(0,0,5)	(0,0,0)
5.13	C2	S2(1)P1(1)	(a,-0.325a,b,c,0.809b-0.588c,-0.588b-0.809c),(d,-1.732d)	(0,-2,0),(4,2,0),(0,0,5)	(0,0,1/4)
8.32	*Cm*	4D2(1)P1(2)	(a,b,c,d,a,b),(-2e,0)	(-2,-4,0),(2,0,0),(0,0,5)	(0,0,0)
58.398	*Pnn*'*m*'	P1(1)P2(1)	(a,0,0,0,0,0),(b,0.577b)	(0,0,5),(2,1,0),(0,1,0)	(0,0,0)
59.41	*Pmm*'*n*'	P2(1)P2(1)	(0,a,0,0,0,0),(b,0.577b)	(0,0,5),(0,-1,0),(2,1,0)	(1/2,1/2,0)
64.474	*Cm*'*c*'*a*	P5(1)P2(2)	(a,0,0,0,a,0),(0,-1.155b)	(2,0,0),(2,4,0),(0,0,5)	(0,0,0)
63.462	*Cm*'*c*'*m*	P6(1)P2(2)	(0,a,0,0,0,-a),(0,-1.155b)	(2,0,0),(2,4,0),(0,0,5)	(1/2,0,0)
31.127	*Pm*'*n*'2_1	C1(1)P2(1)	(a,b,0,0,0,0),(c,0.577c)	(0,-1,0),(2,1,0),(0,0,5)	(1/2,1/4,0)
20.33	*C*2'2'2_1	C3(1)P2(2)	(a,b,0,0,a,-b),(0,-1.155c)	(2,0,0),(2,4,0),(0,0,5)	(1/2,0,0)
12.62	*C*2'/*m*'	C7(1)P2(2)	(a,0,b,0,a,0,0),(-1.155c)	(-2,-4,0),(2,0,0),(0,0,5)	(0,0,0)
12.62	*C*2'/*m*'	C8(1)P2(2)	(0,a,b,0,0,-a),(0,-1.155c)	(-2,-4,0),(2,0,0),(0,0,5)	(1/2,0,0)
38.19	Amm'2'	C9(1)P2(1)	(a,-0.325a,b,-0.325b,b,-0.325b),(c,0.577c)	(0,0,5),(0,2,0),(-4,-2,0)	(0,0,1/4)
39.198	Abm'2'	C10(1)P2(1)	(a,-0.325a,b,3.078b,-b,-3.078b),(c,0.577c)	(0,0,5),(0,2,0),(-4,-2,0)	(0,0,1/4)

36.176	*Cm*'*c*'2$_1$	C11(1)P2(2)	(a,b,0,0,a,b),(0,-1.155c)	(2,0,0),(2,4,0),(0,0,5)	(1/2,-1,0)
5.15	*C*2'	S1(1)P2(2)	(a,b,c,0,a,-b),(0,-1.155d)	(-2,-4,0),(2,0,0),(0,0,5)	(0,0,0)
5.15	C2'	S2(1)P2(1)	(a,-0.325a,b,c,0.809b-0.588c,-0.588b-0.809c), (d,0.577d)	(0,-2,0),(4,2,0),(0,0,5)	(0,0,1/4)
8.34	*Cm*'	4D2(1)P2(2)	(a,b,c,d,a,b),(0,-1.155e)	(-2,-4,0),(2,0,0),(0,0,5)	(0,0,0)
14.75	$P2_1/c$	P1(1)C1(1)	(a,0,0,0,0,0),(b,c)	(0,1,0),(0,0,5),(2,0,0)	(0,0,0)
11.5	$P2_1/m$	P2(1)C1(1)	(0,a,0,0,0,0),(b,c)	(-2,0,0),(0,0,5),(0,1,0)	(-1/2,0,0)
4.7	$P2_1$	C1(1)C1(1)	(a,b,0,0,0,0),(c,d)	(-2,0,0),(0,0,5),(0,1,0)	(-1/2,0,0)
14.75	$P2_1/c$	C4(1)C1(1)	(0,0,a,0,b,0),(c,d)	(-2,0,0),(0,0,5),(0,2,0)	(0,0,0)
11.5	$P2_1/m$	C5(1)C1(1)	(0,0,0,a,0,b),(c,d)	(-2,0,0),(0,0,5),(0,2,0)	(0,1/2,0)
14.75	$P2_1/c$	C6(1)C1(1)	(a,0,0,0,0,b),(c,d)	(-2,0,0),(0,0,5),(2,2,0)	(0,1/2,0)
2.4	$P\bar{1}$	S3(1)C1(1)	(a,0,b,0,c,0),(d,e)	(0,0,5),(0,2,0),(-2,0,0)	(0,0,0)
2.4	$P\bar{1}$	S4(1)C1(1)	(a,0,0,b,0,c),(d,e)	(0,0,5),(0,2,0),(-2,0,0)	(0,1/2,0)
6.18	*Pm*	S5(1)C1(1)	(a,-0.325a,b,0.325b,c,-0.325c),(d,e)	(-2,0,0),(0,0,5),(0,2,0)	(0,0,1/4)
7.24	Pc	S6(1)C1(1)	(a,-0.325a,b,3.078b,c,3.078c), (d,e)	(-2,0,0),(0,0,5),(0,2,0)	(0,0,1/4)
4.7	$P2_1$	4D1(1)C1(1)	(0,0,a,b,c,d),(e,f)	(-2,0,0),(0,0,5),(0,2,0)	(0,1/2,0)
1.1	*P*1	6D1(1)C1(1)	(a,b,c,d,e,f),(g,h)	(0,0,5),(0,2,0),(-2,0,0)	(0,0,0)

S10. 6C

S11. U_1

Table S7 Order parameter components and unit cell configurations for subgroups of $P6_3/mmc$ which can arise from phase transitions in which irrep $U_1(1/2,0,1/6)$ is the active representation.

SGN	Space Group	OPD Name	OPD Vector	Basis Vectors	Origin
12	*C*2/*m*	P1	(a,0,0,0,0,0)	(2,1,-6),(0,1,0),(2,1,0)	(0,0,0)
44	*Imm*2	P2	(a,-0.268a,0,0,0,0)	(0,0,6),(0,1,0),(-2,-1,0)	(-11/12,1/24,-11/4)
12	*C*2/*m*	P3	(a,0,a,0,0,0)	(2,-2,0),(2,2,0),(-1,1,3)	(0,0,0)
15	*C*2/*c*	P4	(a,0,0,a,0,0)	(2,2,0),(-2,2,0),(1,1,3)	(0,1/2,0)
43	*Fdd*2	P5	(a,-0.268a,0.268a,a,0,0)	(0,0,6),(-2,2,0),(-2,-2,0)	(-4/3,-1/3,1)
42	*Fmm*2	P6	(a,-0.268a,a,-0.268a,0,0)	(0,0,6),(2,2,0),(-2,2,0)	(-1/12,1/12,1/4)
164	$P\bar{3}m1$	P7	(a,0,a,0,a,0)	(2,0,0),(0,2,0),(0,0,6)	(0,0,0)
187	$P\bar{6}m2$	P8	(a,-0.268a,a,-0.268a,a,-0.268a)	(0,-2,0),(2,2,0),(0,0,6)	(0,0,1/4)
152	P3121	P9	(a,1.732a,-2a,0,a,-1.732a)	(2,0,0),(0,2,0),(0,0,6)	(0,0,1)
151	$P3_112$	P10	(a,a,-1.366a,0.366a,0.366a,1.366a)	(0,-2,0),(2,2,0),(0,0,6) -	(0,0,5/4)
8	*Cm*	C1	(a,b,0,0,0,0)	(2,1,-6),(0,1,0),(2,1,0)	(0,0,0)
5	*C*2	C2	(a,b,a,-b,0,0)	(2,-2,0),(2,2,0),(-1,1,3)	(0,0,0)
5	*C*2	C3	(a,b,0.866a0.500b,-0.500a0.866b,0,0)	(2,2,0),(-2,2,0),(1,1,3)	(1/12,23/12,1/4)
2	$P\bar{1}$	C4	(a,0,b,0,0,0)	(1,1,3),(0,2,0),(-2,0,0)	(0,0,0)
2	$P\bar{1}$	C5	(a,0,0,b,0,0)	(1,1,3),(0,2,0),(-2,0,0)	(0,1/2,0)
8	*Cm*	C6	(a,-0.268a,b,-0.268b,0,0)	(-2,-2,0),(0,0,6),(-2,0,0)	(-1/12,-1/12,1/4)
9	*Cc*	C7	(a,-0.268a,b,3.732b,0,0)	(-2,-2,0),(0,0,6),(-2,0,0)	(-7/12,-7/12,7/4)
8	*Cm*	C8	(a,b,a,b,0,0)	(2,-2,0),(2,2,0),(-1,1,3)	(0,0,0)
9	*Cc*	C9	(a,b,b,-a,0,0)	(2,2,0),(-2,2,0),(1,1,3)	(0,3/2,0)
156	*P*3*m*1	C10	(a,b,a,b,a,b)	(2,0,0),(0,2,0),(0,0,6)	(0,0,0)

12	*C*2/*m*	C11	(a,0,b,0,a,0)	(-2,-4,0),(2,0,0),(0,0,6)	(0,0,0)
12	*C*2/*m*	C12	(0,a,b,0,0,-a)	(-2,-4,0),(2,0,0),(0,0,6)	(1/2,0,0)
38	*Amm*2	C13	(a,-0.268a,b,-0.268b,b,-0.268b)	(0,0,6),(0,2,0),(-4,-2,0)	(0,0,1/4)
39	*Abm*2	C14	(a,-0.268a,b,3.732b,-b,3.732b)	(0,0,6),(0,2,0),(-4,-2,0)	(0,0,1/4)
144	$P3_1$	C15	(a,b,-0.500a0.866b,0.866a-0.500b,-0.500a+0.866b,-0.866a-0.500b)	(2,2,0),(-2,0,0),(0,0,6)	(0,0,0)
5	*C*2	S1	(a,b,c,0,a,-b)	(-2,-4,0),(2,0,0),(0,0,6)	(0,0,0)
5	*C*2	S2	(a,-0.268a,b,c,0.866b0.500c,-0.500b0.866c)	(0,-2,0),(4,2,0),(0,0,6)	(0,0,1/4)
2	$P\acute{1}$	S3	(a,0,b,0,c,0)	(0,0,6),(0,2,0),(-2,0,0)	(0,0,0)
2	$P\acute{1}$	S4	(a,0,0,b,0,c)	(0,0,6),(0,2,0),(-2,0,0)	(0,1/2,0)
6	*Pm*	S5	(a,-0.268a,b,-0.268b,c,-0.268c)	(-2,0,0),(0,0,6),(0,2,0)	(0,0,1/4)
7	*Pc*	S6	(a,-0.268a,b,3.732b,c,3.732c)	(-2,0,0),(0,0,6),(0,2,0)	(0,0,1/4)
1	*P*1	4D1	(a,b,c,d,0,0)	(1,1,3),(0,2,0),(-2,0,0)	(0,0,0)
8	*Cm*	4D2	(a,b,c,d,a,b)	(-2,-4,0),(2,0,0),(0,0,6)	(0,0,0)
1	*P*1	6D1	(a,b,c,d,e,f)	(0,0,6),(0,2,0),(-2,0,0)	(0,0,0)

S12. U_1 and mΓ_4^+

Table S8 Magnetic subgroups arising from coupling of irreps $m\Gamma_4^{+¿¿}$ and U_1(1/2,0,1/6), with respect to the parent space group $P6_3/mmc$.

SGN.M	Space group	OPD Name U_1(1/2,0,1/6) $m\Gamma_4^{+¿¿}$	OPD Vector U_1(1/2,0,1/6), $m\Gamma_4^{+¿¿}$	Basis Vectors	Origin
12.62	C2'/m'	P1(1)P1(1)	(a,0,0,0,0,0),(b)	(2,1,-6),(0,1,0),(2,1,0)	(0,0,0)
44.232	Im'm'2	P2(1)P1(1)	(a,-0.268a,0,0,0,0),(b)	(0,0,6),(0,1,0),(-2,-1,0)	(-11/12,1/24,-11/4)
12.62	C2'/m'	P3(1)P1(1)	(a,0,a,0,0,0),(b)	(2,-2,0),(2,2,0),(-1,1,3)	(0,0,0)
15.85	C2/c	P4(1)P1(1)	(a,0,0,a,0,0),(b)	(2,2,0),(-2,2,0),(1,1,3)	(0,1/2,0)
43.226	Fd'd2'	P5(1)P1(1)	(a,-0.268a,0.268a,a,0,0),(b)	(0,0,6),(-2,2,0),(-2,-2,0)	(-4/3,-1/3,1)
42.222	Fm'm'2	P6(1)P1(1)	(a,-0.268a,a,-0.268a,0,0),(b)	(0,0,6),(2,2,0),(-2,2,0)	(-1/12,1/12,1/4)
164.89	$P\acute{3}m$'1	P7(1)P1(1)	(a,0,a,0,a,0),(b)	(0,-2,0),(2,2,0),(0,0,6)	(0,0,0)
187.21			(a,-0.268a,a,-0.268a,a,-	(2,2,0),(-2,0,0),	
1	$P\acute{6}$'m'2	P8(1)P1(1)	0.268a),(b)	(0,0,6)	(0,0,1/4)
152.35	P312'1	P9(1)P1(1)	(a,1.732a,-2a,0,a,-1.732a),(b)	(0,-2,0),(2,2,0),(0,0,6)	(0,0,0)
151.29	P3112	P10(1)P1(1)	(a,a,-1.366a,0.366a,0.366a,-1.366a),(b)	(2,2,0),(-2,0,0),(0,0,6)	(0,0,1/4)
8.34	Cm'	C1(1)P1(1)	(a,b,0,0,0,0),(c)	(2,1,-6),(0,1,0),(2,1,0)	(0,0,0)
5.15	C2'	C2(1)P1(1)	(a,b,a,-b,0,0),(c)	(2,-2,0),(2,2,0),(-1,1,3)	(0,0,0)
5.13	C2	C3(1)P1(1)	(a,b,0.866a-0.500b,-0.500a-0.866b,0,0),(c)	(2,2,0),(-2,2,0),(1,1,3)	(1/12,23/12,1/4)
2.4	$P\acute{1}$	C4(1)P1(1)	(a,0,b,0,0,0),(c)	(1,1,3),(0,2,0),(-2,0,0)	(0,0,0)
2.4	$P\acute{1}$	C5(1)P1(1)	(a,0,0,b,0,0),(c)	(1,1,3),(0,2,0),(-2,0,0)	(0,1/2,0)

8.34	Cm'	C6(1)P1(1)	(a,-0.268a,b,-0.268b,0,0),(c)	(-2,-2,0),(0,0,6),(-2,0,0)	(-1/12,-1/12,1/4)
9.39	Cc'	C7(1)P1(1)	(a,-0.268a,b,3.732b,0,0),(c)	(-2,-2,0),(0,0,6),(-2,0,0)	(-7/12,-7/12,7/4)
8.34	Cm'	C8(1)P1(1)	(a,b,a,b,0,0),(c)	(2,-2,0),(2,2,0),(-1,1,3)	(0,0,0)
9.37	Cc	C9(1)P1(1)	(a,b,b,-a,0,0),(c)	(2,2,0),(-2,2,0),(1,1,3)	(0,3/2,0)
156.51	P3m'1	C10(1)P1(1)	(a,b,a,b,a,b),(c)	(0,-2,0),(2,2,0),(0,0,6)	(0,0,0)
12.62	C2'/m'	C11(1)P1(1)	(a,0,b,0,a,0),(c)	(-2,-4,0),(2,0,0),(0,0,6)	(0,0,0)
12.62	C2'/m'	C12(1)P1(1)	(0,a,b,0,0,-a),(c)	(-2,-4,0),(2,0,0),(0,0,6)	(1/2,0,0)
38.191	Am'm'2	C13(1)P1(1)	(a,-0.268a,b,-0.268b,b,-0.268b),(c)	(0,0,6),(0,2,0),(-4,-2,0)	(0,0,1/4)
39.199	Ab'm'2	C14(1)P1(1)	(a,-0.268a,b,3.732b,-b,-3.732b),(c)	(0,0,6),(0,2,0),(-4,-2,0)	(0,0,1/4)
144.4	P31	C15(1)P1(1)	(a,b,-0.500a-0.866b,0.866a-0.500b,-0.500a+0.866b,-0.866a-0.500b),(c)	(2,2,0),(-2,0,0),(0,0,6)	(0,0,0)
5.15	C2'	S1(1)P1(1)	(a,b,c,0,a,-b),(d)	(-2,-4,0),(2,0,0),(0,0,6)	(0,0,0)
5.13	C2	S2(1)P1(1)	(a,-0.268a,b,c,0.866b-0.500c,-0.500b-0.866c),(d)	(0,-2,0),(4,2,0),(0,0,6)	(0,0,1/4)
2.4	P$\bar{1}$	S3(1)P1(1)	(a,0,b,0,c,0),(d)	(0,0,6),(0,2,0),(-2,0,0)	(0,0,0)
2.4	P$\bar{1}$	S4(1)P1(1)	(a,0,0,b,0,c),(d)	(0,0,6),(0,2,0),(-2,0,0)	(0,1/2,0)
6.2	Pm'	S5(1)P1(1)	(a,-0.268a,b,-0.268b,c,-0.268c),(d)	(-2,0,0),(0,0,6),(0,2,0)	(0,0,1/4)
7.26	Pc'	S6(1)P1(1)	(a,-0.268a,b,3.732b,c,3.732c),(d)	(-2,0,0),(0,0,6),(0,2,0)	(0,0,1/4)
1.1	P1	4D1(1)P1(1)	(a,b,c,d,0,0),(e)	(1,1,3),(0,2,0),(-2,0,0)	(0,0,0)
8.34	Cm'	4D2(1)P1(1)	(a,b,c,d,a,b),(e)	(-2,-4,0),(2,0,0),(0,0,6)	(0,0,0)
1.1	P1	6D1(1)P1(1)	(a,b,c,d,e,f),(g)	(0,0,6),(0,2,0),(-2,0,0)	(0,0,0)

S13. U_1 and $m\Gamma_5^+$

Table S9 Magnetic subgroups arising from coupling of irreps $m\Gamma_5^{+¿¿}$ and $U_1(1/2,0,1/6)$, with respect to the parent space group $P6_3/mmc$.

SGN.M	Space Group	OPD Name $U_1(1/2,0,1/6)$ $m\Gamma_5^{+¿¿}$	OPD Vector $U_1(1/2,0,1/6)$, $m\Gamma_5^{+¿¿}$	Basis Vectors	Origin
12.58	C2/m	P1(1)P1(1)	(a,0,0,0,0,0),(b,-1.732b)	(2,1,-6),(0,1,0),(2,1,0)	(0,0,0)
44.229	*Imm*2	P2(1)P1(1)	(a,-0.268a,0,0,0,0),(b,-1.732b)	(0,1,0),(0,0,6),(2,1,0)	(0,0,1/4)
12.58	C2/m	P3(1)P1(3)	(a,0,a,0,0,0),(b,1.732b)	(2,-2,0),(2,2,0),(-1,1,3)	(0,0,0)
15.85	C2/c	P4(1)P1(3)	(a,0,0,a,0,0),(b,1.732b)	(2,2,0),(-2,2,0),(1,1,3)	(0,1/2,0)
43.224	Fdd2	P5(1)P1(3)	(a,-0.268a,0.268a,a,0,0),(b,1.732b)	(-2,2,0),(0,0,6),(2,2,0)	(5/6,5/6,5/2)
42.219	Fmm2	P6(1)P1(3)	(a,-0.268a,a,-0.268a,0,0),(b,1.732b)	(2,2,0),(0,0,6),(2,-2,0)	(1/12,-1/12,1/4)

8.32	Cm	C1(1)P1(1)	(a,b,0,0,0,0),(c,-1.732c)	(2,1,-6),(0,1,0),(2,1,0)	(0,0,0)
5.13	C2	C2(1)P1(3)	(a,b,a,-b,0,0),(c,1.732c)	(2,-2,0),(2,2,0),(-1,1,3)	(0,0,0)
5.13	C2	C3(1)P1(3)	(a,b,0.866a-0.500b,-0.500a-0.866b,0,0),(c,1.732c)	(2,2,0),(-2,2,0),(1,1,3)	(1/12,23/12,1/4)
8.32	Cm	C8(1)P1(3)	(a,b,a,b,0,0),(c,1.732c)	(2,-2,0),(2,2,0),(-1,1,3)	(0,0,0)
9.37	Cc	C9(1)P1(3)	(a,b,b,-a,0,0),(c,1.732c)	(2,2,0),(-2,2,0),(1,1,3)	(0,3/2,0)
12.58	C2/m	C11(1)P1(2)	(a,0,b,0,a,0),(-2c,0)	(-2,-4,0),(2,0,0),(0,0,6)	(0,0,0)
12.58	C2/m	C12(1)P1(2)	(0,a,b,0,0,-a),(-2c,0)	(-2,-4,0),(2,0,0),(0,0,6)	(1/2,0,0)
38.187	Amm2	C13(1)P1(1)	(a,-0.268a,b,-0.268b,b,-0.268b),(c,-1.732c)	(0,0,6),(0,2,0),(-4,-2,0)	(0,0,1/4)
39.195	Abm2	C14(1)P1(1)	(a,-0.268a,b,3.732b,-b,-3.732b),(c,-1.732c)	(0,0,6),(0,2,0),(-4,-2,0)	(0,0,1/4)
5.13	C2	S1(1)P1(2)	(a,b,c,0,a,-b),(-2d,0)	(-2,-4,0),(2,0,0),(0,0,6)	(0,0,0)
5.13	C2	S2(1)P1(1)	(a,-0.268a,b,c,0.866b-0.500c,-0.500b-0.866c),(d,-1.732d)	(0,-2,0),(4,2,0),(0,0,6)	(0,0,1/4)
8.32	Cm	4D2(1)P1(2)	(a,b,c,d,a,b),(-2e,0)	(-2,-4,0),(2,0,0),(0,0,6)	(0,0,0)
12.62	C2'/m'	P1(1)P2(1)	(a,0,0,0,0,0),(b,0.577b)	(2,1,-6),(0,1,0),(2,1,0)	(0,0,0)
44.231	*Im*'*m*2'	P2(1)P2(1)	(a,-0.268a,0,0,0,0),(b,0.577b)	(0,1,0),(0,0,6),(2,1,0)	(0,0,1/4)
12.62	C2'/m'	P3(1)P2(3)	(a,0,a,0,0,0),(-b,0.577b)	(2,-2,0),(2,2,0),(-1,1,3)	(0,0,0)
15.89	C2'/c'	P4(1)P2(3)	(a,0,0,a,0,0),(-b,0.577b)	(2,2,0),(-2,2,0),(1,1,3)	(0,1/2,0)
43.226	Fd'd2'	P5(1)P2(3)	(a,-0.268a,0.268a,a,0,0),(-b,0.577b)	(-2,2,0),(0,0,6),(2,2,0)	(5/6,5/6,5/2)
42.221	Fm'm2'	P6(1)P2(3)	(a,-0.268a,a,-0.268a,0,0),(-b,0.577b)	(2,2,0),(0,0,6),(2,-2,0)	(1/12,-1/12,1/4)
8.34	Cm'	C1(1)P2(1)	(a,b,0,0,0,0),(c,0.577c)	(2,1,-6),(0,1,0),(2,1,0)	(0,0,0)
5.15	C2'	C2(1)P2(3)	(a,b,a,-b,0,0),(-c,0.577c)	(2,-2,0),(2,2,0),(-1,1,3)	(0,0,0)
5.15	C2'	C3(1)P2(3)	(a,b,0.866a-0.500b,-0.500a-0.866b,0,0),(-c,0.577c)	(2,2,0),(-2,2,0),(1,1,3)	(1/12,23/12,1/4)
8.34	Cm'	C8(1)P2(3)	(a,b,a,b,0,0),(-c,0.577c)	(2,-2,0),(2,2,0),(-1,1,3)	(0,0,0)
9.39	Cc'	C9(1)P2(3)	(a,b,b,-a,0,0),(-c,0.577c)	(2,2,0),(-2,2,0),(1,1,3)	(0,3/2,0)
12.62	C2'/m'	C11(1)P2(2)	(a,0,b,0,a,0),(0,-1.155c)	(-2,-4,0),(2,0,0),(0,0,6)	(0,0,0)
12.62	C2'/m'	C12(1)P2(2)	(0,a,b,0,0,-a),(0,-1.155c)	(-2,-4,0),(2,0,0),(0,0,6)	(1/2,0,0)
38.19	Amm'2'	C13(1)P2(1)	(a,-0.268a,b,-0.268b,b,-0.268b),(c,0.577c)	(0,0,6),(0,2,0),(-4,-2,0)	(0,0,1/4)
39.198	Abm'2'	C14(1)P2(1)	(a,-0.268a,b,3.732b,-b,-3.732b),(c,0.577c)	(0,0,6),(0,2,0),(-4,-2,0)	(0,0,1/4)
5.15	C2'	S1(1)P2(2)	(a,b,c,0,a,-b),(0,-1.155d)	(-2,-4,0),(2,0,0),(0,0,6)	(0,0,0)
5.15	C2'	S2(1)P2(1)	(a,-0.268a,b,c,0.866b-0.500c,-0.500b-0.866c),(d,0.577d)	(0,-2,0),(4,2,0),(0,0,6)	(0,0,1/4)
8.34	Cm'	4D2(1)P2(2)	(a,b,c,d,a,b),(0,-1.155e)	(-2,-4,0),(2,0,0),(0,0,6)	(0,0,0)

2.4	$P\bar{1}$	P1(1)C1(1)	(a,0,0,0,0,0),(b,c)	(1,0,3),(0,1,0),(-2,0,0)	(0,0,0)
8.32	Cm	P2(1)C1(1)	(a,-0.268a,0,0,0,0),(b,c)	(-2,0,0),(0,0,6),(0,1,0)	(-1/12,0,1/4)
1.1	P1	C1(1)C1(1)	(a,b,0,0,0,0),(c,d)	(1,0,3),(0,1,0),(-2,0,0)	(0,0,0)
2.4	$P\bar{1}$	C4(1)C1(1)	(a,0,b,0,0,0),(c,d)	(1,1,3),(0,2,0),(-2,0,0)	(0,0,0)
2.4	$P\bar{1}$	C5(1)C1(1)	(a,0,0,b,0,0),(c,d)	(1,1,3),(0,2,0),(-2,0,0)	(0,1/2,0)
8.32	Cm	C6(1)C1(1)	(a,-0.268a,b,-0.268b,0,0),(c,d)	(-2,-2,0),(0,0,6),(-2,0,0)	(-1/12,-1/12,1/4)
9.37	Cc	C7(1)C1(1)	(a,-0.268a,b,3.732b,0,0),(c,d)	(-2,-2,0),(0,0,6),(-2,0,0)	(-7/12,-7/12,7/4)
2.4	$P\bar{1}$	S3(1)C1(1)	(a,0,b,0,c,0),(d,e)	(0,0,6),(0,2,0),(-2,0,0)	(0,0,0)
2.4	$P\bar{1}$	S4(1)C1(1)	(a,0,0,b,0,c),(d,e)	(0,0,6),(0,2,0),(-2,0,0)	(0,1/2,0)
6.18	Pm	S5(1)C1(1)	(a,-0.268a,b,-0.268b,c,-0.268c),(d,e)	(-2,0,0),(0,0,6),(0,2,0)	(0,0,1/4)
7.24	Pc	S6(1)C1(1)	(a,-0.268a,b,3.732b,c,3.732c),(d,e)	(-2,0,0),(0,0,6),(0,2,0)	(0,0,1/4)
1.1	P1	4D1(1)C1(1)	(a,b,c,d,0,0),(e,f)	(1,1,3),(0,2,0),(-2,0,0)	(0,0,0)
1.1	P1	6D1(1)C1(1)	(a,b,c,d,e,f),(g,h)	(0,0,6),(0,2,0),(-2,0,0)	(0,0,0)

S14. 3C

S15. U_1

Table S10 Order parameter components and unit cell configurations for subgroups of $P6_3/mmc$ which can arise from phase transitions in which irrep $U_1(1/2,0,1/3)$ is the active representation.

SGN	Space Group	OPD Name	OPD Vector	Basis Vectors	Origin
58	*Pnnm*	P1	(a,0,0,0,0,0)	(0,0,3),(2,1,0),(0,1,0)	(0,0,0)
59	*Pmmn*	P2	(0,a,0,0,0,0)	(0,0,3),(0,-1,0),(2,1,0)	(1/2,1/2,0)
164	$P\bar{3}m1$	P3	(a,0,a,0,a,0)	(2,0,0),(0,2,0),(0,0,3)	(0,0,0)
187	$P\bar{6}m2$	P4	(a,-0.577a,a,-0.577a,a,-0.577a)	(0,-2,0),(2,2,0),(0,0,3)	(0,0,1/4)
64	*Cmc*a	P5	(a,0,0,0,a,0)	(2,0,0),(2,4,0),(0,0,3)	(0,0,0)
63	*Cmcm*	P6	(0,a,0,0,0,-a)	(2,0,0),(2,4,0),(0,0,3)	(1/2,0,0)
152	$P3_121$	P7	(a,1.732a,-2a,0,a,-1.732a)	(2,0,0),(0,2,0),(0,0,3)	(0,0,1/2)
151	$P3_112$	P8	(a,0.577a,a,0.577a,0,-1.155a)	(0,-2,0),(2,2,0),(0,0,3)	(0,0,3/4)
31	$Pmn2_1$	C1	(a,b,0,0,0,0)	(0,-1,0),(2,1,0),(0,0,3)	(1/2,1/4,0)
156	*P*3*m*1	C2	(a,b,a,b,a,b)	(2,0,0),(0,2,0),(0,0,3)	(0,0,0)
20	$C222_1$	C3	(a,b,0,0,a,-b)	(2,0,0),(2,4,0),(0,0,3)	(1/2,0,0)
14	$P2_1/c$	C4	(0,0,a,0,b,0)	(-2,0,0),(0,0,3),(0,2,0)	(0,0,0)
11	$P2_1/m$	C5	(0,0,0,a,0,b)	(-2,0,0),(0,0,3),(0,2,0)	(0,1/2,0)
14	$P2_1/c$	C6	(a,0,0,0,0,b)	(-2,0,0),(0,0,3),(2,2,0)	(0,1/2,0)
12	*C*2/*m*	C7	(a,0,b,0,a,0)	(-2,-4,0),(2,0,0),(0,0,3)	(0,0,0)
12	*C*2/*m*	C8	(0,a,b,0,0,-a)	(-2,-4,0),(2,0,0),(0,0,3)	(1/2,0,0)
38	*Amm*2	C9	(a,-0.577a,b,-0.577b,b,-0.577b)	(0,0,3),(0,2,0),(-4,-2,0)	(0,0,1/4)

39	*Abm*2	C10	(a,-0.577a,b,1.732b,-b,1.732b)	(0,0,3),(0,2,0),(-4,-2,0)	(0,0,1/4)
36	$Cmc2_1$	C11	(a,b,0,0,a,b)	(2,0,0),(2,4,0),(0,0,3)	(1/2,-1,0)
144	$P3_1$	C12	(a,b,-0.500a0.866b,0.866a-0.500b,-0.500a+0.866b,-0.866a-0.500b)	(2,2,0),(-2,0,0),(0,0,3)	(0,0,0)
5	*C*2	S1	(a,b,c,0,a,-b)	(-2,-4,0),(2,0,0),(0,0,3)	(0,0,0)
5	*C*2	S2	(a,-0.577a,b,c,0.500b0.866c,-0.866b0.500c)	(0,-2,0),(4,2,0),(0,0,3)	(0,0,1/4)
2	$P\acute{1}$	S3	(a,0,b,0,c,0)	(0,0,3),(0,2,0),(-2,0,0)	(0,0,0)
2	$P\acute{1}$	S4	(a,0,0,b,0,c)	(0,0,3),(0,2,0),(-2,0,0)	(0,1/2,0)
6	*Pm*	S5	(a,-0.577a,b,-0.577b,c,-0.577c)	(-2,0,0),(0,0,3),(0,2,0)	(0,0,1/4)
7	*Pc*	S6	(a,-0.577a,b,1.732b,c,1.732c)	(-2,0,0),(0,0,3),(0,2,0)	(0,0,1/4)
4	$P2_1$	4D1	(0,0,a,b,c,d)	(-2,0,0),(0,0,3),(0,2,0)	(0,1/2,0)
8	*Cm*	4D2	(a,b,c,d,a,b)	(-2,-4,0),(2,0,0),(0,0,3)	(0,0,0)
1	*P*1	6D1	(a,b,c,d,e,f)	(0,0,3),(0,2,0),(-2,0,0)	(0,0,0)

S16. U_1 and mΓ_4^+

Table S11 Magnetic subgroups arising from coupling of irreps $m\Gamma_4^{+¿¿}$ and $U_1(1/2,0,1/3)$, with respect to the parent space group $P6_3/mmc$.

SGN.M	Space group	OPD Name $U_1(1/2,0,1/3)$ $m\Gamma_4^{+¿¿}$	OPD Vector $U_1(1/2,0,1/3)$, $m\Gamma_4^{+¿¿}$	Basis Vectors	Origin
58.398	Pnn'm'	P1(1)P1(1)	(a,0,0,0,0,0),(b)	(-2,-1,0),(0,0,3),(0,1,0)	(0,0,0)
59.409	*Pm'm'n*	P2(1)P1(1)	(0,a,0,0,0,0),(b)	(0,0,3),(0,-1,0),(2,1,0)	(1/2,1/2,0)
164.89	$P\acute{3}m'1$	P3(1)P1(1)	(a,0,a,0,a,0),(b)	(0,-2,0),(2,2,0),(0,0,3)	(0,0,0)
187.211	$P\acute{6}'m'2$	P4(1)P1(1)	(a,-0.577a,a,-0.577a,a,-0.577a),(b)	(2,2,0),(-2,0,0),(0,0,3)	(0,0,1/4)
64.476	*Cm'ca'*	P5(1)P1(1)	(a,0,0,0,a,0),(b)	(2,0,0),(2,4,0),(0,0,3)	(0,0,0)
63.464	*Cm'cm'*	P6(1)P1(1)	(0,a,0,0,0,-a),(b)	(2,0,0),(2,4,0),(0,0,3)	(1/2,0,0)
152.35	*P*312'1	P7(1)P1(1)	(a,1.732a,-2a,0,a,-1.732a),(b)	(0,-2,0),(2,2,0),(0,0,3)	(0,0,0)
151.29	P3112	P8(1)P1(1)	(a,0.577a,-a,0.577a,0,-1.155a),(b)	(2,2,0),(-2,0,0),(0,0,3)	(0,0,1/4)
31.125	$Pm'n2_1'$	C1(1)P1(1)	(a,b,0,0,0,0),(c)	(0,-1,0),(2,1,0),(0,0,3)	(1/2,1/4,0)
156.51	*P*3*m*'1	C2(1)P1(1)	(a,b,a,b,a,b),(c)	(0,-2,0),(2,2,0),(0,0,3)	(0,0,0)
20.34	$C22'2_1'$	C3(1)P1(1)	(a,b,0,0,a,-b),(c)	(2,4,0),(-2,0,0),(0,0,3)	(3/2,2,3/4)
14.79	$P2_1'/c'$	C4(1)P1(1)	(0,0,a,0,b,0),(c)	(-2,0,0),(0,0,3),(0,2,0)	(0,0,0)
11.54	$P2_1'/m'$	C5(1)P1(1)	(0,0,0,a,0,b),(c)	(-2,0,0),(0,0,3),(0,2,0)	(0,1/2,0)
14.79	$P2_1'/c'$	C6(1)P1(1)	(a,0,0,0,0,b),(c)	(-2,0,0),(0,0,3),(2,2,0)	(0,1/2,0)
12.62	C2'/m'	C7(1)P1(1)	(a,0,b,0,a,0),(c)	(-2,-4,0),(2,0,0),(0,0,3)	(0,0,0)
12.62	C2'/m'	C8(1)P1(1)	(0,a,b,0,0,-a),(c)	(-2,-4,0),(2,0,0),(0,0,3)	(1/2,0,0)
38.191	Am'm'2	C9(1)P1(1)	(a,-0.577a,b,-0.577b,b,-0.577b),(c)	(0,0,3),(0,2,0),(-4,-2,0)	(0,0,1/4)
39.199	Ab'm'2	C10(1)P1(1)	(a,-0.577a,b,1.732b,-b,-	(0,0,3),(0,2,0),(-4,-	(0,0,1/4)

36.174	*Cm*'*c*2$_1$'	C11(1)P1(1)	1.732b),(c) (a,b,0,0,a,b),(c)	2,0) (2,0,0),(2,4,0),(0,0,3)	(1/2,-1,0)
144.4	P31	C12(1)P1(1)	(a,b,-0.500a-0.866b,0.866a-0.500b,-0.500a+0.866b,-0.866a-0.500b),(c)	(2,2,0),(-2,0,0),(0,0,3)	(0,0,0)
5.15	C2'	S1(1)P1(1)	(a,b,c,0,a,-b),(d)	(-2,-4,0),(2,0,0),(0,0,3)	(0,0,0)
5.13	C2	S2(1)P1(1)	(a,-0.577a,b,c,0.500b-0.866c,-0.866b-0.500c),(d)	(0,-2,0),(4,2,0),(0,0,3)	(0,0,1/4)
2.4	$P\acute{1}$	S3(1)P1(1)	(a,0,b,0,c,0),(d)	(0,0,3),(0,2,0),(-2,0,0)	(0,0,0)
2.4	$P\acute{1}$	S4(1)P1(1)	(a,0,0,b,0,c),(d)	(0,0,3),(0,2,0),(-2,0,0)	(0,1/2,0)
6.2	Pm'	S5(1)P1(1)	(a,-0.577a,b,-0.577b,c,-0.577c),(d)	(-2,0,0),(0,0,3),(0,2,0)	(0,0,1/4)
7.26	Pc'	S6(1)P1(1)	(a,-0.577a,b,1.732b,c,1.732c),(d)	(-2,0,0),(0,0,3),(0,2,0)	(0,0,1/4)
4.9	*P*2$_1$'	4D1(1)P1(1)	(0,0,a,b,c,d),(e)	(-2,0,0),(0,0,3),(0,2,0)	(0,1/2,0)
8.34	Cm'	4D2(1)P1(1)	(a,b,c,d,a,b),(e)	(-2,-4,0),(2,0,0),(0,0,3)	(0,0,0)
1.1	*P*1	6D1(1)P1(1)	(a,b,c,d,e,f),(g)	(0,0,3),(0,2,0),(-2,0,0)	(0,0,0)

S17. U_1 and mΓ_5^+

Table S12 Magnetic subgroups arising from coupling of irreps $m\Gamma_5^{+¿¿}$ and U_1(1/2,0,1/3), with respect to the parent space group *P*6$_3$/*mmc*.

SGN.M	Space Group	OPD Name U_1(1/2,0,1/3) $m\Gamma_5^{+¿¿}$	OPD Vector U_1(1/2,0,1/3), $m\Gamma_5^{+¿¿}$	Basis Vectors	Origin
58.393	Pnnm	P1(1)P1(1)	(a,0,0,0,0,0),(b,-1.732b)	(-2,-1,0),(0,0,3),(0,1,0)	(0,0,0)
59.405	*Pmmn*	P2(1)P1(1)	(0,a,0,0,0,0),(b,-1.732b)	(0,1,0),(0,0,3),(2,1,0)	(1/2,0,0)
64.469	*Cmca*	P5(1)P1(2)	(a,0,0,0,a,0),(-2b,0)	(2,0,0),(2,4,0),(0,0,3)	(0,0,0)
63.457	*Cmcm*	P6(1)P1(2)	(0,a,0,0,0,-a),(-2b,0)	(2,0,0),(2,4,0),(0,0,3)	(1/2,0,0)
31.123	Pmn21	C1(1)P1(1)	(a,b,0,0,0,0),(c,-1.732c)	(0,-1,0),(2,1,0),(0,0,3)	(1/2,1/4,0)
20.31	*C*222$_1$	C3(1)P1(2)	(a,b,0,0,a,-b),(-2c,0)	(2,0,0),(2,4,0),(0,0,3)	(1/2,0,0)
12.58	*C*2/*m*	C7(1)P1(2)	(a,0,b,0,a,0),(-2c,0)	(-2,-4,0),(2,0,0),(0,0,3)	(0,0,0)
12.58	C2/m	C8(1)P1(2)	(0,a,b,0,0,-a),(-2c,0)	(-2,-4,0),(2,0,0),(0,0,3)	(1/2,0,0)
38.187	Amm2	C9(1)P1(1)	(a,-0.577a,b,-0.577b,b,-0.577b),(c,-1.732c)	(0,0,3),(0,2,0),(-4,-2,0)	(0,0,1/4)
39.195	Abm2	C10(1)P1(1)	(a,-0.577a,b,1.732b,-b,-1.732b),(c,-1.732c)	(0,0,3),(0,2,0),(-4,-2,0)	(0,0,1/4)
36.172	*Cmc*2$_1$	C11(1)P1(2)	(a,b,0,0,a,b),(-2c,0)	(2,0,0),(2,4,0),(0,0,3)	(1/2,-1,0)
5.13	C2	S1(1)P1(2)	(a,b,c,0,a,-b),(-2d,0)	(-2,-4,0),(2,0,0),(0,0,3)	(0,0,0)
5.13	C2	S2(1)P1(1)	(a,-0.577a,b,c,0.500b-0.866c,-0.866b-0.500c),(d,-1.732d)	(0,-2,0),(4,2,0),(0,0,3)	(0,0,1/4)
8.32	Cm	4D2(1)P1(2)	(a,b,c,d,a,b),(-2e,0)	(-2,-4,0),(2,0,0),(0,0,3)	(0,0,0)
58.398	*Pnn*'*m*'	P1(1)P2(1)	(a,0,0,0,0,0),(b,0.577b)	(0,0,3),(2,1,0),(0,1,0)	(0,0,0)
59.41	Pmm'n'	P2(1)P2(1)	(0,a,0,0,0,0),(b,0.577b)	(0,0,3),(0,-1,0),(2,1,0)	(1/2,1/2,0)
64.474	*Cm*'*c*'*a*	P5(1)P2(2)	(a,0,0,0,a,0),(0,-1.155b)	(2,0,0),(2,4,0),(0,0,3)	(0,0,0)
63.462	*Cm*'*c*'*m*	P6(1)P2(2)	(0,a,0,0,0,-a),(0,-1.155b)	(2,0,0),(2,4,0),(0,0,3)	(1/2,0,0)
31.127	Pm'n'21	C1(1)P2(1)	(a,b,0,0,0,0),(c,0.577c)	(0,-1,0),(2,1,0),	(1/2,1/4,0

				(0,0,3)	)
20.33	*C*2'2'2$_1$	C3(1)P2(2)	(a,b,0,0,a,-b),(0,-1.155c)	(2,0,0),(2,4,0),(0,0,3)	(1/2,0,0)
12.62	C2'/m'	C7(1)P2(2)	(a,0,b,0,a,0),(0,-1.155c)	(-2,-4,0),(2,0,0), (0,0,3)	(0,0,0)
12.62	C2'/m'	C8(1)P2(2)	(0,a,b,0,0,-a),(0,-1.155c)	(-2,-4,0),(2,0,0), (0,0,3)	(1/2,0,0)
38.19	Amm'2'	C9(1)P2(1)	(a,-0.577a,b,-0.577b,b,-0.577b),(c,0.577c)	(0,0,3),(0,2,0),(-4,-2,0)	(0,0,1/4)
39.198	Abm'2'	C10(1)P2(1)	(a,-0.577a,b,1.732b,-b,-1.732b),(c,0.577c)	(0,0,3),(0,2,0),(-4,-2,0)	(0,0,1/4)
36.176	*Cm*'*c*'2$_1$	C11(1)P2(2)	(a,b,0,0,a,b),(0,-1.155c)	(2,0,0),(2,4,0),(0,0,3)	(1/2,-1,0)
5.15	C2'	S1(1)P2(2)	(a,b,c,0,a,-b),(0,-1.155d)	(-2,-4,0),(2,0,0), (0,0,3)	(0,0,0)
5.15	C2'	S2(1)P2(1)	(a,-0.577a,b,c,0.500b-0.866c,-0.866b-0.500c),(d,0.577d)	(0,-2,0),(4,2,0), (0,0,3)	(0,0,1/4)
8.34	Cm'	4D2(1)P2(2)	(a,b,c,d,a,b),(0,-1.155e)	(-2,-4,0),(2,0,0), (0,0,3)	(0,0,0)
14.75	*P*2$_1$/*c*	P1(1)C1(1)	(a,0,0,0,0,0),(b,c)	(0,1,0),(0,0,3),(2,0,0)	(0,0,0)
11.5	P21/m	P2(1)C1(1)	(0,a,0,0,0,0),(b,c)	(-2,0,0),(0,0,3), (0,1,0)	(-1/2,0,0)
4.7	P21	C1(1)C1(1)	(a,b,0,0,0,0),(c,d)	(-2,0,0),(0,0,3), (0,1,0)	(-1/2,0,0)
14.75	P21/c	C4(1)C1(1)	(0,0,a,0,b,0),(c,d)	(-2,0,0),(0,0,3), (0,2,0)	(0,0,0)
11.5	P21/m	C5(1)C1(1)	(0,0,0,a,0,b),(c,d)	(-2,0,0),(0,0,3), (0,2,0)	(0,1/2,0)
14.75	P21/c	C6(1)C1(1)	(a,0,0,0,0,b),(c,d)	(-2,0,0),(0,0,3), (2,2,0)	(0,1/2,0)
2.4	$P\bar{1}$	S3(1)C1(1)	(a,0,b,0,c,0),(d,e)	(0,0,3),(0,2,0),(-2,0,0)	(0,0,0)
2.4	$P\bar{1}$	S4(1)C1(1)	(a,0,0,b,0,c),(d,e)	(0,0,3),(0,2,0),(-2,0,0)	(0,1/2,0)
6.18	Pm	S5(1)C1(1)	(a,-0.577a,b,-0.577b,c,-0.577c),(d,e)	(-2,0,0),(0,0,3), (0,2,0)	(0,0,1/4)
7.24	Pc	S6(1)C1(1)	(a,-0.577a,b,1.732b,c,1.732c), (d,e)	(-2,0,0),(0,0,3), (0,2,0)	(0,0,1/4)
4.7	P21	4D1(1)C1(1)	(0,0,a,b,c,d),(e,f)	(-2,0,0),(0,0,3), (0,2,0)	(0,1/2,0)
1.1	P1	6D1(1)C1(1)	(a,b,c,d,e,f),(g,h)	(0,0,3),(0,2,0),(-2,0,0)	(0,0,0)